AN AUTOMATED LAB-ON-A-CD SYSTEM FOR PARALLEL WHOLE BLOOD ANALYSES

(Spine title: A Lab-on-a-CD System for Blood Analyses)

(Thesis format: Integrated Article)

by

Tingjie Li

Department of Mechanical and Materials Engineering
Faculty of Engineering

A thesis submitted in partial fulfillment
of the requirements for the degree of
Doctor of Philosophy

The School of Graduate and Postdoctoral Studies
The University of Western Ontario
London, Ontario, Canada

© Tingjie Li 2012

www.manaraa.com

THE UNIVERSITY OF WESTERN ONTARIO
School of Graduate and Postdoctoral Studies

CERTIFICATE OF EXAMINATION

Supervisor

Dr. Jun Yang

Supervisory Committee

Dr. Andy (Xueliang) Sun

Dr. Liying Jiang

Examiners

Dr. Andy (Xueliang) Sun

Dr. Christopher G. Ellis

Dr. George K Knopf

Dr. Xinyu Liu

The thesis by

Tingjie Li

entitled:

An Automated Lab-on-a-CD System for Parallel Whole Blood Analyses

is accepted in partial fulfillment of the
requirements for the degree of
Doctor of Philosophy

Date

Chair of the Thesis Examination Board

www.manaraa.com

Abstract

Medical diagnostics plays a critical role in human healthcare. Blood analysis is one of the most common clinical diagnostic assays. Biomedical engineers have been developing portable and inexpensive diagnostic tools that enable fast and accurate tests for individuals who have limited resources in places that require such field applications. The emergence of Lab-on-a-CD technology provides a compact centrifugal platform for high throughput blood analysis in point-of-care (POC) diagnostics. The objective of this thesis work is to develop a Lab-on-a-CD system for parallel quantitative detection of blood contents.

Blood separation is a key step in blood analysis. By integrating out-of-plane microvalves into the Lab-on-a-CD system, pure plasma is separated from human whole blood sample for subsequent blood detection. These out-of-plane microvalves show excellent performance in preventing backflow or reverse mixing due to blood cell diffusion. The concentrations of certain blood contents in the separated plasma can be detected using the electrochemical biosensors embedded in the plasma reservoir. To improve sensitivity, a nanoporous structure is created on the surfaces of the biosensors' electrodes through an alloying/dealloying process. The nanoporous electrode has an electroactive surface area up to 60 times larger than that of a flat gold electrode of the same size. As a result, numerous catalysts and enzymes are stably entrapped in the nanoporous structure, leading to high sensitivity, stability and reproducibility of the biosensor.

Based on this devised blood separation technique and the improved electrochemical detection method, a Lab-on-a-CD prototype was constructed and successfully applied in the concentration detection of glucose, lactate and uric acid with linear ranges of 0 – 30 mM, 0 – 1.5 mM and 0 – 5 mM, respectively. Furthermore, the volume of whole blood sample consumed for each section can be as small as 16 μL.

www.manaraa.com

The Lab-on-a-CD platform developed in this thesis is low-cost, robust, and simple-to-use. Potentially, it could be used in clinical diagnostics and will especially aid developing countries where resources are limited.

Keywords

Lab-on-a-CD, point-of-care, blood analyses, out-of-plane microvalves, electrochemical detection.

www.manaraa.com

Co-Authorship Statement

This doctoral thesis has been carefully prepared according to the regulations for an integrated-article format thesis stipulated by the Faculty of Graduate and Postdoctoral Studies at the University of Western Ontario, and has been co-authored as follows:

CHAPTER 3: OUT-OF-PLANE MICROVALVES FOR WHOLE BLOOD SEPARATION ON LAB-ON-A-CD

All the theoretical analyses were conducted by T. Li under the supervision of Dr. J. Yang. Device fabrication and experimental testing were undertaken by T. Li under the supervision of Dr. J. Yang. Drafts of Chapter 3 were prepared by T. Li and reviewed by Dr. J. Yang. A paper co-authored by T. Li, L. Zhang and J. Yang has been published on Journal of Micromechanics and Microengineering.

CHAPTER 4: DESIGN AND OPTIMIZATION OF PRUSSIAN BLUE/CARBON NANOTUBE ELECTRODES FOR BIOSENSING APPLICATIONS

All the theoretical analyses were conducted by T. Li under the supervision of Dr. J. Yang. Material synthesis and experimental testing were undertaken by T. Li under the supervision of Dr. J. Yang. Drafts of Chapter 4 were prepared by T. Li and reviewed by Dr. J. Yang. A paper co-authored by T. Li, J. Yang, Q. Zhang has been submitted to Analytical Letters.

CHAPTER 5: FABRICATION OF NANOPOROUS THIN-FILM WORKING ELECTRODES AND THEIR BIOSENSING APPLICATIONS

All the theoretical analyses were conducted by T. Li under the supervision of Dr. J. Yang. Material synthesis and experimental testing were undertaken by T. Li under the supervision of Dr. J. Yang. Drafts of Chapter 5 were prepared by T. Li and reviewed by Dr. J. Yang. A

www.manaraa.com

paper co-authored by T. Li, F. Jia, Y. Fan, Z. Ding and J. Yang has been submitted to Biosensors and Bioelectronics.

CHAPTER 6: A ROBUST LAB-ON-A-CD SYSTEM FOR HIGH-THROUGHPUT AND AUTOMATED WHOLE BLOOD ANALYSIS

All the theoretical analyses were conducted by T. Li under the supervision of Dr. J. Yang. Device fabrication and experimental testing were undertaken by T. Li under the supervision of Dr. J. Yang. Drafts of Chapter 6 were prepared by T. Li and reviewed by Dr. J. Yang. A paper co-authored by T. Li and J. Yang is to be submitted.

www.manaraa.com

Acknowledgments

After been through four years hard work, I am completing my PhD degree in the summer of 2012. It has been my honor to spend these years in the Department of Mechanical and Materials Engineering at the University of Western Ontario, and its faculty and staff members will always remain dear to me. The best and worst moments of my doctoral journey have been shared with many people.

My deepest gratitude must go to my supervisor, Dr. Jun Yang, for introducing me to this state-of-the-art research area and for his continuous guidance and motivation to me to think outside the box. Besides thesis research, Dr. Yang also taught me how to write research proposals and got me involved an industry/university collaboration project. All of these help me become a qualified Ph.D.

Members of the Lanxess project, including Dr. Leo Lau, Dr. Liying Jiang, Dr. Natalie Suhan, Mr. Lorenzo P. Ferrari, Dr. Gilles Arsenault also deserve my sincerest thanks, their assistance and friendship has meant more to me than I could ever express.

Special thanks to technical support from Surface Science Western, especially Mr. Brad Kobe, Mr. Ross Davidson, Ms. Marry Jane Walzak, and Dr. Heng-yong Nie. I also appreciate the technical support from the staff at the Western Nanofabrication Facility, including Mr. Tim Goldhawk, Dr. Todd Simpson, and Dr. Rick Glew. I would also like to thank the thoughtful discussion and friendly support from my colleagues and friends.

Finally, I wish to express my highest gratefulness to all my family members. Their love provided my inspiration and was my driving force. I owe them everything and wish I could show them just how much I love and appreciate them.

www.manaraa.com

Table of Contents

CERTIFICATE OF EXAMINATION ii

Abstract iii

Co-Authorship Statement v

Table of Contents viii

List of Tables xii

List of Figures xiii

Nomenclature xx

Chapter 1 1

1 Introduction 1

1.1 Background 1

1.2 Research Objectives and Outline of this Thesis 2

1.3 References 4

Chapter 2 5

2 Literature Review 5

2.1 Point-of-care Diagnostics 5

2.2 Lab-on-a-CD Technology 11

2.2.1 Microfluidic Pumps 12

2.2.2 Microfluidic Valves 18

2.3 Blood Analysis 24

2.3.1 Conventional Blood Analysis Methods 24

2.3.2 Point-of-care Blood Analysis Systems 26

2.4 Summary 31

2.5 References 32

Chapter 3 43

www.manaraa.com

3 Out-of-plane Microvalves for Whole Blood Separation on Lab-on-a-CD 43
3.1 Introduction 43
3.2 The Working Mechanisms 47
3.3 Experimental Design and Method 51
3.3.1 Materials 51
3.3.2 Device Fabrication 51
3.3.3 Blood Separation Experiments 57
3.4 Results and Discussion 58
3.4.1 Device Characterization 59
3.4.2 Performance of Whole Blood Separation 59
3.4.3 Discussion 67
3.5 Conclusions 69
3.6 References 70
Chapter 4 73
4 Design and Optimization of Prussian Blue/Carbon Nanotube Electrodes for Biosensing Applications 73
4.1 Introduction 73
4.2 Material and methods 76
4.2.1 Reagents 76
4.2.2 Apparatus 76
4.2.3 Configuration of the biosensor 77
4.3 Results and Discussion 80
4.3.1 Morphology and structures of MWCNT/Au 80
4.3.2 Electrochemical behavior of PB/MWCNT/Au 82
4.3.3 Electrochemical behavior of the Nafion/GOx-chitosan/PB/MWCNT/Au biosensor 86
4.3.4 Investigation on the linear range and the sensitivity of glucose biosensors 87

www.manaraa.com

4.3.5 Interference 93
4.3.6 The application of glucose biosensor 94
4.4 Summary 95
4.5 Conclusions 96
4.6 References 97
Chapter 5 104
5 Fabrication of Nanoporous Thin-film Working Electrodes and their Biosensing Applications 104
5.1 Introduction 104
5.2 Experimental Section 106
5.2.1 Materials and Equipments 106
5.2.2 Fabrication of Nanoporous Thin-film Electrodes 107
5.2.3 Deposition of Prussian Blue, Enzyme and Nafion 107
5.3 Results and Discussion 108
5.3.1 Characterization of nanoporous thin-film electrodes 108
5.3.2 Calibration of the Biosensor 116
5.3.3 Analytical performance 119
5.3.4 Discussion 120
5.4 Conclusions 124
5.5 References 125
Chapter 6 128
6 A Robust Lab-on-a-CD System for High-throughput and Automated Whole Blood Analysis 128
6.1 Introduction 128
6.2 Theory and Design of System 130
6.3 Experimental 132
6.4 Results and Discussion 137

www.manaraa.com

6.5 Conclusions 146
6.6 References 147
Chapter 7 150
7 Thesis Summary and Future Work 150
7.1 Summary 150
7.2 Thesis Contribution 150
7.3 Future Work 152
Curriculum Vitae 153

www.manaraa.com

List of Tables

Table 4.1: The effect of Nafion concentration on the sensitivity and linear range of the biosensor. 93

www.manaraa.com

List of Figures

Figure 2.1:Schematics of conventional POC testing procedures (a) an agglutination diagnostic test. (b) a lateral-flow test such as for malaria antigen detection. (c) Light microscopy using Giemsa stain for the detection of malaria.. 8

Figure 2.2: Picture of a cell phone based automated analysis system, which contains an iPod docked on a recharge port and a disposable microfluidic chip sitting on the door..... 9

Figure 2.3: Microfabricated paper-based analytical chips and their application in a commercial hand-held glucometer..... 9

Figure 2.4: Picture of a camera-enabled mobile phone with filters and LED installed for the diagnosis and screening of hematologic and infectious diseases..... 10

Figure 2.5: Schematics of a Lab-on-a-CD system. 12

Figure 2.6: Schematic forces acting on a liquid plug on a rotating platform..... 15

Figure 2.7: Flow switching in a symmetric, inverse Y-structure. (a) At low frequencies ω, where the Coriolis force is negligible, the flow evenly flows through both outlets. (b) At frequencies beyond ω0, a larger Coriolis force can guide up to 100% of the flow into one outlet according to the direction of rotation..... 16

Figure 2.8: Changes of rotation lead to an Euler force (F_E) on the bead and the liquid. Advective currents due to the FE can speed up mixing..... 17

Figure 2.9: Principal centrifugal approach and schematic sketch of the three valving techniques on the centrifugal platform. (A, B) Hydrophobic valves (C) Geometric capillary valve (D) Siphon valve. By adjusting the rotational speed ω, we can control the open or closed status of these microfluidic valves..... 20

Figure 2.10: Schematic of laser controlled microvalves using paraffin wax. (a) To open the normally closed valve, the laser beam is focused at the valve location and the molten ferrowax flows to the assistant valve chamber, opening the valve. (b) To close the normally

www.manaraa.com

opened valve, the laser beam is focused at the pre-loaded ferrowax chamber located adjacent to the main channel and the molten ferrowax bursts into the main microchannel, closing the channel. 21

Figure 2.11: Schematic of laser melted microvalves. A main channel is separated from a connecting channel by a piece of polymer foil (valve closed). A laser beam is used to melt orifices between the main channel and the connecting channel (valve opened). 22

Figure 2.12: A schematic representation of a tape underlayment rotary-node valve and its working principle. 23

Figure 2.13: A schematic representation of a polymer-sealed microvalve and its working principle.. 23

Figure 2.14: (a) sample taking (b) Sample processing (c) Spectrometer used to conduct optical measurement (Beckman 64, UV/Vis) (d) Blood glucose meter for electrochemical measurement (Yellow Springs Instruments 23A).. 26

Figure 2.15: Portable blood analyzer from I-STAT and the exploded view of its cartridge.. 28

Figure 2.16: A compact blood analyzer from Abaxis and the exploded view of its cartridge. 29

Figure 2.17: Schematic of blood test on μPAD. A circular filter membrane catches the red blood cells from a drop of blood. The membrane below contains three microfluidic chambers that can measure the liver enzymes alkaline phosphatase (ALP) and aspartate aminotransferase (AST) as well as serum protein. Colors indicate levels of the enzymes and serum protein, and can be digitized by a cell phone or desktop scanner for further analysis..30

Figure 3.1 (a) transverse-flow microfilter devices (b) spun blood cells down towards a bottom stagnation point (c) a T-channel network structure (d) a bended microchannel structure..... 44

Figure 3.2: A simple device composed of only an egg beater and a piece of polyethylene tubing for blood separation. 47

www.manaraa.com

Figure 3.3: Schematics of the working mechanism of the out-of-plane microvalve on a Lab-on-a-CD platform. The liquid level is horizontal when the platform is motionless (ω = 0). The liquid surface begins to tilt under a rotational speed ω0 which is smaller than the threshold rotational speed. Under these two situations, the microvalve is in "close" state and blocks the passage of fluid. If the rotation speed is increased above the threshold rotational speed ω1, the microvalve is opened and the liquid sample can flow over it. 48

Figure 3.4: Schematics of (a) the aligned bilayer photoresist mold for the out-of-plane microvalve and (b) a PDMS replicate fabricated out of the mold. 52

Figure 3.5: Detailed microfabrication procedures and dimensions for the Lab-on-a-CD device with an out-of-plane microvalve. (a) Spin the first layer of photoresist, (b) UV exposure with the first photomask, (c) Spin the second layer of photoresist, (d) UV exposure with the second photomask, (e) Develop and cast PDMS, (f) Peel off and bond with a glass wafer... 53

Figure 3.6: Graphic illustration of photolithography process for the fabrication of molds.... 54

Figure 3.7: Graphic illustration of softlithography process for the fabrication of PDMS microfluidic structures. 55

Figure 3.8: Characteristics of the Lab-on-a-CD device. (a) The full view of the Lab-on-a-CD system including a motor, a control board and the Lab-on-a-CD device. (b) The sandwich structure of the Lab-on-a-CD device. The top layer is a glass wafer with sample inlets and vents. The PDMS layer comprises 4 sections of identical microstructure including a blood inlet, a supernatant reservoir, a sedimentation reservoir, an out-of-plane microvalve and two air vents. Another smooth glass wafer is used as a support layer. (c) Profiles of the out-of-plane microvalve in the mold and in PDMS casting scanned by a surface profilometer. The profiles of the PDMS casting and the inverted mold are compared. (d) SEM (scanning electron microscope) image taken at the out-of-plane microvalve. A protrusion shown in the microchannel is the out-of-plane microvalve. 56

Figure 3.9: Blood separation. (a) 9.4 μl of the whole blood was loaded into the device. (b) After separation, clear plasma was retained in front of the microvalve in the supernatant reservoir, and the blood cells were centrifuged to the sedimentation reservoir. A clear interface settled down in the sedimentation reservoir. (c) The inset taken at the square area

www.manaraa.com

near the microvalve indicates how the blood cells accumulate at one side. The diffusion of blood cells was restrained by the out-of-plane microvalve. The scale bar is 50 μm. (d) Optical microscope image of a spot in supernatant reservoir showed only few blood cells there. The plasma purity can reach up to 99.9%. The scale bar is 20 μm (e) Optical microscope image of a spot in sedimentation reservoir. Blood cells are tightly stacked together. The scale bar is 50 μm. 58

Figure 3.10: Plasma yield vs. rotation speed. The curve indicates the correlation between plasma yield and rotation speed. The centrifugal force is proportional to the square of the rotation speed. The higher the speed, the faster the plasma-blood cells interface moves outward for a certain time period (200 seconds). Therefore the plasma yield goes up as the rotation speed increases. 61

Figure 3.11: Plasma yield vs. rotation time. The curve shows the plasma yield under 2000 rpm, with different rotation time. The longer the centrifugal force was exerted on the blood sample, the further outward the plasma-blood cells interface moved. Therefore the plasma yield rises as the rotation time increases. 62

Figure 3.12: Rotational speed vs. rotational time for a predetermined plasma yield. For a given rotational speed, each data point of time was collected when the plasma-blood cells interface moved just across the microvalve. The images of the interface, which help us to observe the movement of the plasma-blood cells interface, were captured with the interval of 1 sec without stopping the CD platform. 64

Figure 3.13: Blood cells reflowed back to the supernatant reservoir right after the Lab-on-a-CD device without the out-of-plane microvalve stopped. Blood cell aggregates flushed from the sedimentation reservoir, crossed the original valve area, and back to the supernatant reservoir. a) at 10 seconds after the device stopped. b) at 15 seconds after the device stopped. c) at 20 seconds after the device stopped. d) at 25 seconds after the device stopped. The circle tracks movement of the same cell aggregate. 66

Figure 4.1: Electrochemical cleaning and activation of electrodes in 0.5 M sulfuric acid by cycling between 0.4 V and 1.6 V at a sweep rate of 40 mV s^{-1}. 78

Figure 4.2: Cyclic voltammograms of Pb electropolymerization. 79

www.manaraa.com

Figure 4.3: Cyclic voltammograms of Pb activation. 79

Figure 4.4: SEM images of (a) PDDA-MWCNT composite and (b) unmodified MWCNT on the surfaces of Au electrodes. 81

Figure 4.5: The cyclic voltammograms of PB/MWCNT/Au electrode at different scan rates: 50, 80, 100, 150, 200, 250, and 300 mV/s in PBS (pH 6.8). (b) The dependence of redox peak currents on the square root of scan rates. 83

Figure 4.6: (a) The effects of pH on the oxidation peak current of PB/Au and PB/MWCNT/Au electrodes; (b) Cyclic voltammograms for the biosensor in the absent of glucose and in the presence of 5 mM glucose. Scan rate 50 mV/s; (c) The effects of pH on the sensitivity of the biosensor; (d) The effect of working potential on the sensitivity of the biosensor. Data in (b, c, d) are based on the Nafion/GOx-chitosan/PB/MWCNT/Au biosensors. 85

Figure 4.7: The current-time response curves (a) and their calibration curves (b) of biosensors fabricated using four kinds of enzyme immobilization methods: a GOx-chitosan without cross-linking; b, c and d GOx-chitosan, GOx-BSA and GOx-BSA-chitosan, cross-linked with glutaraldehyde. PBS (pH 6.8) and working potential (0 V) were applied in the experiments. 89

Figure 4.8: The current-time response curves (a) and their calibration curves (b) for the Nafion/GOx-BSA/PB/MWCNT/Au at the amount of GOx of (A)15 U, (B)10 U and (C) 5 U. PBS (pH 6.8) and working potential (0 V) were applied in the experiments. 91

Figure 4.9: Current response of Nafion/GOx-BSA/PB/MWCNT/Au to different substances: (a) 1 mM glucose, (b) 0.6 mM ascorbic acid, (c) 0.6 mM uric acid, (d) 0.6 mM lactic acid, (e) 1 mM glucose. PBS (pH 6.8) and working potential (0 V) were applied in the experiments. 94

Figure 5.1: SEM and AFM images show (a, c) the smooth and flat surface of a gold electrode before nanoporous treatment; (b, d) the nanoporous surface of a gold electrode after nanoporous treatment. 110

www.manaraa.com

Figure 5.2: (a) The EDX spectrum of a nanoporous electrode immersed in 50% HNO_3 solution for 120 sec. (b) Cyclic voltammograms recorded in 0.5 M H_2SO_4 for a flat Au electrode and nanoporous Au electrode show that the cathodic peak of the non-porous Au electrode is only one fortieth of that of the nanoporous Au electrode..... 111

Figure 5.3: SEM images of uniform and compact PB film deposited on a nanoporous electrode (a) and subjected to twenty cycles in a PBS (c); lumpy and loose PB film deposited on a flat electrode (b) and subjected to twenty cycles of potential scan in a PBS (d) All the scale bars are 1 μm..... 113

Figure 5.4: (a) Cyclic voltammogram of the PB-modified nanoporous electrodes at a scan rate of 25 mV s^{-1} in the PBS; (b) The plot of anodic and cathodic currents vs. the square root of the scan rates. The regression equation of the linear fit to anodic response is: y=-0.74+0.26x (R^2=0.9984, n=5), and to cathodic response is: y=0.44-0.28x (R^2=0.9998, n=5). 115

Figure 5.5: (a) Chronoamperograms of glucose with concentration from 0 mM to 40 mM. The working electrode with a diameter of 3 mm was used to record data at 0 V versus Ag/AgCl. (b) Currents of chronoamperometric curves at 100 seconds plotted as a function of the concentration of glucose. Square dots and circular dots represent data from nanoporous biosensors and conventional biosensors, respectively. The regression equation for the linear fit is: y=25.71+3.19x (R^2=0.9971, n=5)..... 118

Figure 5.6: Amperometric response to successive adding of glucose and interferents. The experiment was conducted in the stirring PBS at 0 V versus Ag/AgCl. Under this condition, the adding of 0.2 mM lactate (LA), 0.3 mM uric acid (UA) and 0.1 mM ascorbic acid (AA) introduced 0.7% and 0.3% increasing, and 1.5% decreasing, respectively. 120

Figure 5.7: (a) A nanoporous, thin film and planar electrode system fabricated on a piece of silicon wafer. The diameter of the working electrode is 3 mm. (b) A biosensor embedded in a microfluidic chip. The depth of the microchannel is 50 μm. Control experiments were conducted using this configuration to show the advantages of nanoporous working electrodes in the microfluidic system..... 122

Figure 5.8: The duration of DI water flowing vs. the measured concentrations. 123

www.manaraa.com

Figure 6.1: Exploded view of the configuration of one Lab-on-a-CD section. It is comprised of a microfluidic layer, an insulating layer and a biosensing layer. 131

Figure 6.2: Photos of components and assembled device. (a) a microfluidic cartridge made of PDMS; (b) An array of electrochemical biosensors built on a Si wafer; (c) assembly of the PDMS chip and the Si wafer..... 135

Figure 6.3: Schematics of the experimental steps. A blood sample was loaded into the system at 0 rpm. The rotational speed was ramped from 0 rpm up to 2000 rpm in the first 10 sec. The speed was kept at 2000 rpm for 110 sec, and then slowly decreased to 0 rpm. Electrochemical measurements were conducted when the circular platform was stationary. 137

Figure 6.4: Whole blood analysis using a Lab-on-a-CD system. (a) sample loading and ready for rotation; (b) Rotation ceased and electrochemical signals measured..... 138

Figure 6.5:(a) Chronoamperograms of glucose with concentration from 0 mM to 25 mM.(b) Currents at 150 seconds plotted as a function of the concentration of glucose. 141

Figure 6.6:(a) Chronoamperograms of lactate with concentration from 0 mM to 1.5 mM.(b) Currents at 150 seconds plotted as a function of the concentration of lactate. 142

Figure 6.7:Chronoamperograms of uric acid with concentration from 0 mM to 5 mM.(b) Currents at 150 seconds plotted as a function of the concentration of uric acid. 143

Figure 6.8: The measured concentrations of glucose, lactate and uric acid with the spectrophotometric method and the electrochemical method. The value differences between these two methods are 4.2%, 5.2% and 6.0 %, respectively..... 144

www.manaraa.com

Nomenclature

Mathematical Symbols

A	cross-sectional area of the out-of-plane valve
C_{FC}	cell concentration of the whole blood
C_{PC}	cell concentration in the supernatant reservoir
F_c	centrifugal force
F_h	hydrostatic force
f_c	capillary force
g	gravitational acceleration
H	height of the microvalve
H_{ct},	volume fraction of blood cells
L	length of the upstream reservoir
b, h	width and height of the narrowed microchannel above the microvalve
$\bar{b}$, $\bar{h}$	width and height in the reservoir near the microvalve
V_P	volume occupied by the pure plasma in supernatant reservoir
V_W	volume of the loaded whole blood
W_F	the work of the centrifugal force
W_g	the work of the gravitational force
W_{f_c}	the work of the capillary force
Δs	virtual displacement of liquid on out-of-plane valve

www.manaraa.com

Greek Symbols

ω	rotational speed of the Lab-on-a-CD platform
ρ	sample density
σ	surface tension
θ	contact angle of sample on the channel wall
σ_P	plasma purity
η_P	plasma yield

www.manaraa.com

Chapter 1

1 Introduction

The background of this thesis work is briefly introduced in this chapter, followed by the research objectives and outline of this thesis.

1.1 Background

Diagnostics plays a critical role in health care by providing a timely health care for patients and high-risk groups as well. Approximately 740 tests are currently offered by a central clinical laboratory [1]. 700 out of the 740 tests are used as diagnostic tests and most of them are conducted on blood. The market for blood analysis is valued at $50 billion across the globe: $17 billion goes to the manufacturers of in vitro diagnostic equipment and supplies, and $33 billion is used for medical technology/clinical chemistry staff and other associated service costs [2]. Obviously, new technologies are needed to reduce the cost of blood analysis in order to make it accessible for people all over the world.

Further, the time factor of diagnostic testing is important. The accuracy of the result is higher if the test result is immediately obtained compared to the one obtained hours later for the large majority of diagnostics [3]. For example, real time results for blood glucose tests are often mandatory as the concentration of physiological chemicals rapidly changes. That increases the weightiness of point-of-care analysis devices [4-6]. Currently, a number of high accuracy biotechnologies have been developed and used (more details are available in Chapter 2). However, not all these technologies could be transferred and affordable for people in developing countries. Meanwhile, a formal lab environment is often not possible for health care workers in the field.

www.manaraa.com

Lab-on-a-CD [7] technology, a main branch of Lab-on-a-chip [8] technology, turns out to be an ideal miniaturization for chemical/biochemical tests, which is realized by the intrinsic pumping and separation mechanisms based on the centrifugal field on the entire circular disc (CD) platform. The separation mechanism is ideal for blood analysis because blood separation is the first step for whole blood analysis [9]. The accuracy of whole blood analysis may be disturbed by the existence of blood cells. These characteristics of Lab-on-a-CD technology inspire this thesis work in further exploring an automatic, portable, point-of-care, cost-effective and fast system for blood analyses.

1.2 Research Objectives and Outline of this Thesis

It is the aim of this thesis work to explore a portable and low-cost system for one-step blood separation and analysis. To achieve this aim, a microfluidic cartridge for whole blood separation and an innovative electrode system for electrochemical detection in microfluidic channel were designed and studied. A Lab-on-a-CD prototype was built to conduct multiple tests simultaneously.

Chapter 2 presents a review of the status of point-of-care (POC) diagnostics and the major features of the Lab-on-a-CD platform. Meanwhile, comparisons are made between the conventional blood analysis systems and other POC systems, leading to the research objectives of this thesis.

Since blood separation of whole blood is the first step for clinical blood diagnosis, Chapter 3 describes a novel design for an out-of-plane microvalve that enables high performance of whole blood separation on Lab-on-a-CD centrifugal devices. The principle of design and experimental details of device fabrication are presented. Further, the control experiment without out-of-plane microvalves was conducted to evaluate the performance of the microvalves.

www.manaraa.com

Chapter 4 focuses on design and optimization of prussian blue (PB) and multi-wall carbon nanotubes (MWCNT) based electrodes for electrochemical biosensing of analytes in the separated plasma. The factors that might affect the performance of the biosensor were evaluated. It was found that the immobilization methods and the amount of glucose oxidase (GOx) mainly influenced the sensitivity of the glucose biosensor, while the amount of Nafion affected both the sensitivity and the linear range of the glucose biosensor.

In Chapter 5, a nanoporous structure was created on the surfaces of electrodes through an alloying/dealloying process. The creation of the nanoporous electrode is to compensate the reduced surface area due to the miniaturization of the electrodes in the Lab-on-a-CD system. Meanwhile, the electrode system embedded in the microfluidic system may experience sample flow rates from nl s-1 to liter s-1 in the centrifugal platform. Abundant catalysts and enzymes were stably entrapped in the nanoporous structure, leading to high stability and reproducibility of the biosensor.

Chapter 6 demonstrates the performance of the completed Lab-on-a-CD prototype. The prototype was assembled with a microfluidic cartridge for blood separation and an electrochemical system for quantitative detection. Although only glucose, lactate and uric acid were analyzed, the Lab-on-a-CD prototype is designed as a universal platform to detect the concentration of analytes in whole blood only if hydrogen peroxide is produced in enzymatic reactions.

This thesis ends with a summary of current research results and a prospective of further research directions. Most of the work presented in this thesis has been published in peer-reviewed journals or submitted for publication.

www.manaraa.com

1.3 References

1. Bailey, T., A practicum on making point-of-care testing work. American Clinical Laboratory, 1997. **16**: p. 10-11.

2. MedPro Month, Diagnostic testing, outcomes and POC. Medical Data International, January 1997. Vol. VII: No. 1.

3. Kanji, S., Buffie, J., Hutton, B., Bunting, P., Singh, A., McDonald, K., Fergusson, D., McIntyre, L. and Hebert, P., Reliability of point-of-care testing for glucose measurement in critically ill adults. Critical Care Medicine, 2005. **33**(12): p. 2778-2785..

4. Ahn, C.H., Choi, J., Beaucage, G., Nevin, J.H., Lee, J., Puntambekar, A. and Lee, J.Y., Disposable smart lab on a chip for point-of-care clinical diagnostics. Proceedings of the IEEE, 2004. **92**(1): p. 154-173.

5. Tüdős, A.J., Besselink, G.A.J., and Schasfoort, R.B.M., Trends in miniaturized total analysis systems for point-of-care testing in clinical chemistry. Lab on a Chip, 2001. **1**(2): p. 83-95.

6. Yager, P., Domingo, G.J. and Gerdes, J., Point-of-care diagnostics for global health. Annual Review of Biomedical Engineering, 2008. **10**: p. 107-144.

7. Madou, M., Zoval, J., Jia, G., Kido, H., Kim, J. and Kim, N., Lab on a CD. Annual Review of Biomedical Engineering, 2006. **8**: p. 601-628.

8. Chin, C.D., Linder, V. and Sia, S.K., Lab-on-a-chip devices for global health: past studies and future opportunities. Lab on a Chip, 2006. **7** (1): p. 41-57.

9. Zhang, J., Guo, Q., Liu, M., snd Yang, J., A lab-on-CD prototype for high-speed blood separation. Journal of Micromechanics and Microengineering, 2008, **18**, 125025.

www.manaraa.com

Chapter 2

2 Literature Review

In this chapter, the status of point-of-care (POC) diagnostics is reviewed. POC is normally defined as any testing performed near the patient, and its essence is to miniaturize and integrate diagnostic equipment onto a compact platform. The Lab-on-a-CD technique provides such a compact platform, and its major features are introduced here. Since this thesis focuses on how to transfer the blood analysis process from the macro world into the micro/nano world, conventional blood analysis systems are compared with other POC systems.

2.1 Point-of-care Diagnostics

Diagnostics have already made great contributions to health care in the developed world, e.g. ensuring safe blood banking, providing appropriate and timely care to patients and crucial surveillance data for both emergency public health interventions and long-term public health strategies. Evaluating and improving patients' medical conditions need effective diagnostic tools. For the most part, new diagnostic systems developed by biomedical engineers are in response to the needs of the medical community in only the developed countries due to the new technologies' necessity for highly regulated and quality-weighed environments of centralized laboratories.

However, the majority of people afflicted with various kinds of diseases only have access to poorly resourced health care facilities with almost no supporting clinical laboratory infrastructure. For example, many developing countries do not own modern equipment similar to those in central facilities in developed countries to perform up-to-date diagnostics. Besides hardware, lack of training for operators, lack of standardization in the evaluation of new diagnostics in relevant settings [1], lack of quality assurance [2, 3] and insufficient advocacy to influence adoption rates [4] have all limited the access to appropriate tests for patients. Therefore, approaches used in developed countries do not

www.manaraa.com

fulfill the needs of developing countries. A major task for the biomedical engineering community is to develop POC tests, which allows the test to be brought conveniently and immediately to the patient, meeting the needs of people from various living environment.

The knowledge of what actual constraints and requirements exist in developing countries is important in developing appropriate POC diagnostics for low resource settings. The laboratories in such environments face not only traditional constraints (e.g. low water quality, insufficient power supply and inconsistent refrigeration quality) [5-7], but also additional challenges, which are listed as follows:

1. Inequality of laboratory facilities and capacities within a country and among countries.
2. Poor external quality control and laboratory management systems.
3. Lack of basic essential equipment and laboratory consumables.
4. Unreliable quality of reagents and unsecured supply chains.
5. Insufficiently skilled staff and limited training opportunities.

These factors result in POC diagnostic tests possessing low complexity, while keeping the same level of diagnostic accuracy. The definition of complexity comprises of the number of manual operation steps, the number of instruments involved, the level of necessary training, and the need for user interpretation. The accuracy of the result is characterized by the detection limit, the clinical sensitivity, and specificity. In addition, practical POC testing should be low cost and have short turn-around time. Generic guidelines developed by the World Health Organization (WHO) for the development of POC devices used in the developing world can give more detailed information [8]:

1. Affordable by those at risk of infection.
2. Sensitive (few false positives).
3. Specific (few false negatives).
4. User-friendly (simple to perform and requiring minimal training).
5. Rapid (to enable treatment at first visit) and robust.

www.manaraa.com

6. Equipment-free.
7. Delivered to those who need it.

Apart from clinical needs and user requirements, the political regulation also has a strong impact on the design of POC devices. For example, the US Food and Drug Administration (FDA) defines POC diagnostics as "simple" and as having "insignificant risk of an erroneous result". The design specifications are as follows:

1. Fully automated instrument or unitized, using direct and unprocessed specimens/capillary blood (finger stick), nasal swabs, or urine.
2. Needs only basic specimen and reagent manipulation.
3. Needs no operator calibration, interpretation and intervention during the analysis steps, no technical or specialized training, no electronic or mechanical maintenance.

Under these guidelines, POC diagnostic research has experienced many successes. In the past decade, there has been a continuous growth in publications about early stage technologies for overcoming the hurdles and barriers of introducing diagnostics into the developing world. The conventional POC testing methods include agglutination tests, the detection of the pathogen specific antigen or antibodies by lateral flow tests (rapid diagnostic tests), and direct detection of the infectious agent by microscopy (Figure 2.1). Ideally, these tests can provide helpful information. However, most biological data cannot be extracted by these simple devices, and their robustness and accuracy are not enough. Progress in science and technologies, such as genome sequencing and high-throughput antigen screening, have accelerated the research on disease pathogenesis at a molecular level and the identification of biomarkers for pathogens and diseases. Furthermore, the emergence of microfluidic technique [9-11] and nanotechnology provide a compact platform to integrate sample processing, assay performance, analyte detection, etc.

www.manaraa.com

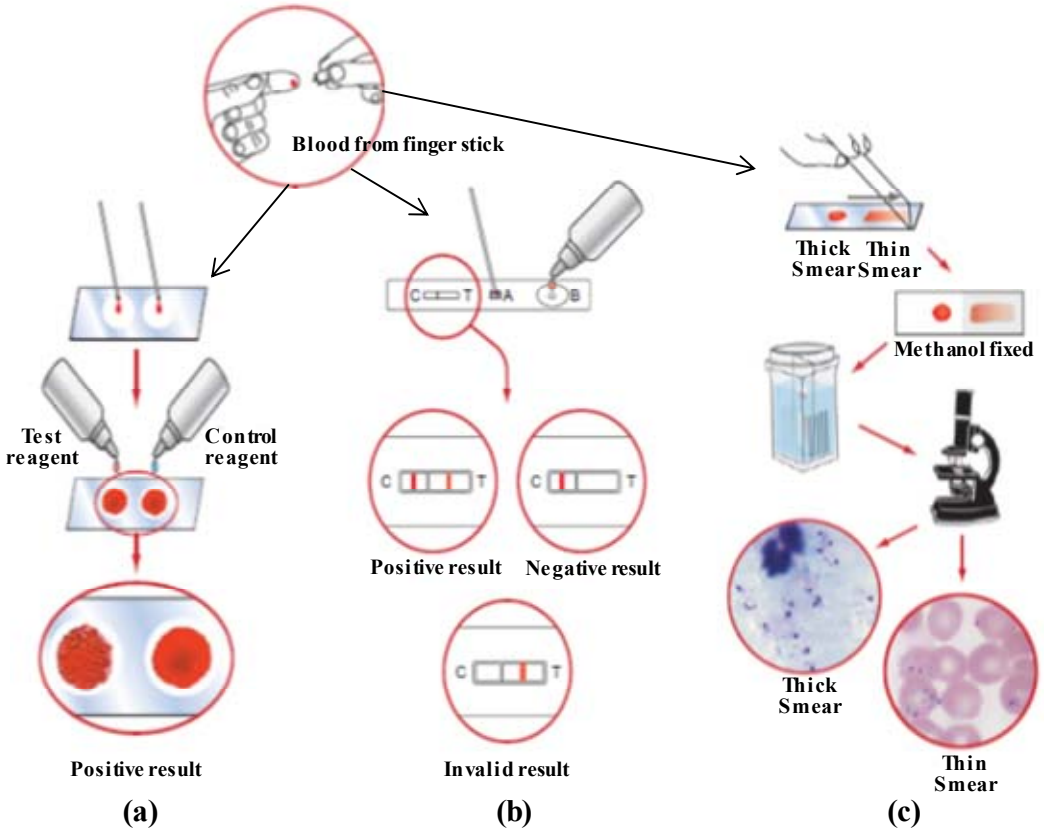

Figure 2.1:Schematics of conventional POC testing procedures (a) An agglutination diagnostic test. (b) A lateral-flow test such as for malaria antigen detection. (c) Light microscopy using Giemsa stain for the detection of malaria. Figures adapted from Ref [12-14].

Recently, our daily tools (cell phones, paper, and cameras) have been creatively involved in the design of POC devices. For example, Stedtfeld et al reported an inexpensive, user-friendly and compact microfluidic device for rapid quantitative detection of multiple genetic markers with high sensitivity and specificity. The device (Figure 2.2) was operated using an iPod Touch, which was used to receive data and carry out automated analysis[15]. Using paper as a platform, Nie et al [16, 17] reported detection of metabolites through the combination of a commercial hand-held glucometer with easily fabricated Micro-Paper-based Analytical Devices (Figure 2.3), and Yang et al [18]

www.manaraa.com

reported detection of glucose with an optical method. Breslauer et al [19] developed camera-enabled mobile phones for the diagnosis and screening of hematologic and infectious diseases (Figure 2.4).

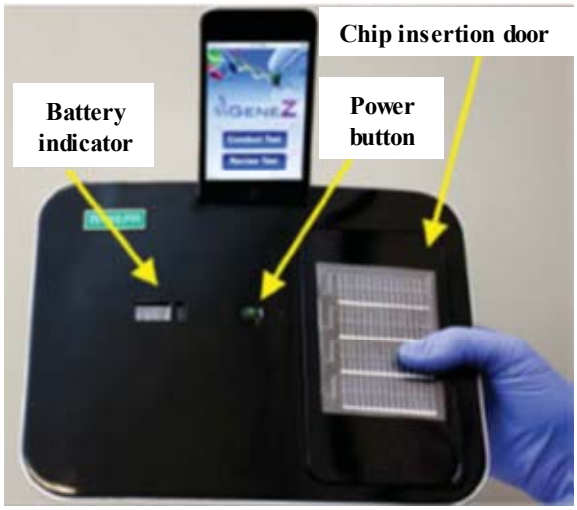

Figure 2.2: Picture of a cell phone based automated analysis system, which contains an iPod docked on a recharge port and a disposable microfluidic chip sitting on the door. Figure adapted from Ref [15].

Figure 2.3: Microfabricated paper-based analytical chips and their application in a commercial hand-held glucometer. Figure adapted from [17].

www.manaraa.com

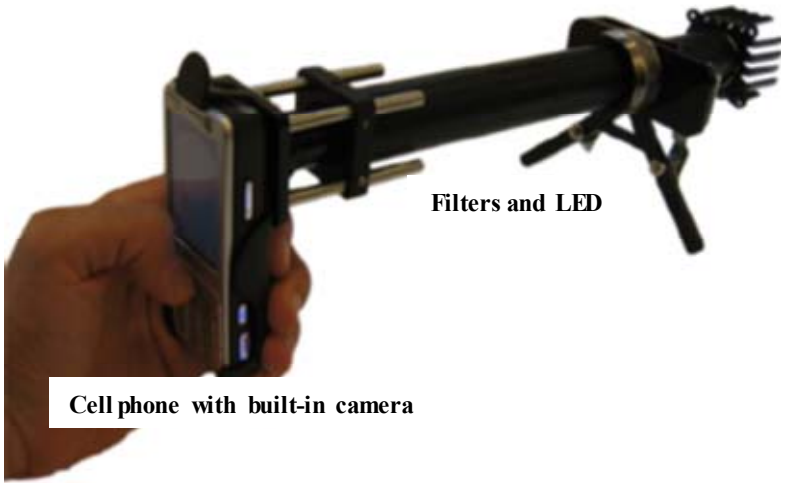

Figure 2.4: Picture of a camera-enabled mobile phone with filters and LED installed for the diagnosis and screening of hematologic and infectious diseases. Figure adapted from Ref [19].

To sum up, miniaturization and integration of existing diagnostics steps into a microfluidic system has been a prominent trend that provides low-cost yet simple diagnostic methods without sacrificing test accuracy. The microfluidic technique solves many issues by lowering test complexity and reducing cost, but the implementation of the existing POC devices heavily depends on complex driving and regulating systems for sample manipulation. For example, microfluidic pumps are widely used to provide driving force [20-22] and compressed air supplied from external sources is employed to offer the microvalve function [23-28]. Based on the microfluidics, nanotechnology and biochemistry, the concept of Lab-on-a-chip [29-33] or Lab-on-a-CD [34] has been established. This has led to the trend of developing accurate and sensitive diagnostic tests for POC [11, 35-37], in both high-income countries and the developing world. Therefore, more work is required to further simplify and miniaturize the POC devices.

www.manaraa.com

2.2 Lab-on-a-CD Technology

Lab-on-a-CD technology is a main branch of Lab-on-a-chip technology. With reservoirs, chambers, connecting microchannels and vents built in, the compact disc (CD) platform can be used to conduct various kinds of chemical and biochemical reactions (Figure 2.5). Inertial forces (centrifugal force, Coriolis force, and Euler force) induced by rotating the CD are utilized to manipulate the liquid's movement from the rotating center to the peripheral, and transport samples and reagents from the inlet reservoirs to the metering, mixing, reaction, detection and waste reservoirs. Sampling processes, such as valving, mixing, metering, sample splitting and separation, are implemented on the CD platform with the combination of inertial forces and designed microfluidic structure. These are a pre-analytical step of the platform, while the analytical step involves analytical measurement using techniques, such as optical measurement and electrochemical measurement. These two parts together make the centrifugal platform a powerful solution for medical and clinical diagnostics. The underlying physical principles of microfluidic manipulation are presented below.

www.manaraa.com

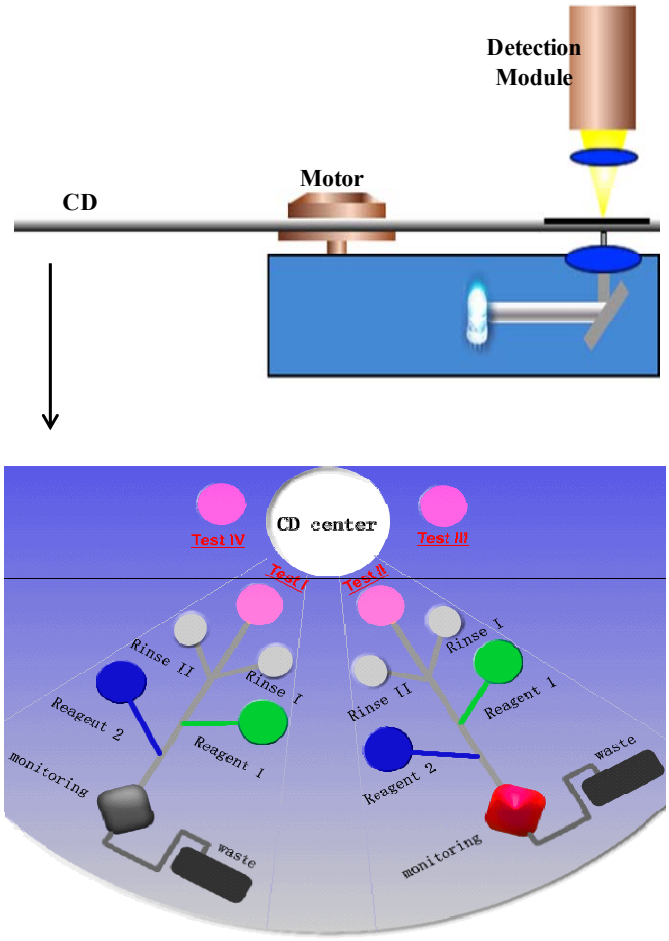

Figure 2.5: Schematics of a Lab-on-a-CD system.

2.2.1 Microfluidic Pumps

Actuation of microflow is a core function in a microfluidic system and several methods of fluid propulsion have been developed to move small quantities of fluids or suspended particles from reservoirs to mixing and reaction sites, to detectors, and eventually to waste chambers. Methods to accomplish this include syringe and peristaltic pumps, electrochemical bubble generation, acoustics, magnetics, electrokinetics, centrifuge, etc.[38-42].

www.manaraa.com

Mechanical pumps [43] are based on well-developed, commercially available components. The generated pressure is a volume-dependent force, which scales as L^3 (L, characteristic length corresponding to the capillary diameter), and a diverse range of flow rates is available, from less than nL s^{-1} to L s^{-1}. Electro-osmotic, electrowetting, and electrohydrodynamic pumps [44-49] possess better performance in small and long channels compared to mechanical pumping because they all scale as surface forces (L^2). No moving parts are needed, and the average flow rates for these pumps are from 1 nL s^{-1} to 1 μL s^{-1}. By oscillating the sound field at the solid/fluid boundary, the acoustic pump produces a constant fluid motion with a flow rate up to 20 μL s^{-1}. The problem for this type of micropump is that heat can be generated in sample fluids due to the dissipation of acoustic energy. The centrifugal pump herein means the rotating circular platform. Its flow rates depend on disc geometry, spinning speed, and fluid properties, ranging from less than 10 nL s^{-1} to greater than 100 μL s^{-1}. The advantages of centrifugal pumps are revealed with its simple driving mechanism, which reduces the need for an external pumping system, and its relative insensitivity to physicochemical properties, such as pH, ionic strength, or chemical composition, which are important factors for AC and DC electrokinetic means of pumping.

Four types of forces may be produced on a liquid plug on a rotating CD. The first one is centrifugal force that commonly occurred in a rotating and non-inertial reference frame and is defined as an outward force away from the rotational center (Figure 2.6). The centrifugal force occurring at a liquid plug on a rotational platform can be defined as:

$$F_{\omega} = m\vec{\omega} \times (\vec{\omega} \times \vec{r}) = mr\omega^2 \tag{2.1}$$

where m is the mass of the liquid plug, r is the distance from the center of the liquid plug to the center of the platform, and ω is the rotating speed. The centrifugal force radially points outward, and exerts a pressure difference upon each liquid segment, which can be expressed by [50]:

www.manaraa.com

$$dP_{\omega} = \frac{F_{\omega}}{A} = \rho r \omega^2 dr \tag{2.2}$$

where dr is the length of the liquid segment. Integrating this pressure difference along the whole length (R_1 to R_2) of the liquid plug, we can calculate the pumping pressure acting on this liquid plug, which is given by Equation 2.3:

$$\Delta P_{\omega} = \frac{1}{2}\rho\omega^2(R_2^2 - R_1^2) \tag{2.3}$$

Since the pressure induced by centrifugal force is known, we can infer the flow rate in a rectangular channel. It is assumed that it is a laminar and incompressible flow with a non-slip boundary condition (Poiseuille flow).The volumetric flow rate Q can be

$$Q = \frac{\Delta P W H^3}{12\mu L} \tag{2.4}$$

Where ΔP is pressure drop and μ is dynamic viscosity. W, H and L are the channel's width, height, and length respectively. Substituting ΔP in Equation 2.3 to Equation 2.4, the flow rate can be expressed as a function of rotating speed:

$$Q = \frac{\rho\omega^2(R_2^2 - R_2^1)WH^3}{24\mu L} \tag{2.5}$$

In order to demonstrate the feasibility of this centrifugal platform, it is assumed that a water plug located at R_1 (20 mm) and R_2 (30 mm). A pumping pressure of 6 kPa can be generated with rotational speed of 1500 rpm. By properly controlling the rotational speed, distance between the sample and the rotational center, geometry of the channel and fluidic properties, we can make the liquid plug move in the channel at a specific flow rate. Considering water flows in a channel with square cross (50 um), a flow rate of 0.12 μl/s can be achieved.

www.manaraa.com

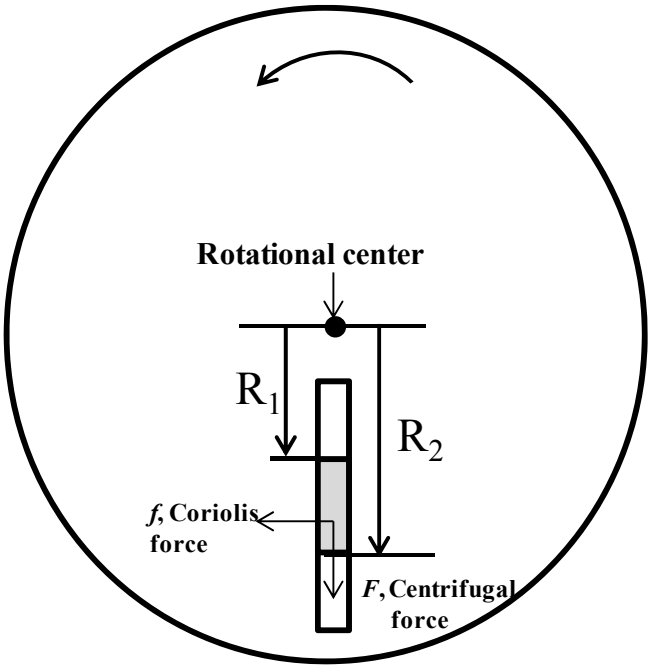

Figure 2.6: Schematic forces acting on a liquid plug on a rotating platform.

The movement of the sample in a rotational platform is affected by another factor, called the Coriolis effect, which is the behavior added by the Coriolis acceleration. The Coriolis acceleration is perpendicular both to the direction of the velocity of the moving mass and to the frame's rotation axis, and the magnitude of the Coriolis acceleration is proportional to the velocity of the object. The induced Coriolis force can be expressed as:

$$\vec{F} = -2m\vec{\omega} \times \vec{V} \tag{2.6}$$

Where m is the mass of the sample in the rotating system, $\vec{\omega}$ is the angular velocity vector (perpendicular to the plane of CD) and $\vec{V}$ is the velocity of the object in the rotating CD platform. Therefore, the Coriolis force commonly occurs in the rotating CD and acts in a direction perpendicular to the velocity of the sample. This force can work with centrifugal force together to change the flow path of fluid samples (Figure 2.7). The typical applications of the Coriolis effect are shown in enhancing mixing for laminar flow in microfluidic channels [51], controlling flow direction at a bifurcation [52], etc.

www.manaraa.com

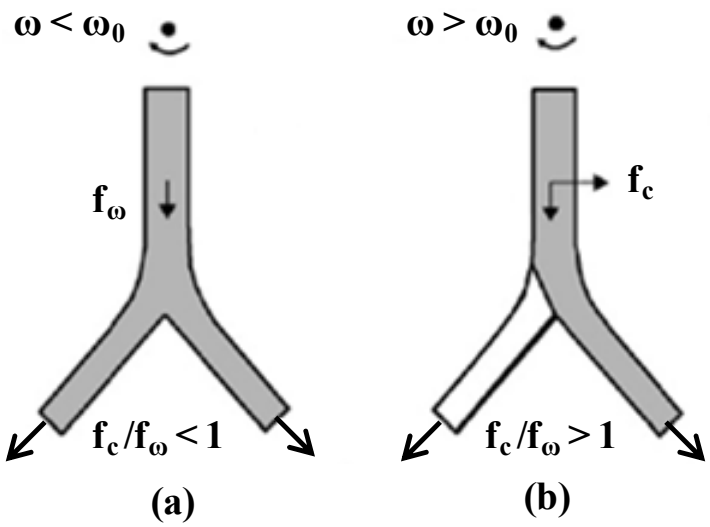

Figure 2.7: Flow switching in a symmetric, inverse Y-structure. (a) At low frequencies ω, where the Coriolis force is negligible, the flow evenly flows through both outlets. (b) At frequencies beyond ω_0, a larger Coriolis force can guide up to 100% of the flow into one outlet according to the direction of rotation. Figure adapted from Ref [53].

Furthermore, if the angular frequency of a rotating CD varies, a third force, called Euler force, will be generated as a function of the angular acceleration. Based on Newton's second law of motion, Euler force F_E acting on the fluid elements can be derived from $-m\frac{d\omega}{dt}\times r$, where r is the radial distance of the accelerating point from the center of rotation. The Euler force has been reported to help mixing samples as well (Figure 2.8).

www.manaraa.com

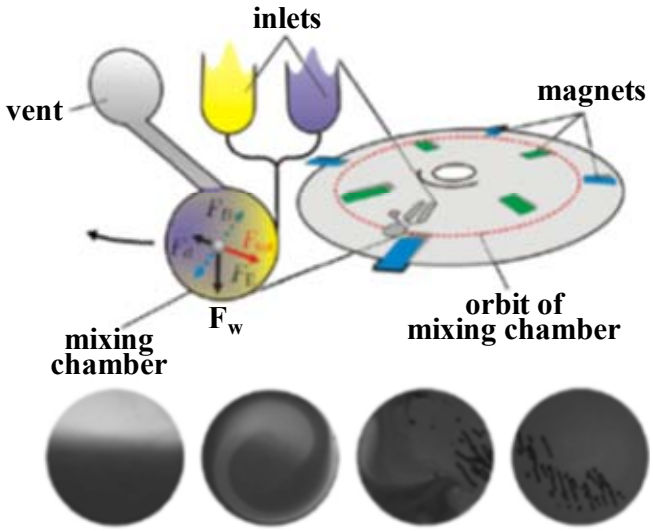

Figure 2.8: Changes of rotation lead to an Euler force (F_E) on the bead and the liquid. Advective currents due to the FE can speed up mixing. Figure adapted from Ref [54].

Another dominant force acting on microfluidic platforms is capillary force. It is different from the previous forces because it does not rely on the rotation of the CD platform. Capillary force exists in any microfluidic channel, and can be either a driving force or a resisting force, depending on the surface tension of the fluid and the surface energy of the channel surface. Surface tension, caused by the inter-molecular attractive forces of the liquid, is the force that holds a liquid together. Take the interface between water and air, for example. All the water molecules close to the surface are pulled inwards, forming a spherical droplet. This tensile force divided by the length of the contact line on the interface (*N/m*) is defined as surface tension (σ).

Surface energy is used to quantify the breakdown of intermolecular bonds on a freshly created surface. The surface energy is quantified with the forces acting on a unit length at the solid-air or the solid-liquid interface, sharing the same unit as the surface tension.

www.manaraa.com

When liquids are in contact with solids, the formation of droplets or thin films depends on the force balance of surface tension and surface energy.

Affinity of a flat surface towards a certain liquid is defined in terms of the "flat" (or *intrinsic*, or Young's) contact angle,

$$\cos(\theta_{flat}) = \frac{\gamma_{SA} - \gamma_{SL}}{\gamma_{LA}} \tag{2.7}$$

where γrepresents the surface energies (or surface tensions), subscript *S* stands for solid, *L* – for liquid, *A* - for air The solid-liquid surface energy can be approximately estimated via the other two as follows [55]:

$$\gamma_{SL} = \gamma_{SA} + \gamma_{LA} - 2\sqrt{\gamma_{SA}\gamma_{LA}} \tag{2.8}$$

The surface is called (hydro-, oleo-, etc.)-*phobic* if $\theta > 90^{\circ}$, and *-philic* if otherwise.

Due to the surface tension, a pressure gradient exists across the interface. Assuming a droplet forms a curve interface in a cylindrical channel (radius: R), the pressure difference across the interface can be deduced from the following force balance:

$$\sigma\cos(\theta)(2\pi R) = (P_i - P_j)\pi R^2 \tag{2.9}$$

where P_i and P_j are pressures on both sides of the interface. As $\Delta P = 2\sigma\cos(\theta)/R$, the capillary action makes a great contribution to the force balance on a microscale channel.

2.2.2 Microfluidic Valves

Microfluidic pumps provide driving force for the microfluidic network, but the precise manipulation of the fluidic movement requires the participation of microfluidic valves. In

www.manaraa.com

a multi-step assay, sample fluid flows through different sites in sequence. For example, the sample needs to remain at specific places for processing and is then released to the next chambers. Based on the differences of actuating mechanisms, microfluidic valves can be divided into passive valves and active valves. Passive valves involve the control of geometries and material properties of channels as well as the rotational speed, while active valves employ external excitation to control the opening or closing of the valves.

As shown in Equation 2.9, pressure drops across a microfluidic channel are related to the size and wettability of the channel. If the channel is hydrophobic, the fluid flow will experience resistance. By abruptly narrowing down a section of the hydrophobic channel, thus reducing R, we can apply much stronger resistance to the fluid flow. Alternatively, if a channel is hydrophilic, a driving force will be exerted on the fluid flow. By placing a hydrophobic patch (changing θ) in the hydrophilic channel, we can switch the driving force to a resisting force [56]. Therefore, the narrow section and the hydrophobic patch can both serve as passive microfluidic valves, categorized as hydrophobic valves (Figure 2.9 A, B). Further, if a channel is completely hydrophilic, the fluid flow can be retained by abruptly expanding the cross section of the microchannel (enlarging R), resulting in a smaller pressure drop. This abrupt expansion of the microchannel is used as a capillary valve, which is also a kind of passive valves (Figure 2.9 C). Operations of the hydrophobic valves and capillary valves are determined by balancing the centrifugal force due to rotation and the resisting force due to surface properties and geometry of the valve. The liquid meniscus is stopped at the valve area until the pressure induced by centrifugal force overcomes the one induced by the microfluidic valve. These microfluidic valves can be easily adapted to CD platforms and do not require external actuation forces. However, these valves are not compatible with low surface tension liquids as they have small contact angles and readily wet polymer surfaces, rendering the valve structures useless [57].

www.manaraa.com

Inspired by the siphon effect, a hydrophilic channel, like Figure 2.9 D, can serve as a microfluidic valve, called a siphon valve [58-60]. The siphon valves are inverted U-shaped channels bent at a crest point located radially farther inward with hydrophilic inner surfaces, fluidically connecting two chambers. The outflow chamber has a higher relative energy potential than the inflow chamber within a centrifugal acceleration field. At a high angular frequency ω_c, the centrifugal force F_c prevails over the capillary force F_θ in the inbound section, localizing the liquid in the first chamber at a level below the crest of the siphon. When the angular frequency is reduced or the rotation ceases, liquid spontaneously primes the siphon by capillary action. Maintaining this capillary priming until the advancing meniscus has passed the crest point of the siphon and settles below the position of the receding meniscus in the first chamber. Now a low angular frequency is sufficient to drive the fluid and finally connect these two chambers. Once these two chambers are connected, the movement of fluid will not cease until air is sucked into the inbound channel. These valves depend exclusively on the surface properties of the channels and require precise control of rotation, so their usages are limited.

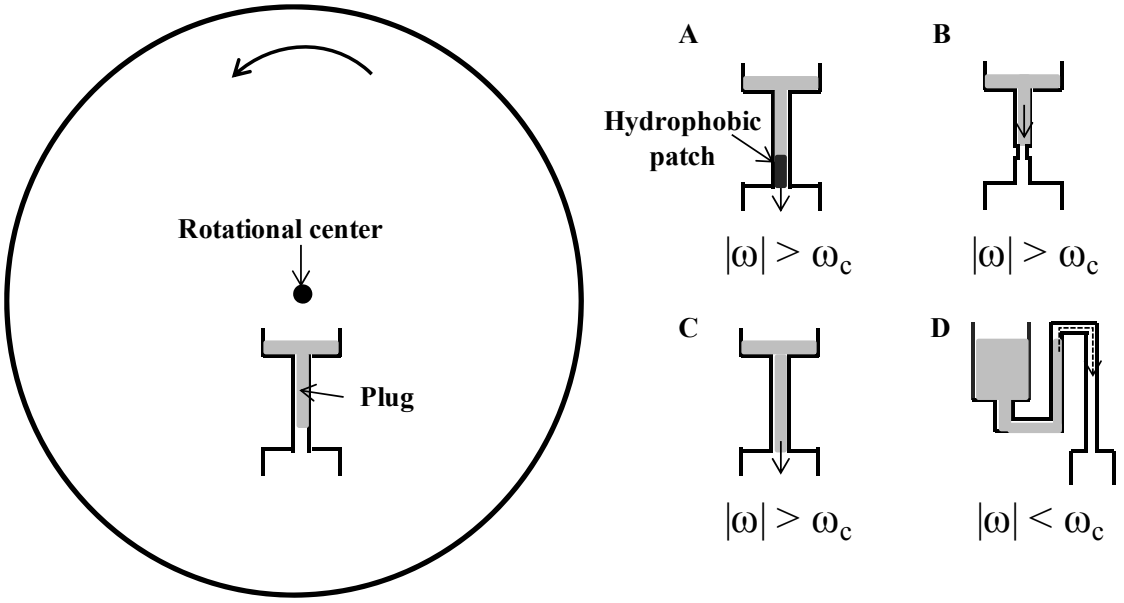

Figure 2.9: Principal centrifugal approach and schematic sketch of the three valving techniques on the centrifugal platform. (A, B) Hydrophobic valves (C) Geometric capillary valve (D) Siphon valve. By adjusting the rotational speed ω, we can control the open or closed status of these microfluidic valves.

www.manaraa.com

Among many active microvalves used in microfluidic applications, optofluidic valves, opened by directing optical energy from a solid-state laser, are particularly attractive for disposable biochip applications because they are simple to implement, cost-effective and biocompatible. Park et al reported phase change based microvalves using paraffin wax mixed with nanoheaters (Figure 2.10) [61], and Garcia-Cordero et al used a laser to localize heating to melt an orifice in the polymer layer, connecting previously isolated fluidic components or compartments (Figure 2.11) [62]. The disadvantage of this kind of valve is that they are only for single use. Researchers are still trying to develop more robust active microfluidic valves. For example, Markov et al [63] fabricated a tape underlayment rotary-node microvalve (Figure 2.12), and Park et al [64] created a membrane-type microvalve in rectangular microfluidic channels through seal photopolymerization (Figure 2.13).

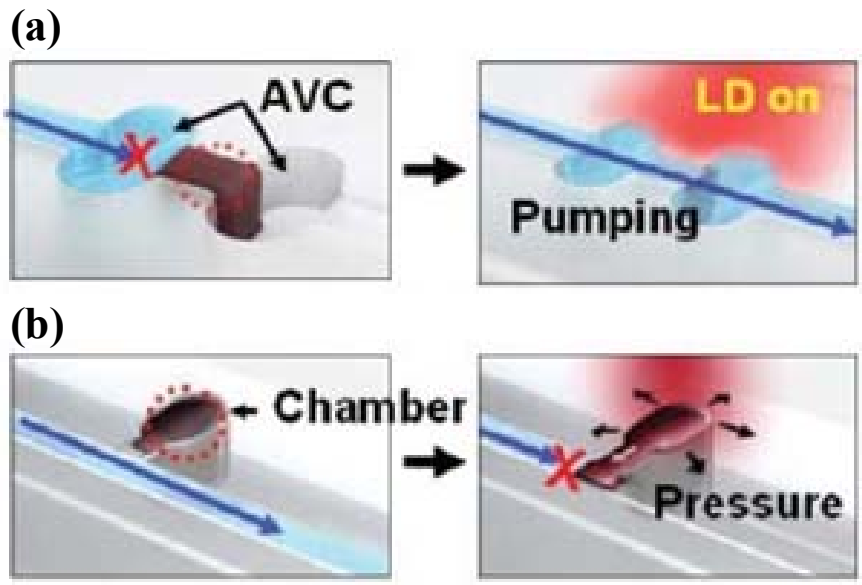

Figure 2.10: Schematic of laser controlled microvalves using paraffin wax. (a) To open the normally closed valve, the laser beam is focused at the valve location and the molten ferrowax flows to the assistant valve chamber, opening the valve. (b) To close the normally opened valve, the laser beam is focused at the pre-loaded ferrowax chamber located adjacent to the main channel and the molten ferrowax bursts into the main microchannel, closing the channel. Figure adapted from Ref [61].

www.manaraa.com

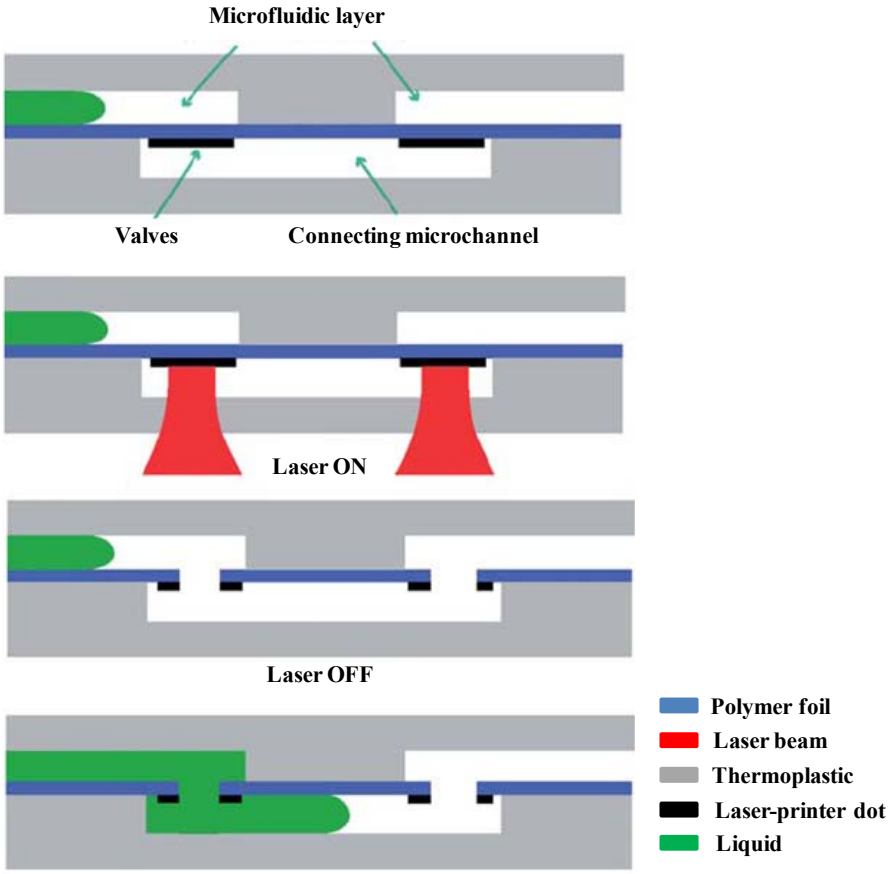

Figure 2.11: Schematic of laser melted microvalves. A main channel is separated from a connecting channel by a piece of polymer foil (valve closed). A laser beam is used to melt orifices between the main channel and the connecting channel (valve opened). Figure adapted from Ref [62].

www.manaraa.com

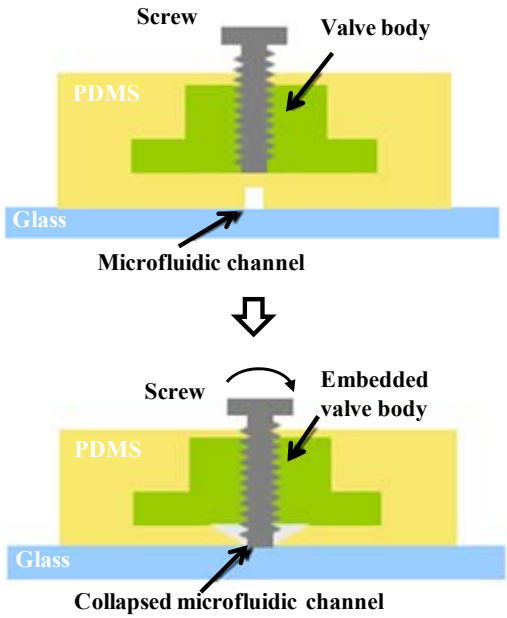

Figure 2.12: A schematic representation of a tape underlayment rotary-node valve and its working principle.

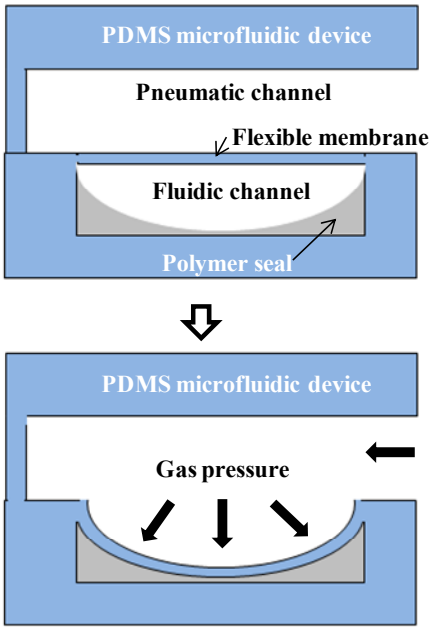

Figure 2.13: A schematic representation of a polymer-sealed microvalve and its working principle. Figures adapted from Ref [63, 64].

www.manaraa.com

2.3 Blood Analysis

Blood analysis is the most commonly-used diagnostic method nowadays due to the definitive information of patients' medical conditions provided by blood tests.

2.3.1 Conventional Blood Analysis Methods

Traditional blood analysis includes sample collection, preparation and detection. These three processes are commonly conducted in diverse locations and at different time periods. Blood samples are taken from patients by nurses at hospitals or clinics. Five to ten mL of whole blood is stored in labeled tubes (Figure 2.14 a). These tubes are then collected and sent to central laboratories for further processing by specific laboratory technicians. Plasma is separated from blood cells by centrifuging the tubes, effectively trapping the blood cells in the sediment and lifting the plasma up to the supernatant (Figure 2.14 b). The plasma is extracted for subsequent quantitative detections. These detections can be conducted using colorimetric analysis methods and electrochemical analysis methods. Large scale spectrometers are employed in the colorimetric measurements and standard electrochemical working stations are utilized in the electrochemical detections (Figure 2.14 c, d). This blood analysis regime has been successfully applied to provide accurate results for physicians in the diagnosis of symptomatic patients or in the preventative program.

Since numerous personnel and process steps are involved in the blood test, the possibility of quality failure is increased. The entire blood test can be categorized into two processes: Process I, which occurs in the patient-care department, such as test requisition (nurse), sample acquisition (nurse or phlebotomist), labeling (nurse or phlebotomist), transportation (transporter), and receipt of results (nurse); and Process II, which takes place in the laboratory, such as sample receipt and aliquoting (clerk), and centrifuging, analysis, and results reporting (medical technologist). Any mistake that occurs during this

www.manaraa.com

process, e.g. mislabeled samples or deteriorated samples during transportation, would lead to failure of testing.

People have to pay attention to the method of recognizing the test results, although there is no mistake involved in the process flow. Normally, it takes a few days after taking blood samples from the patient to release the test result to the patient. Unfortunately, the processing time would readily be doubled if the result is doubted and the request to re-measure the blood is made. Considering the issue described above, the patient will feel more confident in the blood result if the procedures for labeling and transporting blood samples are eliminated and the measurement can be performed with a customer-friendly analysis device at the patients' side.

The completed cost of the blood test comes from the sample acquisition and transportation, analytical equipment, reagents and the associated labor cost. Cost savings can be achieved by switching the multistep laboratory process to a one-step patient-side alternative. For example, blood sampling is performed by pricking the finger into receptacle instead of by a nurse. Sample storage, transportation and processes in the patient-care department and laboratory would be eliminated so long as the patient-side device is designed appropriately.

The turn-around time for diagnostic testing is very significant. The high accuracy of results is ensured only when the test result is provided instantaneously, which is hardly realizable by the majority of diagnostics conducted in the central lab. For example, real time results for blood glucose tests are often mandatory as the concentration of physiological chemicals rapidly change. The timely manner further increases the importance of POC analysis devices. Nowadays, a number of high accuracy biotechnologies have been developed and used. However, not all these technologies could be transferred and are affordable for those people with low-resources in developing

www.manaraa.com

countries. Moreover, a formal lab environment and experienced professionals are often not accessible in the field. Developing simpler, more robotic and affordable devices becomes necessary.

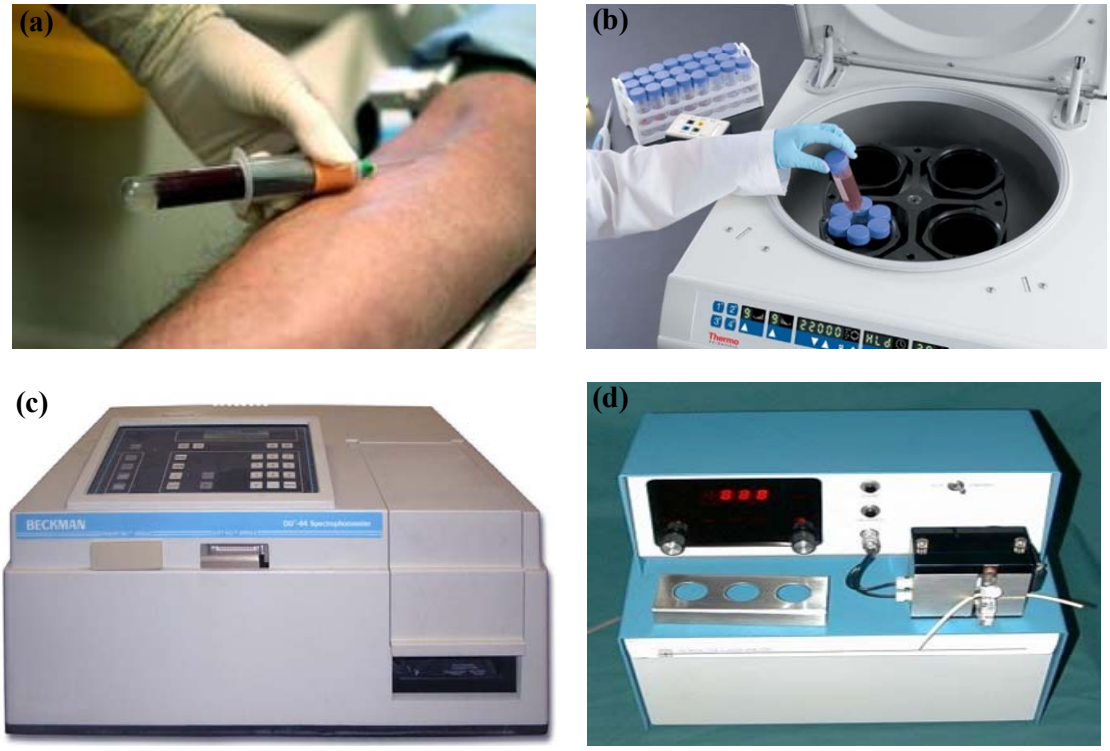

Figure 2.14: (a) Sample taking (b) Sample processing (c) Spectrometer used to conduct optical measurement (Beckman 64, UV/Vis) (d) Blood glucose meter for electrochemical measurement (Yellow Springs Instruments 23A). Figures adapted from www.labx.com.

2.3.2 Point-of-care Blood Analysis Systems

Point-of-care blood analysis systems are aimed at accomplishing blood tests in a simple and robust way, and deliver laboratory accuracy and reliability in patient-side locations which are far less well controlled than the laboratory. The commercialized techniques of POC blood analyses can be sorted into two major groups: electrochemical detection with

www.manaraa.com

whole blood sample, which is represented by i-STAT from Abbott; and colorimetric measurement on plasma extracted from whole blood, which is demonstrated by Piccolo xpress of Abaxis.

The electrochemical method (U.S. Patent 5,200,051) i-STAT employed to analyze whole blood is fast and convenient. The system is composed of three parts: a plastic cartridge as a sample receptacle, a microfabricated biosensor array installed in the plastic housing, and a low-cost general-purpose electromechanical transducer. The cartridge is a total microanalytical system with a sandwich structure formed by bonding a lower plastic component and upper plastic component. In the cartridge, all the necessary fluidics function units, such as chambers, pumps, valves, conduits, mixers, and separators, are built in, and reagents, diluents and biosensor arrays are pre-loaded. The fluid sample inside the cartridge is driven by capillary force and pneumatic pressure, while the cartridge itself does not move. The existence of blood cells, however, leads to an error of 10% - 15%.

www.manaraa.com

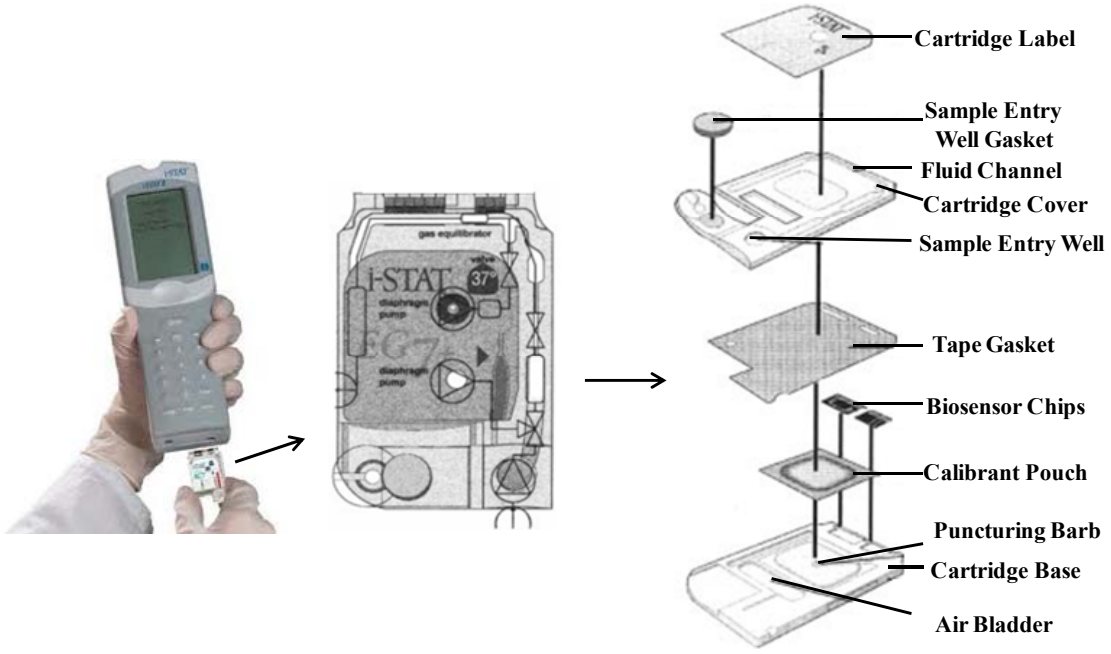

Figure 2.15: Portable blood analyzer from I-STAT and the exploded view of its cartridge. Figure adapted from Ref [65].

Piccolo xpress (U.S. Patent 5,122,284) consists of a single-use reagent rotor and an optical analyser. The system uses capillary force and centrifugal force as driving forces to complete all sample processing and optical analysis. The reagent rotor with a diameter of 80 mm consists of three functional layers, where all the dry reagents and the diluents were preloaded. The bottom and middle layers are bonded to form a fluidic system that is composed of cuvettes, chambers and fluidic channels for the manipulation of the sample fluid. In this microfluidic layer, plasma is separated from whole blood samples and guided to the cuvettes, where lyophilized reagent beads are placed for chemical reactions. The top layer provides imprinted bar-coded, rotor-specific calibration information to the analyser. A sealed container is arranged in the center of the rotor, containing 475 µl of diluents. The coefficient of variation (CV) of measurement results is from 0.07% to 0.47%. Unfortunately, the size of its chip is not within the micron scale, thus the amount of consumed blood for detection is relatively large. Meanwhile, optical devices for colorimetric sensing make the system heavy and expensive (more than $10,000).

www.manaraa.com

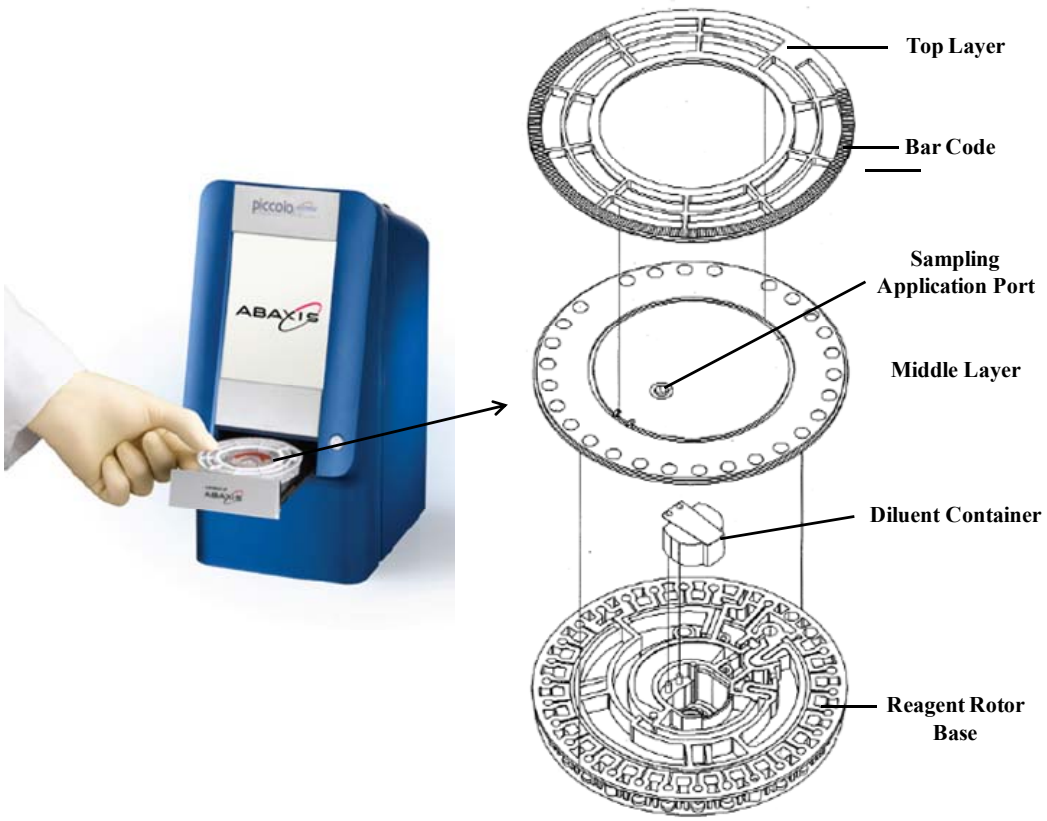

Figure 2.16: A compact blood analyzer from Abaxis and the exploded view of its cartridge. Figure adapted from Ref [66].

In this research field, cost-effective microfluidic paper-based analytical devices (μPADs) have emerged as a promising POC blood analysis technique. Paper possesses a few advantages: extremely low-cost, porous and flexible. Whitesides's group first demonstrated how to fabricate a microfluidic network on paper and conduct optical or electrochemical detections. For example, Vella at al reported that enzymatic markers of liver function can be measured using a micropatterned paper device and blood from a fingerstick (Figure 2.17) [67]. Since then, a large number of scientific reports from various groups have claimed innovative developments in point-of-care devices made from paper [68-79].

www.manaraa.com

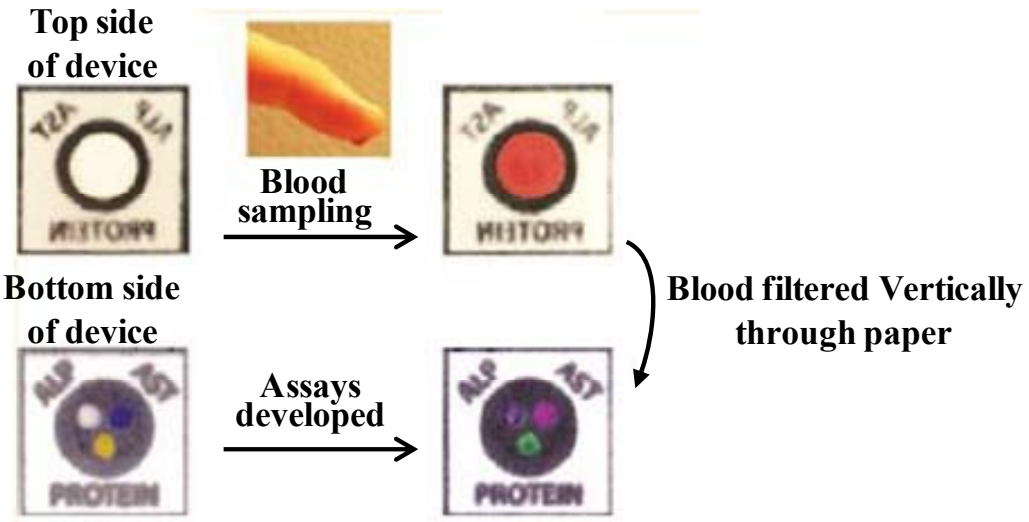

Figure 2.17: Schematic of blood test on µPAD. A circular filter membrane catches the red blood cells from a drop of blood. The membrane below contains three microfluidic chambers that can measure the liver enzymes alkaline phosphatase (ALP) and aspartate aminotransferase (AST) as well as serum protein. Colors indicate levels of the enzymes and serum protein, and can be digitized by a cell phone or desktop scanner for further analysis. Figure adapted from Ref [67].

Due to their huge potential market value, point-of-care techniques are rapidly progressing. Various research groups [29, 80-88] and diverse pharmaceutical companies (Abbott, Bayer, GE, Sumsung, Covidien, Pelican, Gyros, etc) heavily invest in every technique that is possibly helpful for fabricating point-of-care devices. Meanwhile, in pursuit of better diagnostic methods for people in developing countries and low resource areas, the Bill & Melinda Gates Foundation has started the new push for research into POC diagnostic devices [89].

www.manaraa.com

2.4 Summary

Current needs for accurate and low-cost diagnostic methods for global health are critical. Significant advances in the newly developed diagnostic systems have provided quantitative, novel diagnostic techniques with an analytical performance close to those of conventional laboratory tests. However, further simplification of the testing procedures and analyzers is still desirable, and strong efforts are directed towards the development of miniaturized and simple, yet sensitive and quantitative detection technologies to meet the need of POC diagnostics. A major challenge for biomedical engineers in the next few decades will be how to translate recent technologies accomplishments into technologies that are available and affordable at the periphery of the health care system. Of the new techniques, perhaps the most promising at the moment is microfluidics, as it has the potential to add capabilities for sample processing and complex fluidic handling while being compatible with inexpensive materials and fabrication methods. A tiny droplet of blood is enough for multiple blood tests on the microsystem, which dramatically reduces the consumption of blood sample and reagents. The Lab-on-a-CD technique used in this project acts as a special microfluidic platform, integrating sample processing and analytical steps into one continuous process. In the next three chapters, a low-cost, portable Lab-on-a-CD system for multiple and parallel point-of-care blood analyses will be elucidated in detail.

www.manaraa.com

2.5 References

1. Small, P.M. and Perkins, M.D., More rigour needed in trials of new diagnostic agents for tuberculosis. Lancet, 2000. **356** (9235): p. 1048-1048.

2. Belizario, V., Pasay, C., Bersabe, M., de Leon, W., Guerrero, D. and Bugaoisan, V., Field evaluation of malaria rapid diagnostic tests for the diagnosis of P. falciparum and non-P. falciparum infections. The Southeast Asian Journal of Tropical Medicine and Public Health, 2005. **36** (3): p. 552-561.

3. Lona, C., Alcantarab, S., Luchavezb, J., Tsuyuokac, R. and Belld, D., Positive control wells: a potential answer to remote-area quality assurance of malaria rapid diagnostic tests. Transactions of the Royal Society of Tropical Medicine and Hygiene, 2005. **99** (7): p. 493-498.

4. Barat, L., Chipipa, J., Kolczak, M. and Sukwa, T., Does the availability of blood slide microscopy for malaria at health centers improve the management of persons with fever in Zambia? The American journal of tropical medicine and hygiene, 1999. **60** (6): p. 1024-1030.

5. Bates, I. and Maitland, K., Are laboratory services coming of age in Sub-Saharan Africa? Clinical Infectious Diseases, 2006. **42** (3): p. 383-384.

6. Petti, C.A., Polage, C.R., Quinn, T.C., Ronald, A.R. and Sandel, M.A., Laboratory medicine in Africa: a barrier to effective health care. Clinical Infectious Diseases, 2006. **42** (3): p. 377-382.

7. Ridderhof, J.C., van DeunII, A., KamIII, K.M., NarayananIV, P.R. and AzizV, M.A., Roles of laboratories and laboratory systems in effective tuberculosis programmes. Bulletin of the World Health Organization, 2007. **85** (5): p. 354-359.

8. Mabey, D., Peeling, R. W., Ustianowski, A., and Perkins, M. D., Tropical infectious diseases: diagnostics for the developing world. Nature Reviews Microbiology, 2004. **2** (3): p. 231-240.

www.manaraa.com

9. Duffy, D. C., Gillis, H. L., Lin, J., Sheppard Jr, N. F., and Kellogg, G. J., Microfabricated centrifugal microfluidic systems: Characterization and multiple enzymatic assays. Analytical Chemistry, 1999. **71** (20): p. 4669-4678.

10. Verpoorte, E., Microfluidic chips for clinical and forensic analysis. Electrophoresis, 2002. **23** (5): p. 677-712.

11. Yager, P., Edwards, T., Fu, E., Helton, K., Nelson, K., Tam, M. R., and Weigl, B. H., Microfluidic diagnostic technologies for global public health. Nature, 2006. **442** (7101): p. 412-418.

12. Bührer-Sékula, S., Smits, H., Gussenhoven, G., Van Leeuwen, J., Amador, S., Fujiwara, T., Klatser, P. R. and Oskam, L., Simple and fast lateral flow test for classification of leprosy patients and identification of contacts with high risk of developing leprosy. Journal of Clinical Microbiology, 2003. **41** (5): p. 1991-1995.

13. Cole Jr, J.R., Sulzer, C.R. and Pursell, A.R., Improved microtechnique for the leptospiral microscopic agglutination test. Applied microbiology, 1973. **25** (6): p. 976-980.

14. Payne, D., Use and limitations of light microscopy for diagnosing malaria at the primary health care level. Bulletin of the World Health Organization, 1988. **66** (5): p. 621-626.

15. Stedtfeld, R. D., Tourlousse, D. M., Seyrig, G., Stedtfeld, T. M., Kronlein, M., Price, S., Ahmad, F., Gulari, E., Tiedje, J. M., and Hashsham, S. A., Gene-Z: a device for point of care genetic testing using a smartphone. Lab on a Chip, 2012. **12** (8): p. 1454-1462.

16. Nie, Z., Deiss, F., Liu, X., Akbulut, O., and Whitesides, G. M., Integration of paper-based microfluidic devices with commercial electrochemical readers. Lab on a Chip, 2010. **10** (22): p. 3163-3169.

www.manaraa.com

17. Nie, Z., Nijhuis, C. A., Gong, J., Chen, X., Kumachev, A., Martinez, A. W., and Whitesides, G. M., Electrochemical sensing in paper-based microfluidic devices. Lab on a Chip, 2009. **10** (4): p. 477-483.

18. Yang, X., Forouzan, O., Brown, T. P., & Shevkoplyas, S. S., Integrated separation of blood plasma from whole blood for microfluidic paper-based analytical devices. Lab on a Chip, 2011. **12** (2): p. 274-280.

19. Breslauer, D. N., Maamari, R. N., Switz, N. A., Lam, W. A., & Fletcher, D. A., Mobile phone based clinical microscopy for global health applications. PLoS One, 2009. **4** (7): p. e6320.

20. Terray, A., Oakey, J., and Marr, D.W.M., Microfluidic control using colloidal devices. Science, 2002. **296** (5574): p. 1841-1844.

21. Sia, S.K. and Whitesides, G.M., Microfluidic devices fabricated in poly (dimethylsiloxane) for biological studies. Electrophoresis, 2003. **24** (21): p. 3563-3576.

22. McDonald, J.C. and Whitesides, G.M., Poly (dimethylsiloxane) as a material for fabricating microfluidic devices. Accounts of Chemical Research, 2002. **35** (7): p. 491-499.

23. Wang, C.H. and Lee, G.B., Automatic bio-sampling chips integrated with micro-pumps and micro-valves for disease detection. Biosensors and Bioelectronics, 2005. **21** (3): p. 419-425.

24. Zhang, C., Xing, D. and Li, Y., Micropumps, microvalves, and micromixers within PCR microfluidic chips: Advances and trends. Biotechnology advances, 2007. **25** (5): p. 483-514.

25. Unger, M. A., Chou, H. P., Thorsen, T., Scherer, A., & Quake, S. R., Monolithic microfabricated valves and pumps by multilayer soft lithography. Science, 2000. **288** (5463): p. 113-116.

www.manaraa.com

26. Yang, Y.N., Hsiung, S.K. and Lee, G.B., A pneumatic micropump incorporated with a normally closed valve capable of generating a high pumping rate and a high back pressure. Microfluidics and Nanofluidics, 2009. **6** (6): p. 823-833.

27. Huang, C.W., Huang, S.B. and Lee, G.B., Pneumatic micropumps with serially connected actuation chambers. Journal of Micromechanics and Microengineering, 2006. **16** (11): p. 2265-2272.

28. Wang, C.H. and Lee, G.B., Pneumatically driven peristaltic micropumps utilizing serpentine-shape channels. Journal of Micromechanics and Microengineering, 2006. **16** (12): p. 341-348.

29. Ahn, C. H., Choi, J. W., Beaucage, G., Nevin, J. H., Lee, J. B., Puntambekar, A., and Lee, J. Y., Disposable Smart lab on a chip for point-of-care clinical diagnostics. Proceedings of the IEEE, 2004. **92** (1): p. 154-173.

30. Chin, C.D., Linder, V. and Sia, S.K., Lab-on-a-chip devices for global health: Past studies and future opportunities. Lab on a Chip, 2007. **7** (1): p. 41-57.

31. Srinivasan, V., Pamula,V.K. and Fair, R.B., An integrated digital microfluidic lab-on-a-chip for clinical diagnostics on human physiological fluids. Lab on a Chip, 2004. **4** (4): p. 310-315.

32. Srinivasan, V., Pamula, V.K. and Fair, R.B., Droplet-based microfluidic lab-on-a-chip for glucose detection. Analytica chimica acta, 2004. **507** (1): p. 145-150.

33. Toner, M. and Irimia, D., Blood-on-a-chip. Annual Review of Biomedical Engineering, 2005. **7**: p. 77-103.

34. Madou, M., Zoval, J., Jia, G., Kido, H., Kim, J., and Kim, N., Lab on a CD. Annual Review of Biomedical Engineering, 2006. **8**: p. 601-628.

35. Chin, C.D., Linder, V. and Sia, S.K., Lab-on-a-chip devices for global health: past studies and future opportunities. Lab on a Chip, 2006. **7** (1): p. 41-57.

www.manaraa.com

36. Singer, P.A., et al., Grand challenges in global health: the ethical, social and cultural program. PLoS medicine, 2007. **4** (9): p. e265.

37. Weigl, B.H., Bardell, R.L. and Cabrera, C.R., Lab-on-a-chip for drug development. Advanced Drug Delivery Reviews, 2003. **55** (3): p. 349-377.

38. Haeberle, S., Schmitt, N., Zengerle, R., and Ducrée, J., Centrifugo-magnetic pump for gas-to-liquid sampling. Sensors and Actuators A: Physical, 2007. **135** (1): p. 28-33.

39. Lastochkin, D., Zhou, R., Wang, P., Ben, Y., and Chang, H. C., Electrokinetic micropump and micromixer design based on ac faradaic polarization. Journal of applied physics, 2004. **96** (3): p. 1730-1733.

40. Lemoff, A.V. and Lee, A.P., An AC magnetohydrodynamic micropump. Sensors and actuators B: Chemical, 2000. **63** (3): p. 178-185.

41. Nguyen, N. T., Meng, A. H., Black, J., and White, R. M., Integrated flow sensor for in situ measurement and control of acoustic streaming in flexural plate wave micropumps. Sensors and Actuators A: Physical, 2000. **79** (2): p. 115-121.

42. Tsai, J.H. and Lin, L., Active microfluidic mixer and gas bubble filter driven by thermal bubble micropump. Sensors and Actuators A: Physical, 2002. **97**: p. 665-671.

43. Madou, M. J., Lee, L. J., Daunert, S., Lai, S., and Shih, C. H., Design and fabrication of CD-like microfluidic platforms for diagnostics: microfluidic functions. Biomedical Microdevices, 2001. **3** (3): p. 245-254.

44. García-Sánchez, P. and Ramos, A., The effect of electrode height on the performance of travelling-wave electroosmotic micropumps. Microfluidics and Nanofluidics, 2008. **5** (3): p. 307-312.

45. McBride, S.E. and York, P.K., Electrode combinations for pumping fluids. 2000, Google Patents.

www.manaraa.com

46. Wong, P. K., Wang, T. H., Deval, J. H., and Ho, C. M., Electrokinetics in micro devices for biotechnology applications. IEEE/ASME Transactions on Mechatronics, 2004. **9** (2): p. 366-376.

47. Garcia-Sanchez, P., Ramos, A., Green, N., and Morgan, H., Experiments on AC electrokinetic pumping of liquids using arrays of microelectrodes. IEEE Transactions on Dielectrics and Electrical Insulation, 2006. **13** (3): p. 670-677.

48. Miao, J. Y., Xu, Z. L., Zhang, X. Y., Wang, N., Yang, Z. Y., and Sheng, P., Micropumps based on the enhanced electroosmotic effect of aluminum oxide membranes. Advanced Materials, 2007. **19** (23): p. 4234-4237.

49. Wang, L., L. Flanagan, and Lee, A.P., Side-wall vertical electrodes for lateral field microfluidic applications. Journal of Microelectromechanical Systems, 2007. **16** (2): p. 454-461.

50. Madou, M.J., Fundamentals of microfabrication: the science of miniaturization. 2002: CRC.

51. Ducrée, J., Haeberle, S., Brenner, T., Glatzel, T., and Zengerle, R., Patterning of flow and mixing in rotating radial microchannels. Microfluidics and Nanofluidics, 2006. **2** (2): p. 97-105.

52. Kim, J., Kido, H., Rangel, R. H., and Madou, M. J., Passive flow switching valves on a centrifugal microfluidic platform. Sensors and actuators B: Chemical, 2008. **128** (2): p. 613-621.

53. Brenner, T., Glatzel, T., Zengerle, R., and Ducrée, J., Frequency-dependent transversal flow control in centrifugal microfluidics. Lab on a Chip, 2005. **5** (2): p. 146-150.

54. Ducrée, J., Haeberle, S., Lutz, S., Pausch, S., Von Stetten, F., and Zengerle, R., The centrifugal microfluidic Bio-Disk platform. Journal of Micromechanics and Microengineering, 2007. **17**: p. S103.

www.manaraa.com

55. Israelachvili, J.N., Intermolecular and surface forces. 2011: Academic press.

56. Andersson, P., Jesson, G., Kylberg, G., Ekstrand, G., and Thorsén, G., Parallel nanoliter microfluidic analysis system. Analytical Chemistry, 2007. **79** (11): p. 4022-4030.

57. Duffy, D.C., Gillis, H. L., Lin, J., Sheppard, N. F., Kellogg, G. J., Microfabricated centrifugal microfluidic systems: characterization and multiple enzymatic assays. Analytical Chemistry, 1999. **71** (20): p. 4669-4678.

58. Steigert, J., Brenner, T., Grumann, M., Riegger, L., Lutz, S., and Zengerle, R., Integrated siphon-based metering and sedimentation of whole blood on a hydrophilic lab-on-a-disk. Biomedical Microdevices, 2007. **9**(5): p. 675-679.

59. Haeberle, S. and Zengerle, R., Microfluidic platforms for lab-on-a-chip applications. Lab on a Chip, 2007. **7** (9): p. 1094-1110.

60. Siegrist, J., Gorkin, R., Clime, L., Roy, E., Peytavi, R., Kido, H., Michel Bergeron, M., Veres, T., and Madou, M., Serial siphon valving for centrifugal microfluidic platforms. Microfluidics and Nanofluidics, 2010. **9** (1): p. 55-63.

61. Park, J., Cho, Y., Lee, B., Lee, J., and Ko, C., Multifunctional microvalves control by optical illumination on nanoheaters and its application in centrifugal microfluidic devices. Lab on a Chip, 2007. **7** (5): p. 557-564.

62. Garcia-Cordero, J. L., Kurzbuch, D., Benito-Lopez, F., Diamond, D., Lee, L. P., and Ricco, A. J., Optically addressable single-use microfluidic valves by laser printer lithography. Lab on a Chip, 2010. **10** (20): p. 2680-2687.

63. Markov, D. A., Manuel, S., Shor, L. M., Opalenik, S. R., Wikswo, J. P., and Samson, P. C., Tape underlayment rotary-node (TURN) valves for simple on-chip microfluidic flow control. Biomedical Microdevices, 2010. **12** (1): p. 135-144.

www.manaraa.com

64. Park, W., Han, S. and Kwon, S., Fabrication of membrane-type microvalves in rectangular microfluidic channels via seal photopolymerization. Lab on a Chip, 2010. **10** (20): p. 2814-2817.

65. Erickson, K.A. and Wilding, P., Evaluation of a novel point-of-care system, the i-STAT portable clinical analyzer. Clinical Chemistry, 1993. **39** (2): p. 283-287.

66. Schembri, C., Burd, T., Kopf-Sill, A., Shea, L., and Braynin, B., Centrifugation and capillarity integrated into a multiple analyte whole blood analyser. Journal of Automatic Chemistry, 1995. **17** (3): p. 99-104.

67. Vella, S. J., Beattie, P. D., Cademartiri, R., Laromaine, A., Martinez, A. W., Phillips, S. T., Mirica, K. M., and Whitesides, G. M., Measuring Markers of Liver Function Using a Micro-Patterned Paper Device Designed for Blood from a Fingerstick. Analytical Chemistry, 2012. **84** (6), pp 2883–2891.

68. Allan, Z.C. and Fisher, M.A., Environmental effects on assays in microfluidic paper-based analytical devices. Abstracts of Papers of the American Chemical Society, 2011. **241**.

69. Phillips, S.T., Fluidic "Timers" for paper-based microfluidic devices. Abstracts of Papers of the American Chemical Society, 2010. **240**.

70. Schilling, K. M., Lepore, A. L., Kurian, J. A., and Martinez, A. W., Fully Enclosed Microfluidic Paper-Based Analytical Devices. Analytical Chemistry, 2012. **84** (3): p. 1579-1585.

71. Yang, X. X., Forouzan, O., Brown, T. P., & Shevkoplyas, S. S., Integrated separation of blood plasma from whole blood for microfluidic paper-based analytical devices. Lab on a Chip, 2012. **12** (2): p. 274-280.

72. Noh, N. and Phillips, S.T., Metering the Capillary-Driven Flow of Fluids in Paper-Based Microfluidic Devices. Analytical Chemistry, 2010. **82** (10): p. 4181-4187.

www.manaraa.com

73. Martinez, A.W., Microfluidic paper-based analytical devices: from POCKET to paper-based ELISA. Bioanalysis, 2011. **3** (23): p. 2589-2592.

74. Klasner, S. A., Price, A. K., Hoeman, K. W., Wilson, R. S., Bell, K. J., and Culbertson, C. T., Paper-based microfluidic devices for analysis of clinically relevant analytes present in urine and saliva. Analytical and Bioanalytical Chemistry, 2010. **397** (5): p. 1821-1829.

75. Liu, X. Y., Cheng, C. M., Martinez, A. W., Mirica, K. A., Li, X. J., Phillips, S. T., Mascareñas, M., and Whitesides, G.M., A portable microfluidic paper-based device for ELISA, IEEE 24th International Conference on Micro Electro Mechanical Systems. 2011. p. 75-78.

76. Carvalhal, R.F., Carrilho, E. and Kubota, L.T., The potential and application of microfluidic paper-based separation devices. Bioanalysis, 2010. **2** (10): p. 1663-1665.

77. Ellerbee, A. K., Phillips, S. T., Siegel, A. C., Mirica, K. A., Martinez, A. W., and Striehl, P., Quantifying Colorimetric Assays in Paper-Based Microfluidic Devices by Measuring the Transmission of Light through Paper. Analytical Chemistry, 2009. **81** (20): p. 8447-8452.

78. Phillips, S.T., Strategies for running multiple quantitative assays simultaneously in paper-based microfluidic devices. Abstracts of Papers of the American Chemical Society, 2011. **242**.

79. Dungchai, W., Chailapakul, O. and Henry, C.S., Use of multiple colorimetric indicators for paper-based microfluidic devices. Analytica chimica acta, 2010. **674** (2): p. 227-233.

80. Marcucci, R., Gori, A. M., Paniccia, R., Giusti, B., Valente, S., and Giglioli, C., Cardiovascular Death and Nonfatal Myocardial Infarction in Acute Coronary Syndrome Patients Receiving Coronary Stenting Are Predicted by Residual

www.manaraa.com

Platelet Reactivity to ADP Detected by a Point-of-Care Assay A 12-Month Follow-Up. Circulation, 2009. **119** (2): p. 237-242.

81. Tefferi, A. and Vardiman, J.W., Classification and diagnosis of myeloproliferative neoplasms: The 2008 World Health Organization criteria and point-of-care diagnostic algorithms. Leukemia, 2008. **22** (1): p. 14-22.

82. Wang, J., Electrochemical biosensors: Towards point-of-care cancer diagnostics. Biosensors & bioelectronics, 2006. **21** (10): p. 1887-1892.

83. Sibbing, D., Braun, S., Morath, T., Mehilli, J., Vogt, W., and Schomig, A., Platelet Reactivity After Clopidogrel Treatment Assessed With Point-of-Care Analysis and Early Drug-Eluting Stent Thrombosis. Journal of the American College of Cardiology, 2009. **53** (10): p. 849-856.

84. Steinhubl, S. R., Talley, J. D., Braden, G. A., Tcheng, J. E., Casterella, P. J., and Moliterno, D. J., Point-of-care measured platelet inhibition correlates with a reduced risk of an adverse cardiac event after percutaneous coronary intervention - Results of the GOLD (AU-Assessing Ultegra) multicenter study. Circulation, 2001. **103** (21): p. 2572-2578.

85. Sohn, A. H., Garrett, D. O., Sinkowitz-Cochran, R. L., Grobskopf, L. A., Levine, G. L., and Stover, B. H., Prevalence of nosocomial infections in neonatal intensive care unit patients: Results from the first national point-prevalence survey. Journal of Pediatrics, 2001. **139** (6): p. 821-827.

86. Price, M. J., Endemann, S., Gollapudi, R. R., Valencia, R., Stinis, C. T., and Levisay, J. P., Prognostic significance of post-clopidogrel platelet reactivity assessed by a point-of-care assay on thrombotic events after drug-eluting stent implantation. European Heart Journal, 2008. **29** (8): p. 992-1000.

87. Tudos, A.J., Besselink, G.A.J. and Schasfoort, R.B.M., Trends in miniaturized total analysis systems for point-of-care testing in clinical chemistry. Lab on a Chip, 2001. **1** (2): p. 83-95.

www.manaraa.com

88. Maisel, A. S., Koon, J., Krishnaswamy, P., Kazenegra, R., Clopton, P., and Gardetto, N.,, Utility of B-natriuretic peptide as a rapid, point-of-care test for screening patients undergoing echocardiography to determine left ventricular dysfunction. American Heart Journal, 2001. **141** (3): p. 367-374.

89. McCoy, D., Kembhavi, G., Patel, J., and Luintel, A., The Bill & Melinda Gates Foundation's grant-making programme for global health. The Lancet, 2009. **373** (9675): p. 1645-1653.

www.manaraa.com

Chapter 3

3 Out-of-plane Microvalves for Whole Blood Separation on Lab-on-a-CD

It has been mentioned in the previous chapter that the emergence of Lab-on-a-CD technology provides a centrifugal and compact platform for high throughput blood analysis in point-of-care (POC) diagnostics, and blood separation of the whole blood is the first step for clinical blood diagnosis. This chapter describes a novel design of an out-of-plane microvalve that enables high performance of the whole blood separation on Lab-on-a-CD centrifugal devices. The principle of design and experimental details of device fabrication are presented. Further, the control experiment without out-of-plane microvalve was conducted to evaluate the performance of the microvalve.

3.1 Introduction

Blood tests are the most commonly-used diagnostic methods nowadays because blood analysis provides definitive information of patients' medical conditions [1]. Traditional blood tests, including sample collection, preparation and detection, are conducted using large-scale blood analyzers. The advent of Lab-on-a-chip technology that takes advantage of low volumes of consumed samples, fast response time and low fabrication costs in mass production [2], makes it possible to integrate the whole procedure of blood analysis into miniaturized devices.

Implementing blood separation, one of the key steps of blood analysis, on Lab-on-a-chip devices has long been a major research focus. Crowley et al. employed transverse-flow microfilter devices [3]. Arifin et al. spun blood cells down towards a bottom stagnation point [4]. Yang et al. proposed a T-channel network structure [5]. Blattert et al. used a bended microchannel structure [6] (Figure 3.1).

www.manaraa.com

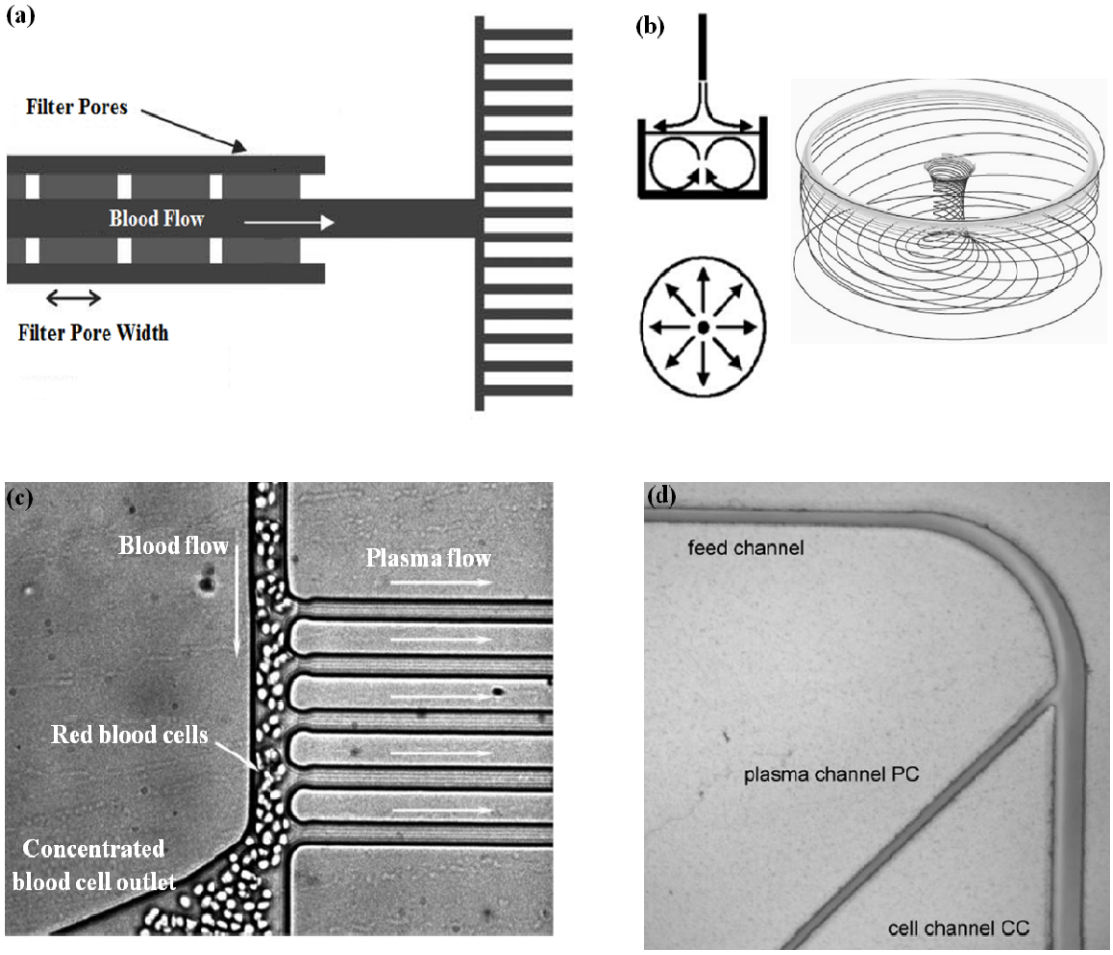

Figure 3.1 (a) Transverse-flow microfilter devices (b) Spun blood cells down towards a bottom stagnation point (c) A T-channel network structure (d) A bended microchannel structure. Figures adapted from Ref [3-6].

The emergence of Lab-on-a-CD technology boosts the development of on-chip blood separation. When rotating, Lab-on-a-CD devices not only act as centrifugal platforms for fluid propulsion, but also provide inherent inertial forces for blood separation. Various blood components of different mass densities will bear diverse body forces under specific physical fields [7]. Haeberle et al. proposed a decanting structure to extract plasma from the whole blood [8]. Recent studies carried out in our laboratory showed that a specially designed curved microchannel network, taking advantage of two centrifugal forces and

www.manaraa.com

Coriolis force due to the system rotation, was capable of separating diluted blood and guiding blood cells and plasma to different reservoirs for subsequent analysis [9]. All of these previous studies have raised more technical challenges that need to be solved, such as, how to improve efficiency of blood separation (or purity of the separated plasma) for the whole blood of high hematocrit; how to improve the plasma yield for subsequent blood analysis; how to improve the readiness of plasma extraction; and how to reduce the complexity of the device to increase reliability. For example, we have found that prevention of blood cells diffusing from the sedimentation back to the supernatant can effectively improve efficiency of blood separation, plasma yield and the readiness of plasma extraction.

Ideally blood cells and plasma are better spatially isolated after separation for subsequent plasma extraction and testing. This is also the main concept of our previous work [9] delivering plasma and blood cells into two separate reservoirs. However, our previous Lab-on-a-CD design worked well for diluted blood of 6% hematocrit, but not for the whole blood of much higher hematocrit. The idea of the present work is to introduce a newly designed microvalve, namely the out-of-plane microvalve, into Lab-on-a-CD devices to spatially isolate plasma from blood cells after blood separation. Indeed, various types of microvalves have been implemented in Lab-on-a-CD devices for different purposes. Park et al. presented a phase change-based microvalve controlled by laser illumination [10]. Madou et al. presented a polymer-based CD platform that utilized capillary microvalve [11]. Steigert et al. brought forward the frequency-dependent microvalve adopting the siphon effect [12]. Mark et al. proposed a novel design of centrifuge-pneumatic valve which does not require ultra-precise structures or local surface modifications [13]. there is continuing demand for microfluidic devices to become lower-cost, easier-to-manufacture and easier-to-use for point-of-care (POC) diagnostics [14]. Whitesides's group developed a simple blood separation device comprising only an egg beater and a piece of polyethylene tubing [15] (Figure 3.2). Therefore our motivation is to integrate microvalves into a Lab-on-a-CD device to form a structurally-simple but functionally-robust device, which is capable of high-performance

www.manaraa.com

blood separation and suitable for simple microfabrication methods like hot-embossing or micro-injection molding.

The essence of the work presented here is the novel design of a simple but effective Lab-on-a-CD device with the three-dimensional out-of-plane microvalves for high-performance whole blood separation. The “close” or “open” status of the out-of-plane microvalve is controlled by the rotational speed that determines the balance of centrifugal force, hydrostatic force and capillary force related to the out-of-plane microvalve. When the Lab-on-a-CD device spins above a certain speed, blood sample flows over the mivrovalve, and sedimentation can be achieved on the rotating platform due to the centrifugal force developed along the radial axis [16]. The accumulated blood cells are confined in the downstream sedimentation reservoir by the microvalve, away from the plasma in the upstream supernatant reservoir. The use of the out-of-plane microvalve helps improve the efficiency of whole blood separation and the plasma yield. The integration of the out-of-plane microvalve(s) into Lab-on-a-CD platforms is a simple, easy-to-make and low-cost solution for blood separation. In next sections, the working mechanism, device fabrication, experiments and blood separation results will be introduced.

www.manaraa.com

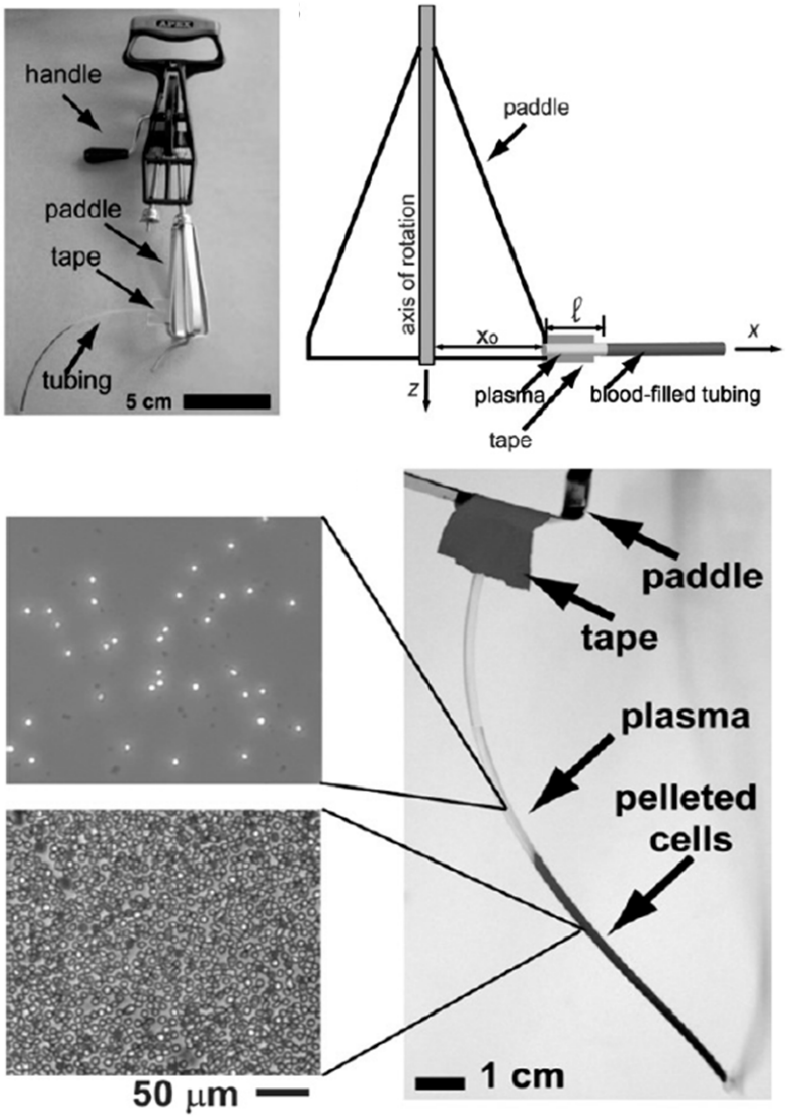

Figure 3.2: A simple device composed of only an egg beater and a piece of polyethylene tubing for blood separation. Figure adapted from Ref [15].

3.2 The Working Mechanisms

The phrase "out-of-plane" literally specifies a rise from the bottom of a microchannel. As shown in Figure 3.3, the out-of-plane microvalve is designed as an upstanding block from the bottom of the channel to a predetermined height inside the channel, leaving a narrowed microchannel. The liquid level is horizontal when the platform remains still.

www.manaraa.com

But it begins to tilt when the CD platform starts to rotate. When the rotational speed is below a threshold value, the microvalve is in "close" state. If the rotational speed is increased above a threshold value, the liquid sample is able to flow over the microvalve.

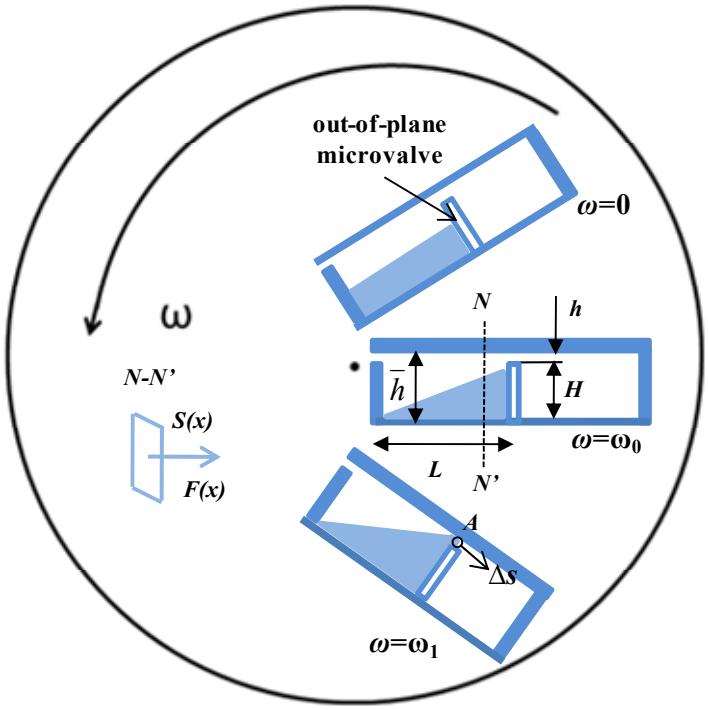

Figure 3.3: Schematics of the working mechanism of the out-of-plane microvalve on a Lab-on-a-CD platform. The liquid level is horizontal when the platform is motionless (ω = 0). The liquid surface begins to tilt under a rotational speed ω_0 which is smaller than the threshold rotational speed. Under these two situations, the microvalve is in "close" state and blocks the passage of fluid. If the rotation speed is increased above the threshold rotational speed ω_1, the microvalve is opened and the liquid sample can flow over it.

Once the platform is stopped, no forces are available for the sample flowing backward, and the microvalve blocks the passage of fluid. In this case, the out-of-plane microvalve functions as a dam stopping the sample flowing backward. This is the core function of the

www.manaraa.com

out-of-plane microvalve designed to improve blood separation. To estimate the threshold rotational speed ω_1, we apply the principle of virtual work on the whole volume of liquid for the moment that the liquid is going to flow over the microvalve.

The forces induced by the centrifugal platform at the out-of-plane microvalve are simplified into three main categories. The first one is centrifugal force (F_c) which is the driving force induced by the centrifugal platform. The other two are hydrostatic force (F_h) and capillary force (f_c) which are obstructive forces. When the sample flow primes the microvalve, the capillary force at the narrowed microchannel above the out-of-plane microvalve actually dominates the obstructive forces. To apply the principle of virtual work, we assume a small amount of liquid ($A\Delta s$) enters the narrowed microchannel by a virtual displacement Δs , where A is the cross-sectional area of the narrowed microchannel. In this case, the centrifugal force is the driving force doing positive work, while the liquid needs to overcome the gravitational force and the capillary force when the channel cross-section varies from wider to narrower, both of which are doing negative work. According to the principle of virtual work, the total virtual work is zero:

$$W_F + W_g + W_{f_c} = 0 \tag{3.1}$$

where W_F , W_g and W_{f_c} are the work of the centrifugal force, the gravitational force and the capillary force, respectively, which are expressed as

$$W_F = \int_0^L F(x) \cdot L(x) \cdot dx \tag{3.2}$$

$$W_g = -\rho A \Delta s \cdot g(h/2 + H) \tag{3.3}$$

$$W_{f_c} = f_c \cdot \Delta s \tag{3.4}$$

In Equations 3.2-3.4, F(x), L(x) and fc are expressed as:

$$F(x) = S(x)\rho\omega^2 x \tag{3.5}$$

www.manaraa.com

$$L(x) = \frac{A\Delta s}{S(x)} \tag{3.6}$$

$$f_c = 2A\sigma\cos\theta\left[\left(\frac{1}{b}+\frac{1}{h}\right)-\left(\frac{1}{\bar{b}}+\frac{1}{\bar{h}}\right)\right] \tag{3.7}$$

In above Equations, S(x) is the cross-sectional area of the sample liquid in the reservoir at the location x, g is the gravitational acceleration, ρ is the sample density, ω is the rotational speed, σ is the surface tension, θ is the contact angle of sample on the channel wall, H is the height of the microvalve and L is the length of the upstream reservoir. b and h are the width and height of the narrowed microchannel above the microvalve, respectively, and $\bar{b}$ and $\bar{h}$ are the width and height in the reservoir near the microvalve, respectively.

From Equations 3.1 to 3.7, we can determine the threshold rotational speed, or so-called the burst frequency [11], as follows:

$$\omega_1 = \sqrt{\frac{\rho g(h+2H) - 4\sigma\cos\theta\left[\left(\frac{1}{b}+\frac{1}{h}\right)-\left(\frac{1}{\bar{b}}+\frac{1}{\bar{h}}\right)\right]}{\rho L^2}} \tag{3.8}$$

The term "$4\sigma\cos\theta\left[\left(\frac{1}{b}+\frac{1}{h}\right)-\left(\frac{1}{\bar{b}}+\frac{1}{\bar{h}}\right)\right]$" due to the capillary force is three orders of magnitude larger than the term "$\rho g(h+2H)$" due to the gravitational force in Equation 3.8. Since the gravitational force has negligible effect in Equation 3.8, for simplicity. Equation 3.8 of the burst frequency can be derived by Equation 3.9.

$$\omega_1 = \sqrt{\frac{-4\sigma\cos\theta\left[\left(\frac{1}{b}+\frac{1}{h}\right)-\left(\frac{1}{\bar{b}}+\frac{1}{\bar{h}}\right)\right]}{\rho L^2}} \tag{3.9}$$

www.manaraa.com

The analysis above provides us guidance to control the "open" or "close" state of the out-of-plane valve by adjusting the rotational speed. Using the following parameters, blood surface tension (20 °C) $\sigma = 0.052$ N/m [17], density of blood $\rho = 1060$ kg/m^3 [18], $g = 9.8$ m/s^2, $L = 0.02$ m, $h = 1\times10^{-5}$ m, $\bar{h} = 5.5\times10^{-5}$ m, $b = \bar{b} = 2\times10^{-3}$ m, $H = 4.5\times10^{-5}$ m, the ω_1 is in the range between 797 rpm to 1352 rpm when θ varying from 100° to 120°. In numerous experiments we have done, the experimentally observed threshold rotational speed ω_1 falls in the range predicted by Equation 3.9, round 1100 rpm.

3.3 Experimental Design and Method

In this section, we present how the out-of-plane microvalve(s) is built into a centrifugal platform to form a Lab-on-a-CD device for whole blood separation.

3.3.1 Materials

High-resolution (2000DPI) photomask printing service was provided by CAD/Art Services Inc. Polydimethysiloxane (PDMS) replicate was prepared by mixing prepolymer and curing agent (Sylgard 184, Dow Corning, Midland, MI) at a ratio of 10:1. Human raw blood was drawn from a healthy donor at the University Hospital and stored in a vacutainer containing anticoagulant (EDTA) at 4ºC. The stepper motor (RDK-STEPPER) used to provide centrifugal force was purchased from Luminary Micro. Standard materials for photolithography were available in Western Nanofabrication Lab at University of Western Ontario.

3.3.2 Device Fabrication

A Lab-on-a-CD device may comprise a number of identical sectors for parallel blood separation, each of which contains three main parts: a supernatant reservoir (~9.4 μL), a sedimentation reservoir (~4.7 μL) and a connection section within which an out-of-plane microvalve (radial width 250 μm) was built. The total height of the channel network

www.manaraa.com

structure is 55 μm, while the microvalve is 45 μm high leaving a 10 μm narrowed microchannel to allow blood to pass through. The formation of the out-of-plane microvalve involves 3D microfabrication processes. In this work, we develop an innovative technique of fabricating 3D mold masters that are negative-photoresist (SU-8) reliefs comprising multiple layers of photoresist overlaid on top of each other. The fabrication process we proposed involves two major steps:

(1) Fabrication of the 3D photoresist mold with layers of photoresist (Figure 3.4(a)).

(2) Configuration of the microchannel network structure by casting PDMS on the mold (Figure 3.4(b)).

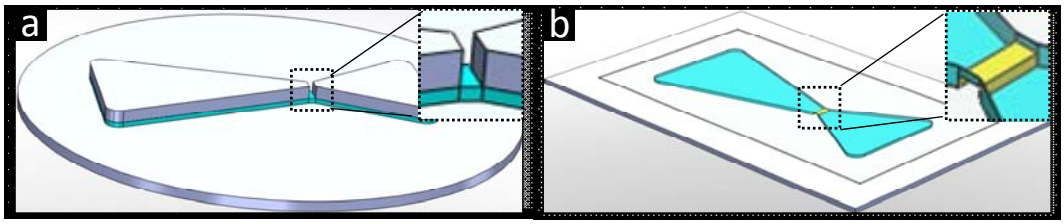

Figure 3.4: Schematics of (a) The aligned bilayer photoresist mold for the out-of-plane microvalve and (b) A PDMS replicate fabricated out of the mold.

The photoresist mold in the first step was prepared by standard photolithographic techniques [19]. To obtain maximum process reliability, silicon (Si) wafers were thoroughly cleaned and dried before use. The bottom layer of photoresist (SU-8 3005, Microchem, USA) was spun at 500 rpm for 5 seconds followed by 1000 rpm for 30 seconds on a Si wafer using a spin coater (Solitec 5110 Spinner) to obtain a thickness of 10 μm (Figure 3.5(a)). This layer was exposed to ultraviolet (UV) light through the first photomask using a mask aligner (Karl Suss MA6 Mask Aligner, sensor wavelength = 405 nm), but not developed yet in this step (Figure 3.5(b)). After post exposure bake, the wafer was spin-coated with another layer of photoresist (SU-8

www.manaraa.com

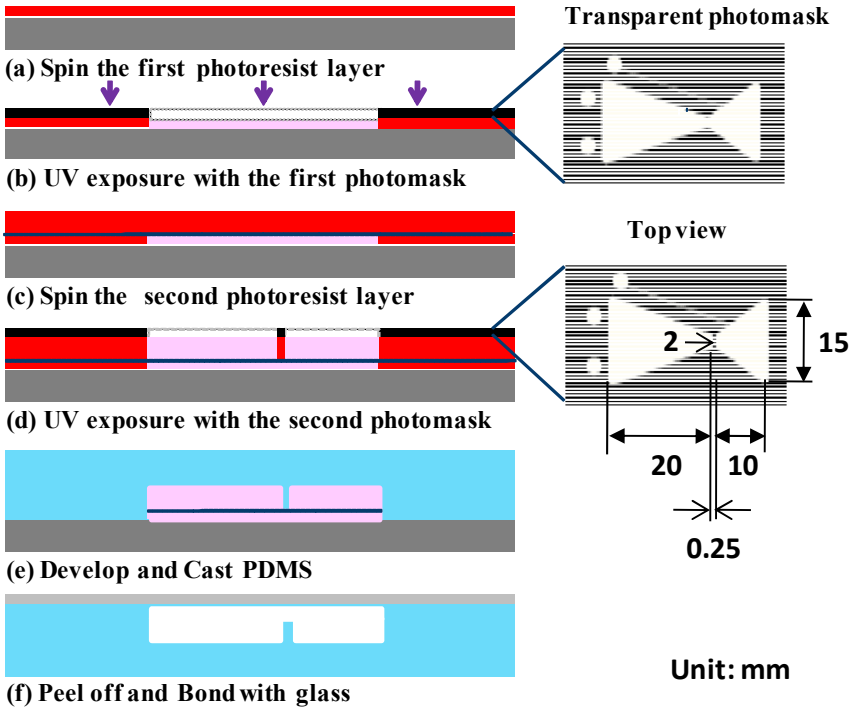

Figure 3.5: Detailed microfabrication procedures and dimensions for the Lab-on-a-CD device with an out-of-plane microvalve. (a) Spin the first layer of photoresist, (b) UV exposure with the first photomask, (c) Spin the second layer of photoresist, (d) UV exposure with the second photomask, (e) Develop and cast PDMS, (f) Peel off and bond with a glass wafer.

3025, thickness 45 μm) (Figure 3.5(c)). The second photomask with similar pattern to the first one, but an opening in the area where the microvalve located, was aligned with the bottom layer, followed by UV exposure (Figure 3.5(d)). After post exposure bake, both photoresist layers were developed using SU-8 developer. Finally, the wafer was rinsed with isopropanol (IPA) followed by deionized (DI) water and baked at 150 °C for 2 minutes, forming a positive and 3D insert mold on a wafer. The steps for fabricating SU-8 structure on Si substrate using photolithography technique are also shown in Figure 3.6.

www.manaraa.com

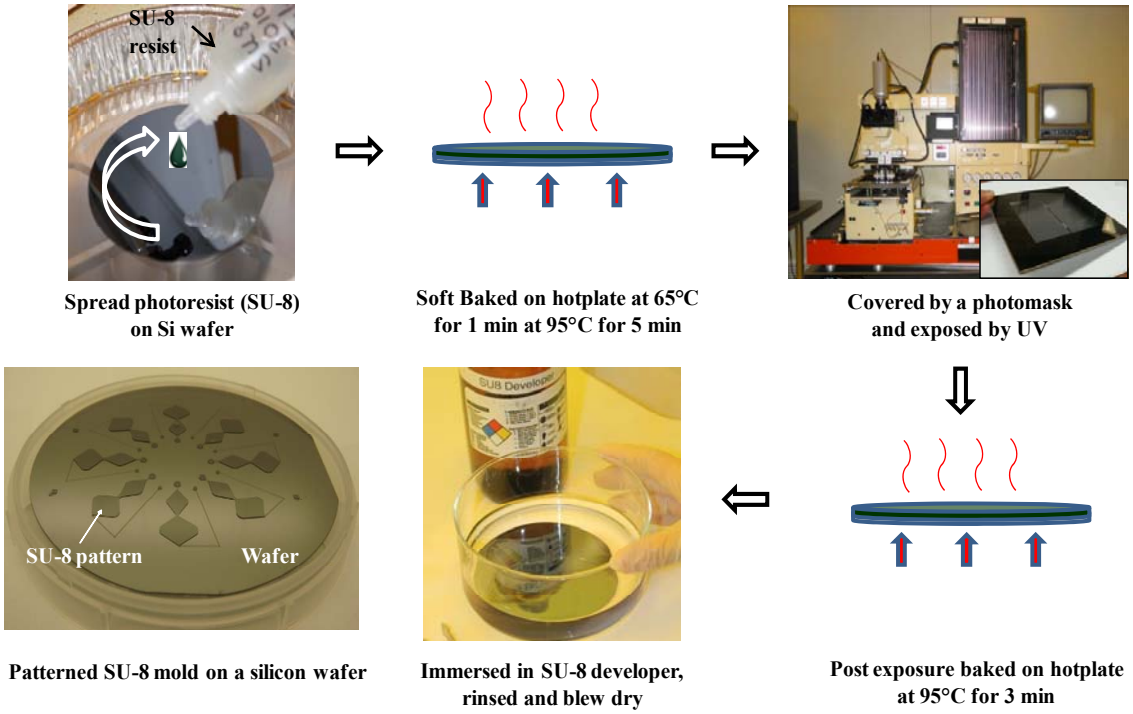

Figure 3.6: Graphic illustration of photolithography process for the fabrication of molds.

In the next step, standard soft lithographic technique was employed to fabricate the Lab-on-a-CD device [20]. 55 g (per master mold) of premixed PDMS was mixed and poured into the SU-8 master mold in a Petri dish and degassed in a vacuum chamber for a minimum of 30 min. After removing all the trapped air, the Petri dish was put on a hotplate (65 °C for 3 h and 80 °C for 2 h) to cure the PDMS (Figure 3.5(e)).

The cured PDMS layer (~5 mm thick) was peeled off from the mold and bonded to a Pyrex glass wafer (Figure 3.5(f))). Holes were drilled using round-headed diamond drill bits (Brasseler, USA) on the glass wafer, serving as inlets and vents for the patterned PDMS layer. Before bonding, the PDMS replica and the glass wafer were cleaned with oxygen plasma (100 mW, 2% oxygen, 1 min) in a PX-250 plasma chamber (March Instruments, Concord, MA) and then immediately placed in contact

www.manaraa.com

followed by baking at 70 °C for 1 hour to enhance the strength of bonding. Another glass wafer was brought into contact with the other side of the PDMS replica as a support layer. The steps for fabricating PDMS devices using softlithography technique are also shown in Figure 3.7. A completed Lab-on-a-CD device is shown in Figure 3.8(b).

As seen in the detailed fabrication steps in Figure 3.4, the height of the out-of-plane microvalve is controlled by the thickness of the second photoresist layer, while the size of the narrowed microchannel above the microvalve is determined by the thickness of the first photoresist layer.

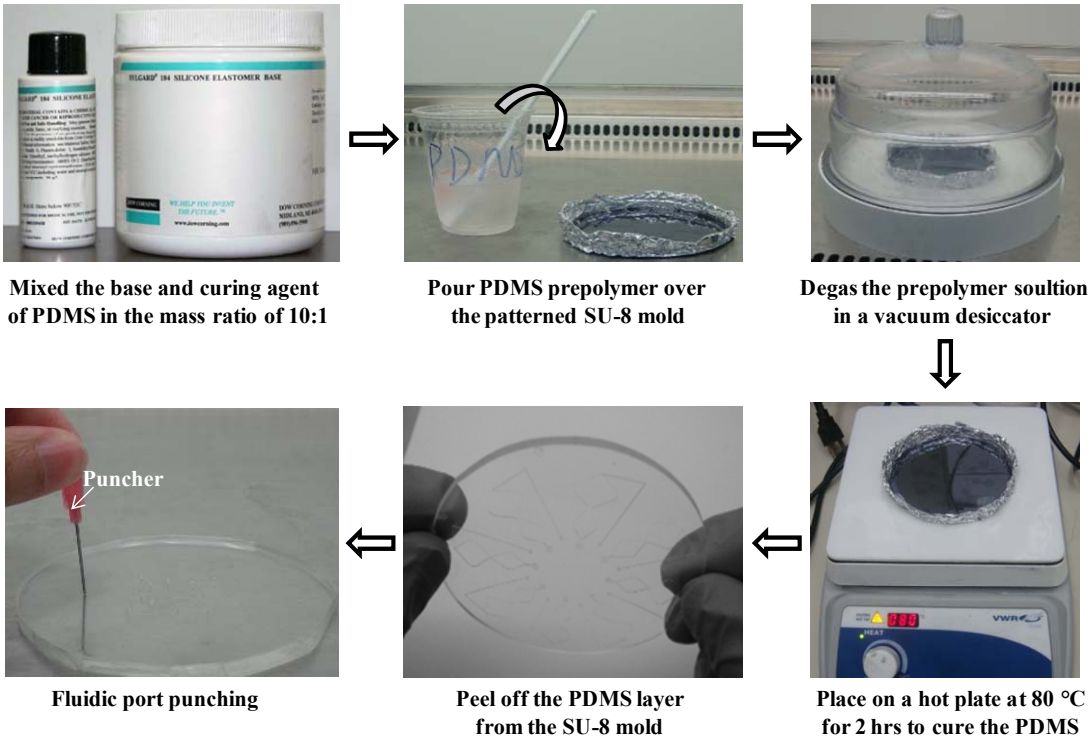

Figure 3.7: Graphic illustration of softlithography process for the fabrication of PDMS microfluidic structures.

www.manaraa.com

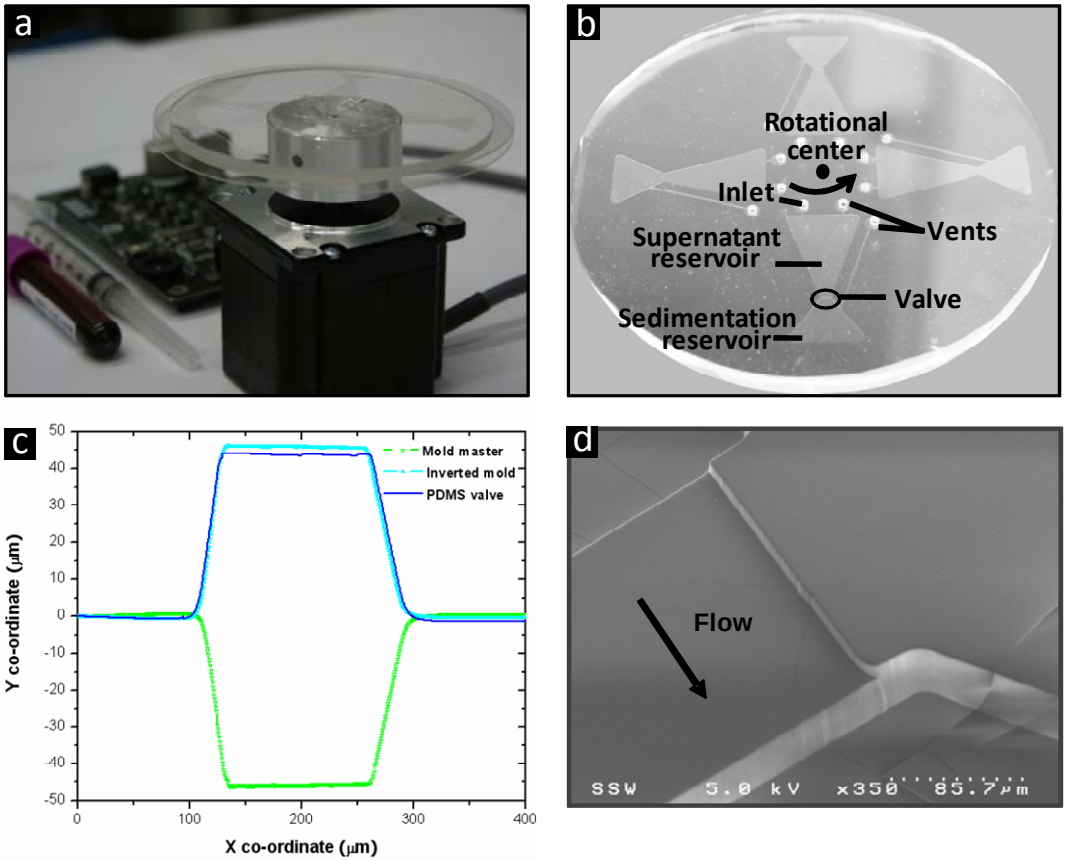

Figure 3.8: Characteristics of the Lab-on-a-CD device. (a) The full view of the Lab-on-a-CD system including a motor, a control board and the Lab-on-a-CD device. (b) The sandwich structure of the Lab-on-a-CD device. The top layer is a glass wafer with sample inlets and vents. The PDMS layer comprises 4 sections of identical microstructure including a blood inlet, a supernatant reservoir, a sedimentation reservoir, an out-of-plane microvalve and two air vents. Another smooth glass wafer is used as a support layer. (c) Profiles of the out-of-plane microvalve in the mold and in PDMS casting scanned by a surface profilometer. The profiles of the PDMS casting and the inverted mold are compared. (d) SEM (scanning electron microscope) image taken at the out-of-plane microvalve. A protrusion shown in the microchannel is the out-of-plane microvalve.

www.manaraa.com

3.3.3 Blood Separation Experiments

9.4 µl of human whole blood was loaded into the upstream reservoir through each inlet port (Figure 3.9(a)). Then the Lab-on-a-CD device was rotated at a set of predetermined speeds which are above the burst frequency calculated using Equation 3.9 to exert different centrifugal forces on the whole blood sample at room temperature.

To investigate the efficiency of blood separation, two sets of experiments were conducted. The first set of experiments varied the rotational speed over a predetermined range (1500 rpm ~ 3000 rpm) while the rotational time was held constant. The second set of tests adjusted the rotational time over a desired range (100 seconds ~ 400 seconds) at a constant rotational speed. The percentage of plasma yield for each experiment was recorded and plotted in Figures 3.10-3.12. When the separation process finished, the motor was stopped and the quality of the extracted plasma was examined under an optical microscope. A control experiment using similar centrifugal platform without microvalves was carried out to prove the necessity to the microvalves.

www.manaraa.com

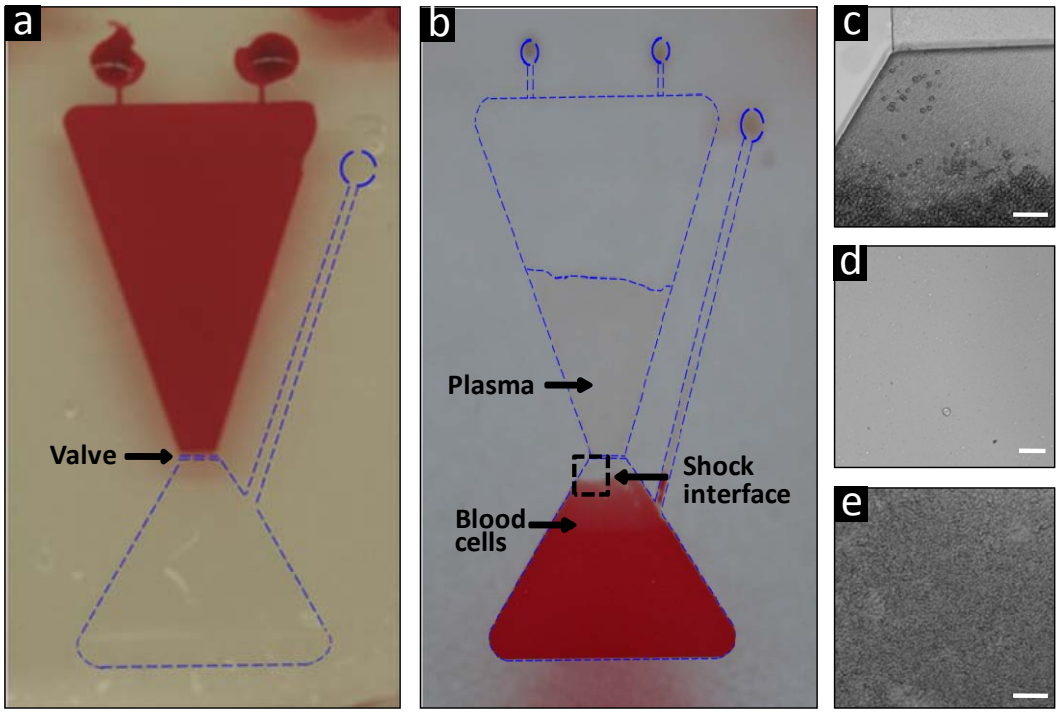

Figure 3.9: Blood separation. (a) 9.4 µl of the whole blood was loaded into the device. (b) After separation, clear plasma was retained in front of the microvalve in the supernatant reservoir, and the blood cells were centrifuged to the sedimentation reservoir. A clear interface settled down in the sedimentation reservoir. (c) The inset taken at the square area near the microvalve indicates how the blood cells accumulate at one side. The diffusion of blood cells was restrained by the out-of-plane microvalve. The scale bar is 50 µm. (d) Optical microscope image of a spot in supernatant reservoir showed only few blood cells there. The plasma purity can reach up to 99.9%. The scale bar is 20 µm (e) Optical microscope image of a spot in sedimentation reservoir. Blood cells are tightly stacked together. The scale bar is 50 µm.

3.4 Results and Discussion

The Lab-on-a-CD device was first characterized for its fabrication quality, and then was evaluated according to performances of blood separation, which are plasma purity and

www.manaraa.com

plasma yield. Finally, the blood separation results of the centrifugal devices with and without the microvalve were compared.

3.4.1 Device Characterization

The quality of the out-of-plane microvalves was evaluated through measuring the cross-sectional profiles of the microvalves with a surface profilometer (Dektak). The profile data were the average value of five measurements over the out-of-plane microvalve area (Figure 3.8(c)) in the mold, and in PDMS casting, respectively. The surfaces of the microstructure including the out-of-plane microvalve were smooth for both the mold and the PDMS casting layer. The real dimensions of the device matched with the anticipated/designed data (height ~45 μm, radial width ~250 μm) very well. The results also indicated that the structure of the mold coincided with the PDMS casting layer. Compared the reversed microvalve profile in the SU-8 mold with the microvalve profile in PDMS casting, we found that they are overlaid in most part, while the microvalve profile in PDMS was 2 ~ 3 μm lower in the height and 3 ~ 4 μm bigger in the width due to deformation of the PDMS polymer. Another method of evaluation is to do SEM imaging. In Figure 3.8(d), the SEM image shows the out-of-plane microvalve is smoothly integrated into the microchannel, leaving a narrowed microchannel.

3.4.2 Performance of Whole Blood Separation

When the Lab-on-a-CD device rotated above the burst frequency estimated using Equation 3.9, we observed the whole blood flow started to flow over the out-of-plane microvalve. However the rotational frequency for the sedimentation process (> 1500 rpm) was beyond the burst frequency of the microvalve, which was less than 1500 rpm in calculation and about 1100 rpm observed in our experiments. During the sedimentation process, due to the density difference between blood cells and plasma, they moved in two opposite directions: the blood cells were prone to flow radially outward beyond the microvalve to the sedimentation reservoir, while the plasma was pushed back into the

www.manaraa.com

supernatant reservoir. An interface, representing the abrupt discontinuity of blood cells concentration, formed, and moved outward gradually. In our experiment, the motor was controlled to stop when the interface moved across the microvalve and located in the sedimentation reservoir. Further sedimentation process could not increase the plasma yield in the supernatant reservoir because the extra separate plasma could only be retained in the sedimentation reservoir. Figure 3.9(b) shows a clear plasma-cell interface settling down in the sedimentation reservoir. The blood cells stacked densely in the sedimentation reservoir, while purified plasma was on the other side of the microvalve (the supernatant reservoir). The inset taken at the interface (square with dashed line in Figure 3.9(b)) indicates how the blood cells accumulate at one side of the out-of-plane microvalve (Figure 3.9(c)).

The blood separation performance of the devices was evaluated in terms of plasma purity and plasma yield. The plasma purity (σ_P) is defined as

$$\sigma_P = (C_{FC} - C_{PC}) / C_{FC} \tag{3.10}$$

where CFC is the cell concentration of the whole blood and CPC is the cell concentration in the supernatant reservoir. A plasma purity of 100% implies that no cells exist in the supernatant reservoir. The cell concentration can be approximately measured using Count/Size function automatically by the Image Pro software of the Olympus microscope indirectly. Thus the plasma purity is calculated based on the data acquired from the image taken under the microscope. In this experiment, only few blood cells existed in the supernatant reservoir (Figure 3.9(d)), and most of the blood cells stacked in the sedimentation reservoir (Figure 3.9(e)). In addition, no clogging or hemolysis of cells was observed under microscope. The obtained plasma purity was as high as 99.9% with the out-of-plane microvalves restraining the cells diffusion.

www.manaraa.com

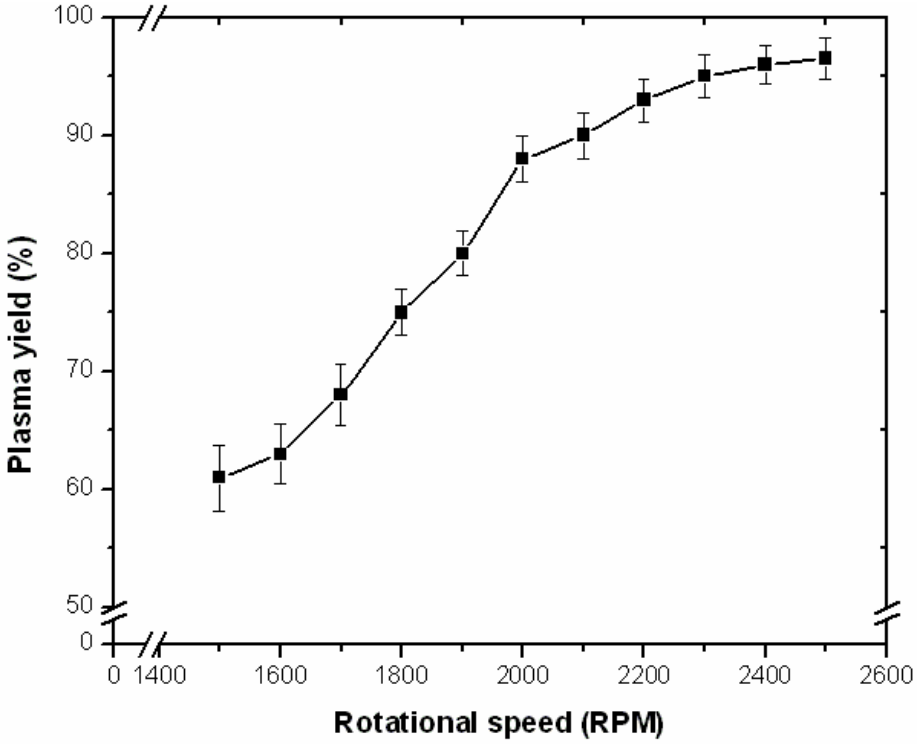

Figure 3.10: Plasma yield vs. rotation speed. The curve indicates the correlation between plasma yield and rotation speed. The centrifugal force is proportional to the square of the rotation speed. The higher the speed, the faster the plasma-blood cells interface moves outward for a certain time period (200 seconds). Therefore the plasma yield goes up as the rotation speed increases.

Plasma yield (η_P), the percentage of the separate pure plasma volume out of the total plasma volume, is another important indicator of blood separation. It is defined as

$$\eta_P = V_P / V_W (1 - H_{ct}) \tag{3.11}$$

where V_P is the volume occupied by the pure plasma in supernatant reservoir, V_W and H_{ct} are the volume and the known hematocrit (H_{ct}, volume fraction of blood cells) of the loaded whole blood, respectively. In order to reduce the sample consumption, as much plasma as possible, in other words, a high plasma yield, should be achieved.

www.manaraa.com

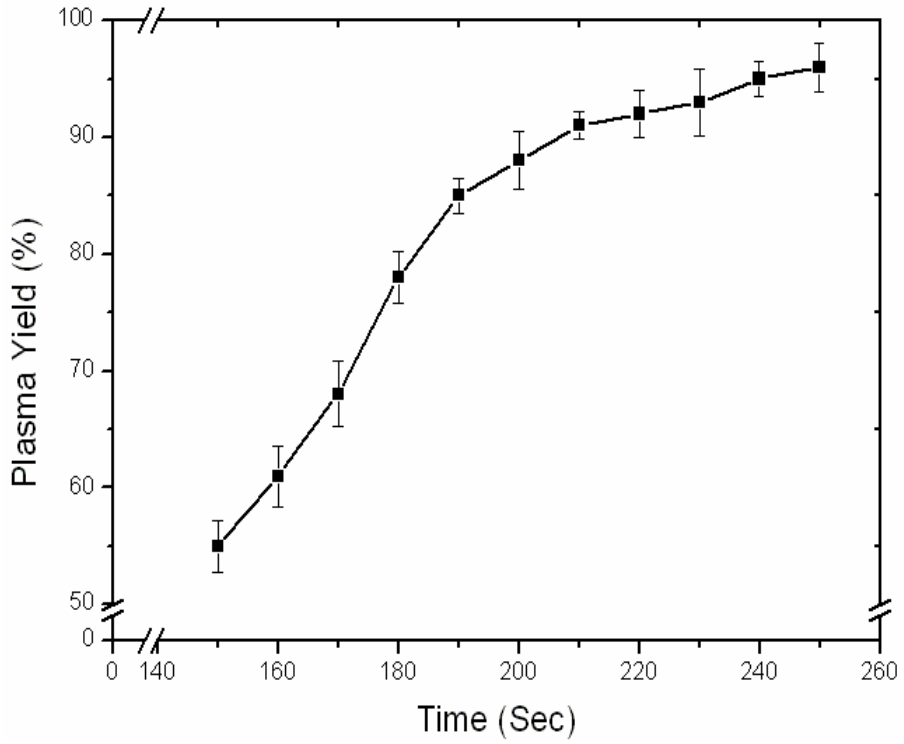

Figure 3.11: Plasma yield vs. rotation time. The curve shows the plasma yield under 2000 rpm, with different rotation time. The longer the centrifugal force was exerted on the blood sample, the further outward the plasma-blood cells interface moved. Therefore the plasma yield rises as the rotation time increases.

The plasma yield is not only dependent on the efficiency of blood separation, but also related to capability of a device for plasma collection. The higher efficiency of blood cell sedimentation, the more plasma is squeezed out from the whole blood.

Only taking the efficiency of sedimentation into account, plasma yield is proportional to the rotational time and the rotational speed of the CD platform. Figure 3.8 shows the plasma yield of whole blood sample (48% H_{ct}) after rotation of 200 seconds, reaching 88% at 2000 rpm and achieving better result (around 96%) at 2500 rpm. It suggests that blood separation proceeded faster when the rotational speed was higher. However, the

www.manaraa.com

speed of sedimentation decreased gradually in the post-separation process, because the viscosity in the sedimentation reservoir increases as the concentration of blood cells increases. On the other hand, when the angular velocity was held constant at 2000 rpm, the plasma yield was proportional to the rotational time (Figure 3.11).

According to Equation 3.11, the plasma yield is proportional to the volume of plasma contained in the supernatant reservoir. For the current device, the ability of plasma collection is also related to the location of out-of-plane microvalves. To achieve the highest plasma purity and plasma yield, the plasma-blood cells interface should be located in the sedimentation reservoir and close to the microvalve. As the hematocrit of the whole blood is normally less than 48%, the volume of sedimentation reservoir over total loaded sample should be slightly larger than 48% (~50% in this work). Therefore, there is enough space to store the blood cells in the sedimentation reservoir when the separation process is thoroughly completed. In our experiments, the measured plasma yield of current design of the device was 96 ± 0.5% for the whole blood samples of 48% hematocrit.

www.manaraa.com

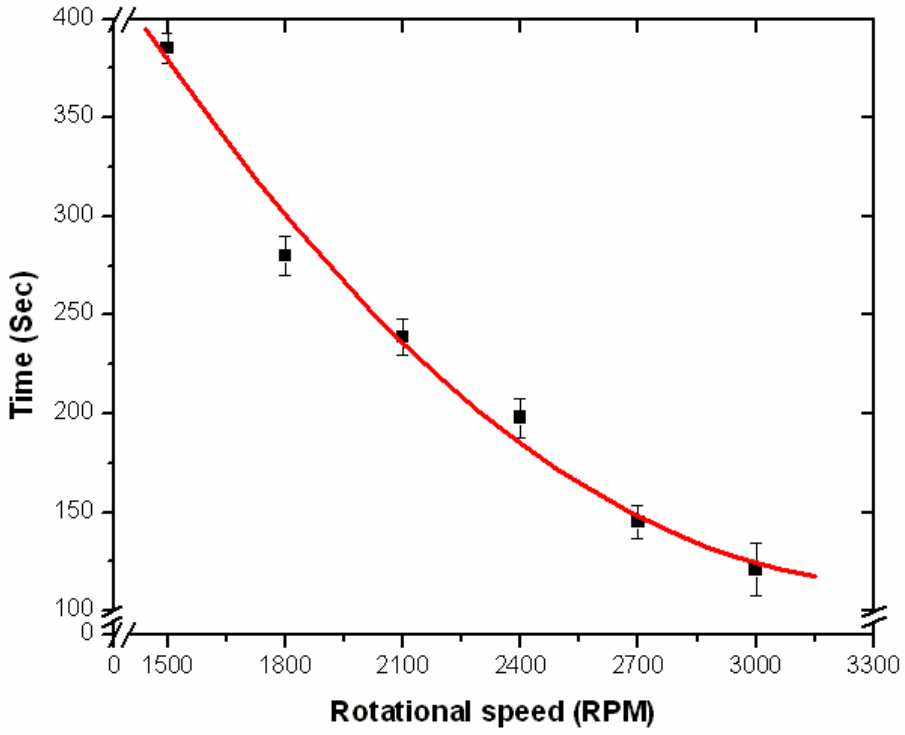

Figure 3.12: Rotational speed vs. rotational time for a predetermined plasma yield. For a given rotational speed, each data point of time was collected when the plasma-blood cells interface moved just across the microvalve. The images of the interface, which help us to observe the movement of the plasma-blood cells interface, were captured with the interval of 1 second without stopping the CD platform.

We also studied the relationship between rotational speed and rotation time (V - T) for the same plasma yield (96%) (Figure 3.12). Controlling the rotational speed at a predetermined value (x-axis), the time (y-axis) at which the plasma-blood cells interface moved just across the microvalve was recorded. The data obtained can be well fitted by a hyperbolic curve. Therefore, when the speed was too slow, the time required for blood separation dramatically increased. On the contrary, the blood cells could be easily separated if the speed was high. However, the rotational speed could not be ultimately high, since the cells might be broken and lysed. We found that a rotational speed of 2000 rpm could achieve the best performance in terms of separation time and cell quality.

www.manaraa.com

The major contribution of the out-of-plane microvalve to Lab-on-a-CD devices for blood analysis is to prevent the separated blood cells flowing/diffusing back and to maintain the purity of the separated plasma. To demonstrate this core function of out-of-plane microvalve, we made another Lab-on-a-CD device with the same design but without the out-of-plane microvalve. Results of blood separation for both centrifugal platforms were compared. The device without the out-of-plane microvalves was rotated on the motor at 2000 rpm for 250 seconds. The separated blood cells spread from the sedimentation reservoir to the supernatant reservoir fairly fast right after the platform stopped. This cell-flowing-back phenomenon was obvious and could be observed clearly by naked eyes. Figure 3.13 shows the blood cell aggregates flowed in the opposite direction of the sedimentation direction. They intruded the area where there was supposed to be an out-of-plane microvalve, and took over the supernatant reservoir mixing with the purified plasma. Actually, the blocking effect of the out-of-plane microvalve can be also found in Figure 3.9(c). When the platform was still, some of the blood cells flowed towards the microvalve. However, they were stopped by the microvalve, which ensures the purity of plasma for subsequent operation and analysis.

www.manaraa.com

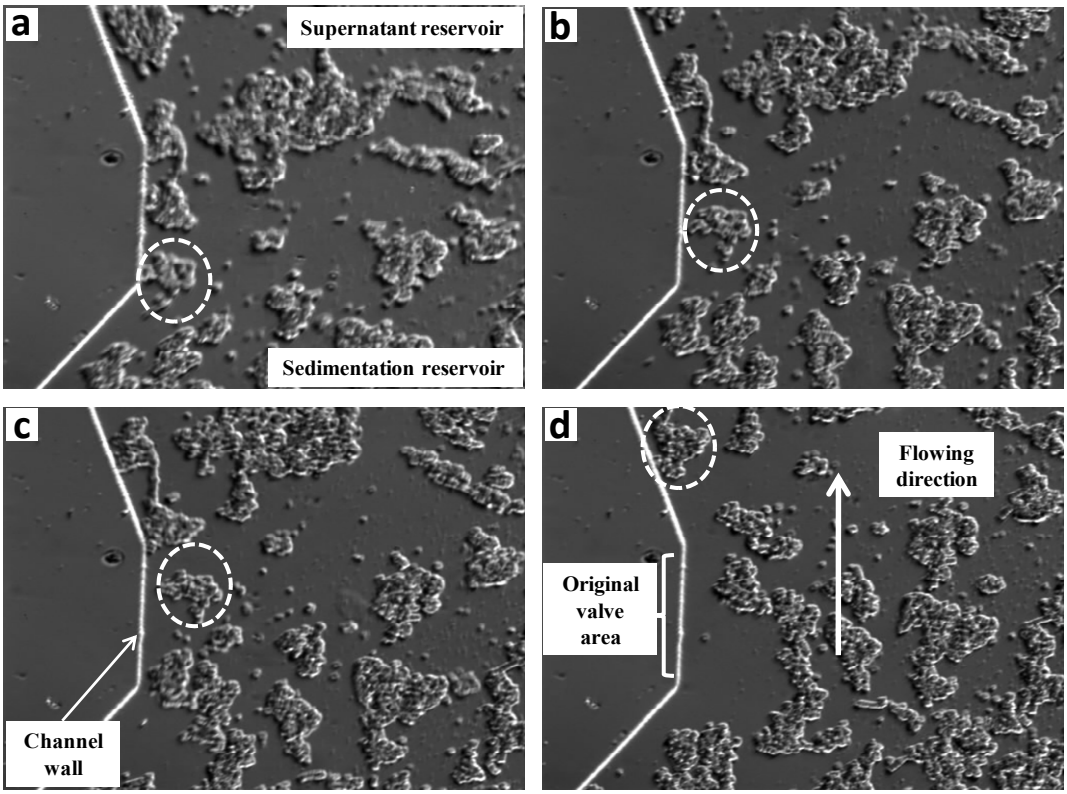

Figure 3.13: Blood cells reflowed back to the supernatant reservoir right after the Lab-on-a-CD device without the out-of-plane microvalve stopped. Blood cell aggregates flushed from the sedimentation reservoir, crossed the original valve area, and back to the supernatant reservoir. a) at 10 seconds after the device stopped. b) at 15 seconds after the device stopped. c) at 20 seconds after the device stopped. d) at 25 seconds after the device stopped. The circle tracks movement of the same cell aggregate.

www.manaraa.com

3.4.3 Discussion

This Lab-on-a-CD design involves 3D structural microfabrication, but removes any need to modify surface properties of microstructure or fill with exotic materials that required by existing microvalving designs. 3D microfabrication is easy, low-cost and industrially applicable. For mass production, hot-embossing or micro-injection molding can be used. For prototype demonstration and laboratory test, the microfabrication method we used in the present work is multi-step photolithography. In this method, 3D structure cast from the multi-layer photoresists has higher alignment accuracy compared with conventional multilayered PDMS structures that require well alignment of multiple PDMS layers. The characterization results of the SU8 master and the fabricated PDMS layer suggest that the present microfabrication method is suitable for the fabrication of Lab-on-a-CD device with out-of-plane microvalves, and is highly reliable and replicable.

Complete blood separation not only means redistribution of blood components using different physical field, but also requires isolation of different components to prevent remixing. Therefore the spatial isolation of different blood components in Lab-on-a-CD devices not only improves blood separation performance, but also help implement the downstream blood analysis.

Two mechanisms can cause separated blood cells to flow back. One is diffusion due to the concentration difference of blood cells between the sedimentation reservoir and the supernatant reservoir. The other is the release of the accumulated elastic energy of compressed blood cells. In the sedimentation process, blood cells aggregated and were largely deformed under centrifugal force. Once the force vanished, the stored elastic energy of the deformed and concentrated blood cells can push themselves back to the supernatant reservoir. Therefore, the blood cells in the sedimentation reservoir were prone to flow backward into purified plasma when the devices have no obstructions like the out-of-plane micorvalves to stop them.

www.manaraa.com

The microvalve not only prevents the diffusion of blood cells from the sedimentation reservoir back to the supernatant reservoir, but also breaks the liquid connection between two reservoirs when the device stops. When it stopped after blood separation, the existence of out-of-plane microvalves interrupted the connection of liquid in the narrowed microchannel on top of the out-of-plane microvalve. As a result, the plasma in the sedimentation reservoir was completely isolated from the blood cells in the sedimentation reservoir.

This out-of-plane microvalve design can be easily integrated into any other centrifugal platforms, and again lead many potential applications. For example, this out-of-plane microvalve can be used together with the siphon microvalve [12] to facilitate plasma extraction.

In summary, the present design of Lab-on-a-CD devices with the out-of-plane microvalve provides a simple, fast and inexpensive approach for high-performance, on-chip blood separation for whole blood. Figure 3.8(a) shows the whole set up of the system. A 12V DC motor controlled by a laptop is enough to provide the required function of the rotational speed over time. Besides its easy fabrication method and simple control mechanism, the whole system is also portable, and allows parallel and multiple blood sample treatment in one Lab-on-a-CD platform.

www.manaraa.com

3.5 Conclusions

This study has demonstrated a simple but highly effective design of Lab-on-a-CD device integrated with out-of-plane microvalves for high performance whole blood separation. 99.9% of plasma purity and 96 ± 0.5% of plasma yield have been achieved for the whole blood with 48% hematocrit. This design significantly improves the plasma yield, the efficiency of blood separation of the whole blood, and the readiness of plasma usage for subsequent blood testing. The 3D microfabrication of the out-of-plane microvalve(s) and its integration into Lab-on-a-CD devices are simple, low-cost, and easy-to-be-implemented in both research laboratories and industry. The present design can also provide a simple and possible solution for developing Lab-on-a-CD products using optical analysis or electrochemical analysis after blood separation.

www.manaraa.com

3.6 References

1. Toner, M. and Irimia, D., Blood-on-a-chip. Annual Review of Biomedical Engineering, 2005. **7**: p. 77-103.

2. Whitesides, G., The origins and the future of microfluidics. Nature, London, 2006. **442**(7101): p. 368.

3. Crowley, T. and Pizziconi, V., Isolation of plasma from whole blood using planar microfilters for lab-on-a-chip applications. Lab on a Chip, 2005. **5**(9): p. 922-929.

4. Yeo, L., Friend, J. and Arifin, D., Electric tempest in a teacup: The tea leaf analogy to microfluidic blood plasma separation. Applied Physics Letters, 2006. **89**: p. 103516

5. Yang, S., Undar, A. and Zahn, J.D., A microfluidic device for continuous, real time blood plasma separation. Lab on a Chip, 2006. **6**(7): p. 871-880.

6. Blattert, C., Jurischka, R., Tahhan, I., Schoth, A., Kerth, P. and Menz, W., Separation of blood in microchannel bends. Conf Proc IEEE Eng Med Biol Soc, 2004. **4**: p. 2627-30.

7. Shinohara, H., Takahashib, Y., Mizunoa, J. and Shojia, S., Surface hydrophilic treatment of polyurea film realized by vacuum ultraviolet light irradiation and its application for poly (methylmethacrylate) blood analysis chip. Sensors and actuators B: Chemical, 2008. **132**(2): p. 374-379.

8. Haeberle, S., Brenner, T., Zengerle, R. and Ducrée, J., Centrifugal extraction of plasma from whole blood on a rotating disk. Lab on a Chip, 2006. **6**(6): p. 776-781.

9. Zhang, J., Guo, Q., Liu, M. and Yang, J., A lab-on-CD prototype for high-speed blood separation. Journal of Micromechanics and Microengineering, 2008. **18**: p. 125025.

www.manaraa.com

10. Cho, Y., Lee, J., Park, J., Lee, B., Lee, Y. and Ko, C., One-step pathogen specific DNA extraction from whole blood on a centrifugal microfluidic device. Lab on a Chip, 2007. **7**(5): p. 565-573.

11. Madou, M., Steigert, J., Brenner, T., Grumann, M., Riegger, L., Lutz, S., Zengerle, R. and Ducrée, J., Design and fabrication of CD-like microfluidic platforms for diagnostics: microfluidic functions. Biomedical Microdevices, 2001. **3**(3): p. 245-254.

12. Steigert, J., et al., Integrated siphon-based metering and sedimentation of whole blood on a hydrophilic lab-on-a-disk. Biomedical Microdevices, 2007. **9**(5): p. 675-679.

13. Mark, D., Metz, T., Haeberle, S., Lutz, S., Ducrée, J., Zengerle, R. and Stetten, F., Centrifugo-pneumatic valve for metering of highly wetting liquids on centrifugal microfluidic platforms. Lab on a Chip, 2009. **9**(24): p. 3599-3603.

14. Driks, J., Diagnostic blood analysis using point-of-care technology. AACN Advanced Critical Care, 1996. **7**(2): p. 249.

15. Wong, A., Gupta, M., Shevkoplyas, S. and Whitesides, G. M., Egg beater as centrifuge: isolating human blood plasma from whole blood in resource-poor settings. Lab on a Chip, 2008. **8**(12): p. 2032-2037.

16. Madou, M., Zoval, J., Jia, G., Kido, H., Kim, J. and Kim, N., Lab on a CD. Annual Review of Biomedical Engineering, 2006. **8**: p. 601-628.

17. Harkins, H. and Harkins, W., The surface tension of blood serum, and the determination of the surface tension of biological fluids. J. Clin. Invest, 1929. **7**(2): p. 263-281.

18. Hinghofer-Szalkay, H. and Greenleaf, J., Continuous monitoring of blood volume changes in humans. Journal of applied physiology, 1987. **63**(3): p. 1003.

www.manaraa.com

19. Madou, M., Fundamentals of microfabrication. 1997. CRC Press LLC. Capítulo. **1**: p. 1-50.

20. Xia, Y. and Whitesides, G., Soft lithography. Annual Review of Materials Science, 1998. **28**(1): p. 153-184.

www.manaraa.com

Chapter 4

4 Design and Optimization of Prussian Blue/Carbon Nanotube Electrodes for Biosensing Applications

In the last Chapter, a blood plasma separation process was successfully conducted on the Lab-on-a-CD platform. Thereafter, the concentrations of blood contents in the separated plasma can be detected with the electrochemical biosensors embedded in the plasma reservoir. Electrochemical detection for point-of-care diagnostics is of great interest due to its high sensitivity, fast analysis time and ability to operate on a micro/nano scale. This work focuses on design and optimization of prussian blue (PB) and multi-wall carbon nanotubes (MWCNT) based electrodes for electrochemical biosensing applications. The factors that might affect the performance of the biosensor were evaluated. It was found that the immobilization methods and the amount of GOx mainly influenced the sensitivity of the glucose biosensor, while the amount of Nafion affected both the sensitivity and the linear range of the glucose biosensor.

4.1 Introduction

Diabetes mellitus is the most common endocrine disorder of carbohydrate metabolism that normally cannot be cured. It is a leading cause of morbidity and mortality, and its prevalence is increasing. Blood glucose concentration is the major diagnostic criterion for diabetes as well as a useful parameter for patient monitoring. Self-monitoring of blood glucose has been established as a valuable tool for the management of diabetes. Regular and frequent measurements of blood glucose have been found to provide data that optimizes or changes patient treatment strategies, resulting in the development of a series of glucose-measuring devices. Biosensing technology plays a key role in providing a powerful analytical tool for glucose measurement [1]. This is a reason that many papers focused on the enzyme-based glucose biosensors since Clark and Lyons reported their enzyme electrode for measuring glucose in 1962 [2].

www.manaraa.com

The majority of the current glucose biosensors are of the electrochemical type due to their excellent sensitivity, easy maintenance and low cost [3]. Electrochemical biosensors can be subdivided into potentiometric, amperometric and conductometric types [4-5]. Enzymatic amperometric glucose biosensors are the most common devices that are commercially available and have been widely studied over the past few decades. Although different kinds of enzymatic amperometric glucose biosensors are available, the basic concept of the glucose biosensor has changed little in principle. Initially, the immobilized glucose oxidase (GOx) catalyzes the oxidation of β-D-glucose by oxygen, producing gluconolactone and hydrogen peroxide [6]. This can be represented as follows：

$$\text{Glucose} + O_2 \xrightarrow{\text{GOD}} \text{Gluconolactone} + H_2O_2 \qquad (4.1)$$

The concentration of glucose can be obtained by electrochemically detecting the enzymatically liberated H_2O_2. However, the applied potential necessary for the oxidation or reduction of H_2O_2 at solid electrodes is extremely high and increases the disturbance from chemical interferences. Therefore, a modified electrode [7] or a transducer such as peroxidase [8-11] and hexacyanoferrate [12-13] are usually used for the reduction of H_2O_2 at low applied potentials. PB, whose composition is expressed as $Fe_4[Fe(CN)_6]_3$, is considered as an “artificial peroxidase” due to its high activity and selectivity toward the reduction of H_2O_2. Its high chemical stability, facile preparation and rich electrochemical properties make it effective in the application of biosensor [14-18]. However, PB is not stable on the surface of bare electrodes in neutral solutions. Therefore, it is necessary to electrodeposite a PB layer on modified electrodes [19] or co-electrodeposit with a modifier [20] to improve its operational stability and increase its use in biosensor fabrication.

Since discovered by Iijima [21], multi-wall carbon nanotubes (MWCNT) have been widely used in the electrochemical field owing to their high chemical stability, large surface area, unique electronic properties, and relatively high mechanical strength. Even

www.manaraa.com

more importantly, PB deposited on the MWCNT modified electrode was found to be stable in neutral solutions. However, MWCNT possesses poor dispersibility in liquid, especially in water, which greatly hinders the corresponding applications. Poly(diallydimethylammonium) (PDDA), a water-soluble quaternary ammonium polyelectrolyte, was reported to improve the dispersibility of CNTs in water [22-24]. Hence, PB was electrodeposited on a Au electrode that was modified with PDDA wrapped MWCNT.

Immobilization of enzymes is a key step in the fabrication of glucose biosensors. Methods based on covalent or cross-linking bonding [25-26], adsorption [27-28], and sol-gel techniques [29-30] have been reported. Glutaraldehyde is commonly employed as an amine-reactive homobifunctional crosslinker, although it may cause the loss of enzyme activity to some extent [31]. Chitosan [32-33] and nanoparticles [7, 34] were explored to aid the immobilization of GOx in order to improve the performance of the glucose biosensors.

In this work, MWCNT wrapped by PDDA were spread onto the surface of a Au electrode. PB, as an electron mediator, was then electrochemically deposited on the MWCNT modified electrode. GOx was immobilized on the PB/MWCNT/Au electrode and a layer of Nafion was used to prevent GOx from leaking off and operated as a glucose diffusion-limited membrane. Based on this configuration, all the possible factors (pH values, detection potentials, GOx immobilization methods, GOx amount and Nafion concentration) that may affect the performance of the glucose biosensors were investigated, and a method of manipulating their linear range and sensitivity was developed.

www.manaraa.com

4.2 Material and methods

4.2.1 Reagents

The reagents were of analytical grade or the highest commercially available purity. All chemicals were employed without further purification. All solutions were prepared with deionized (DI) water with a resistivity that is higher than 18 MΩ cm (Milli-Q, USA). D-(+)-Glucose, GOx (Type X-S, 250 units/mg), human serum with glucose concentration of 5.4 (S2257-1ml), bovine serum albumin (BSA), iron (III) chloride, and potassium ferricyanide (III) were purchased from Sigma. Different concentrations of glucose solution were prepared in DI water and stored at 4 °C (mutarotation was allowed for at least 24 h before use). 20 mM phosphate buffer solutions (PBS) containing 0.1 M KCl were freshly prepared everyweek. GOx was dissolved in PBS (pH 6.8) to a desired concentration. Nafion (20 wt % in lower aliphatic alcohols) and PDDA (20 wt % in water) were purchased from Aldrich. The MWCNT with 95% purity (purchased from US Research Nanomaterials, Inc) are cylindrical with a diameter in the range 5 – 15 nm.

4.2.2 Apparatus

All electrochemical experiments in this work were performed on a computer-controlled CHI1200a (CHI Instruments, Inc., USA). A gold working electrode (2 mm diameter), a platinum wire counter electrode, a Ag/AgCl reference electrode with saturated KCl and a conventional three-electrode electrochemical cell were all purchased from CHI instruments, Inc., USA.

www.manaraa.com

4.2.3 Configuration of the biosensor

4.2.3.1 Preparation of a MWCNT-PDDA modified Au electrode

The Au electrode was sequentially polished with 1.0 and 0.3 μm alumina slurry on microcloth pads. After removing the trace alumina from the surface by rinsing with DI water, the electrode was ultrasonically cleaned for 10 min in a fresh Piranha solution (H_2SO_4: H_2O_2 = 3:1(v/v)). The electrode was then ultrasonicated in DI water, ethanol, and DI water again for 5 min each. Before depositing MWCNT, the electrodes were electrochemically cleaned and activated in 0.5 M sulfuric acid by cycling between 0.4 V and 1.6 V at a sweep rate of 40 mV s^{-1} until a stable voltammogram was obtained (Figure 4.1) [35]. MWCNT were hydrophilically functionalized by adding H_2SO_4 (98%) and HNO_3 (60%), which are in the volume ratio of 3:1 [36-38]. This treatment lasted for 8 hours, after which the acid solution from the supernatant was removed. In order to neutralize the MWCNT solution, NaOH was added into the solution until its pH value reached 7. The salts left with MWCNT were extracted by DI water in a procedure which involved repeating the steps of adding DI water, centrifugation and removing supernatant. MWCNT-PDDA composite was prepared in a 4 mL vial by adding 1 mL of PDDA (8%) and 1 mg MWCNT, and ultrasonicated for about 1.5 hours. The PDDA residual was removed using a high-speed centrifugation technique and the composite was washed with DI water several times until the black stable solution was obtained [34, 39-40]. The modified electrode was prepared by spreading 5 μL of the MWCNT-PDDA solution over the Au electrode surface and evaporating the solvent at room temperature.

www.manaraa.com

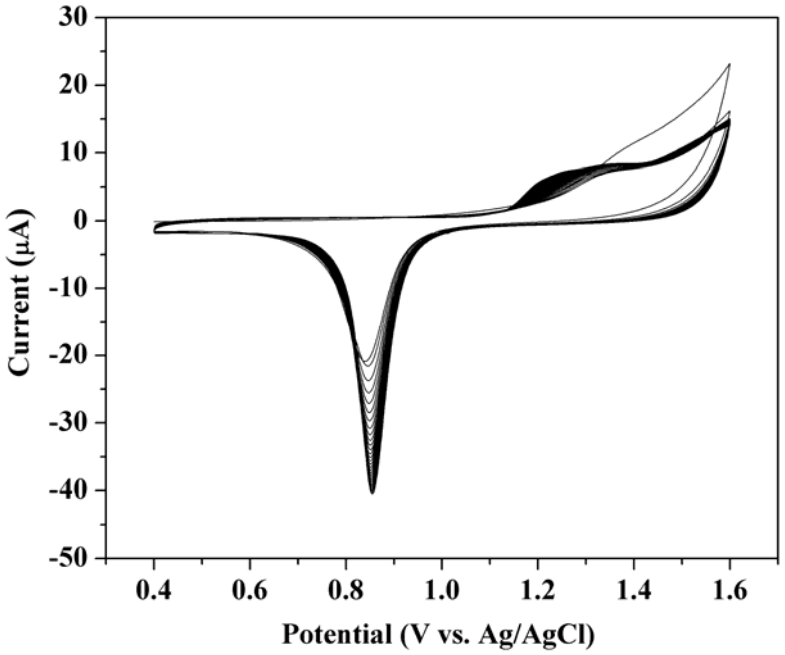

Figure 4.1: Electrochemical cleaning and activation of electrodes in 0.5 M sulfuric acid by cycling between 0.4 V and 1.6 V at a sweep rate of 40 mV s^{-1}.

4.2.3.2 Electropolymerization of PB film

Cyclic voltammetry (CV) was employed to deposit PB film on the surface of the MWCNT modified Au electrode. The electropolymerization of PB was achieved by immersing the electrode in an unstirred fresh solution containing 5 mM $K_3[Fe(CN)_6]$, 5 mM $FeCl_3$, 0.01 M HCl and 0.1 M KCl, followed by a 20 cycle scan in a potential range of -0.1 to 0.4 V at 20 mV/s (Figure 4.2) [41-45]. After it was thoroughly washed with DI water, the electrode was transferred into a supporting electrolyte solution (0.1 M KCl containing 0.01 M HCl) and electrochemically activated by cycling between -0.1 and 0.4 V at 50 mV/s until the stable CV curves emerged (Figure 4.3) [46-48]. The PB/MWCNT/Au electrode was cleaned again in DI water and tempered at 110 °C for 1 h.

www.manaraa.com

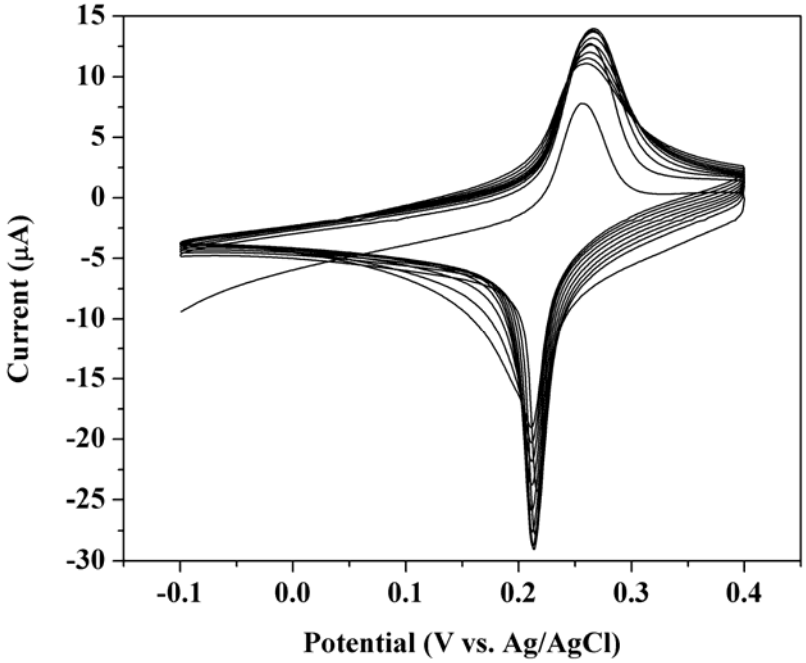

Figure 4.2: Cyclic voltammograms of Pb electropolymerization.

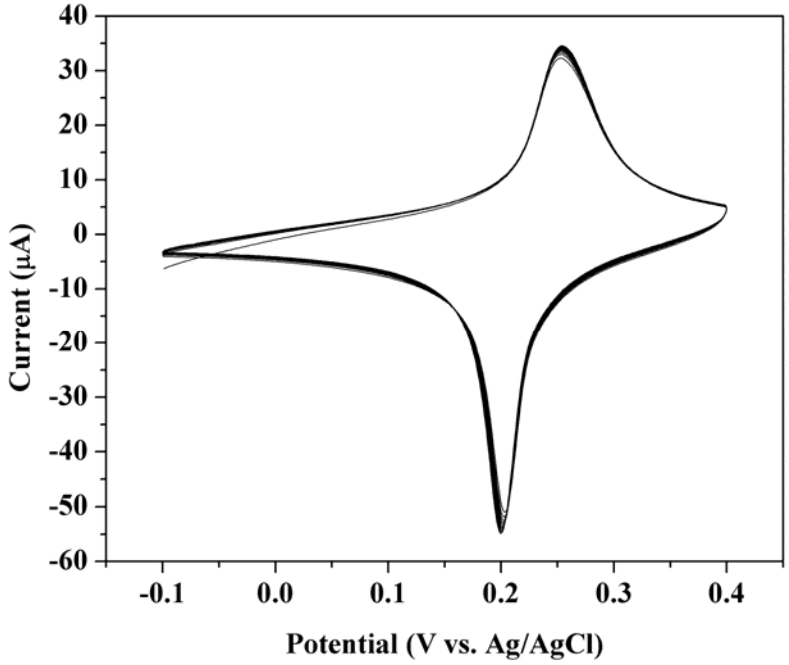

Figure 4.3: Cyclic voltammograms of Pb activation.

www.manaraa.com

4.2.3.3 Glucose biosensors constructed on PB/MWCNT/Au electrode

When the PB/MWCNT/Au electrode was ready to use, the next step was to immobilize the enzyme GOx. Different methodologies of immobilizing GOx were investigated to improve the analytical performance. In the first method, GOx was immobilized with chitosan. GOx-chitosan mixture consisted of 10 μL GOx (10 mg/mL) and 10 μL chitosan (0.5%). 5 μL mixture was dropped onto the PB/MWCNT/Au electrode. The second method involved the cross-linking of GOx-chitosan mixture by adding glutaraldehyde. The GOx-chitosan layer was dipped into 0.25% glutaraldehyde for 20 min. The third and fourth methods were conducted in a similar way as the second one, but the mixture of GOx-chitosan (0.5%, w/V) was replaced by the combination of GOx-BSA (1%, w/V) and GOx-BSA-chitosan (0.5%, w/V), respectively. These four types of glucose biosensor were completely constructed by casting 5 μL Nafion on top of the GOx layer. Finally, the biosensors were cleaned in DI water and stored overnight in a refrigerator (4 °C) and used the next day. When not in use, the biosensor was stored again in the refrigerator for lifetime tests.

4.3 Results and Discussion

4.3.1 Morphology and structures of MWCNT/Au

A homogeneous, well-dispersed suspension of PDDA-MWCNT solution was stable for several months. As shown in Figure 4.4a, the MWCNT-PDDA composite spreads evenly on the surface of a Au electrode and the film is homogeneous and porous. In contrast, the unmodified MWCNT form bundles (Figure 4.4b). The results show that PDDA aids the dispersion of MWCNT and the resulting homogeneous and porous film of PDDA-MWCNT is beneficial not only to the electrodeposition of PB but also to the immobilization of GOx.

www.manaraa.com

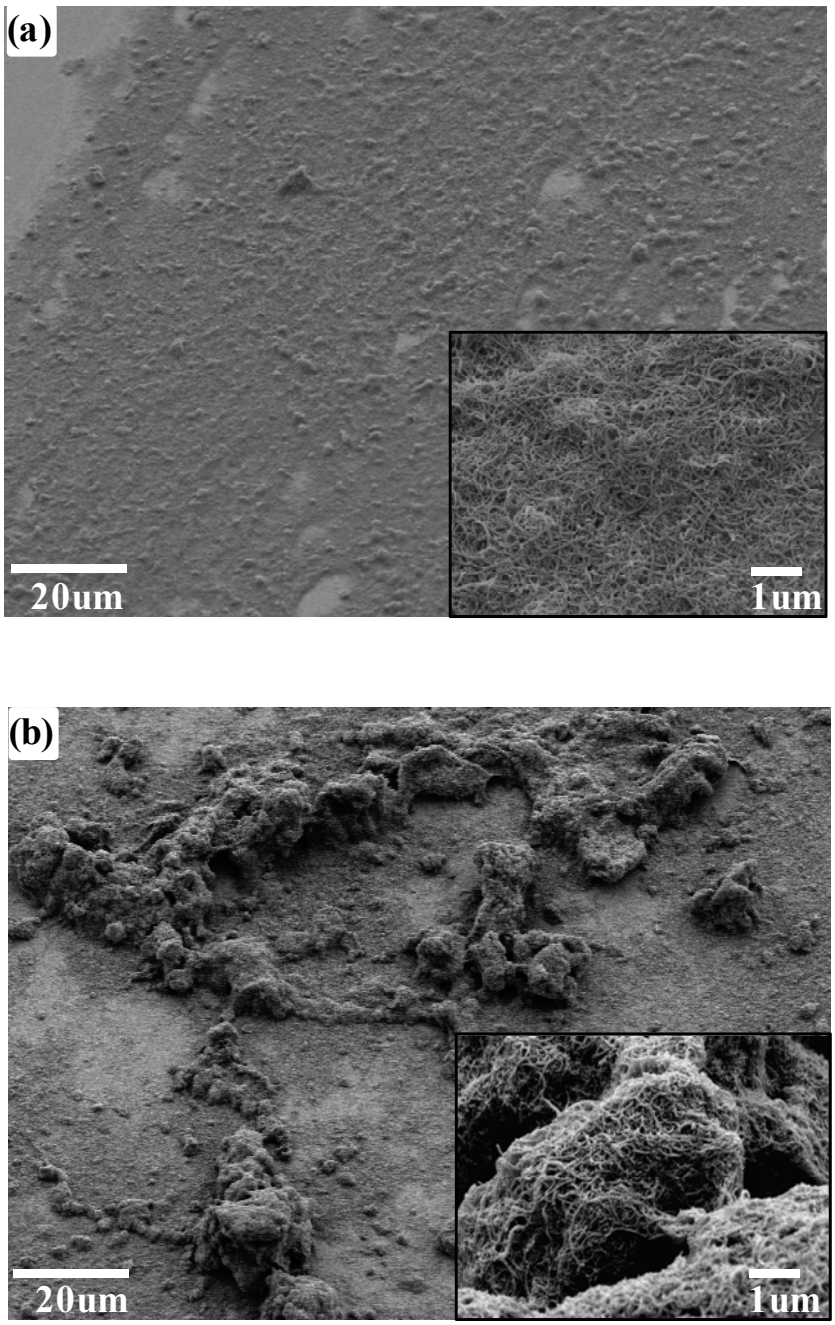

Figure 4.4: SEM images of (a) PDDA-MWCNT composite and (b) unmodified MWCNT on the surfaces of Au electrodes.

www.manaraa.com

4.3.2 Electrochemical behavior of PB/MWCNT/Au

MWCNT/Au electrode did not show any obvious redox peak, while the addition of PB produced a pair of well-defined redox peaks with potential values in the range of 0.2 ~ 0.25 V, which were ascribed to the redox of PB and PW (Prussian white) [49]. The CV curves of PB/MWCNT/Au at various scan rates were shown in Figure 4.5a. With increasing scan rate, both the redox peak currents and the peak-to-peak separation increased. The anodic and cathodic peak currents were linearly proportional to the square root of the scan rate from 30 mV/s to 300 mV/s, indicating that the redox of PB on MWCNT/Au was a diffusion-controlled process (Figure 4.5b).

The existence of MWCNT can alter the electroanalytical performance of PB. MWCNT possess larger electroactive surface area that could facilitate more PB polymerizing on the electrode. Figure 4.6a compares the voltammetric peak current of a pure PB modified electrode and a PB/MWCNT modified electrode in PBS with pH from 4.8 to 7.8. The redox currents of PB/MWCNT modified electrode are larger than the pure PB modified electrode in the whole pH range. The peak current value of the PB/MWCNT/Au electrode at pH 6.8 was 30.57 μA, about 2.5 times higher than that at the PB/Au electode (13.00 μA). Besides providing larger electroactive surface area, MWCNT alleviate pH dependency of PB layer. It is well known that PB is unstable and dissolvable at pH above 7.0 [41], and the higher the value of pH in the solution, the lower the stability of the PB. So far, only a few methods were tried to improve the stability of PB during the raising of pH [9, 21]. As shown in Figure 4.6a, MWCNT retained the electrocatalytic property of PB at higher pH value. The current of the pure PB modified electrode starts dropping at pH 6.3, while the current generated by PB/MWCNT modified electrode does not significantly decrease until pH 6.8. Even at pH 7.4 (the normal pH of human blood), the current signal generated by PB/MWCNT modified electrode is still 80% of the one generated at pH 6.8. The above data clearly show that MWCNT enhance the stability of PB modified electrodes at high pH values. Since MWCNT modified electrode increased

www.manaraa.com

both the response and the stability of PB, PB/MWCNT modified electrode was selected to fabricate glucose biosensors.

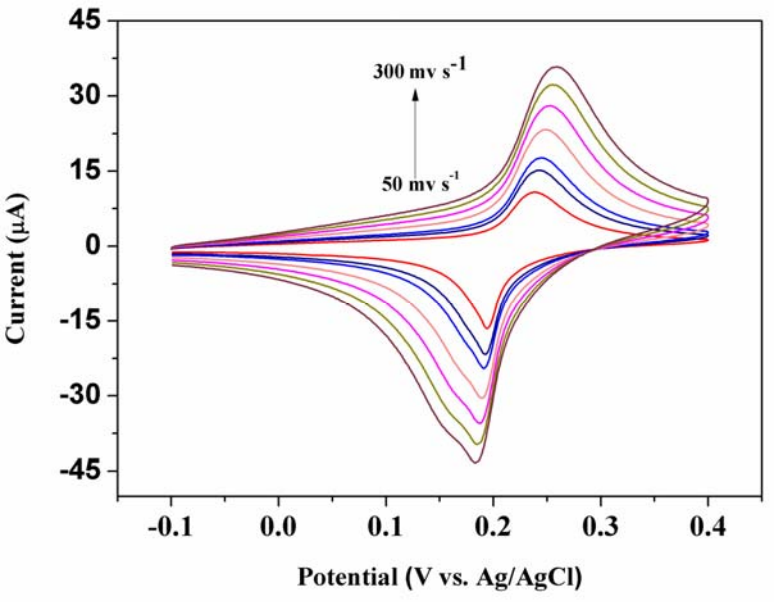

(a)

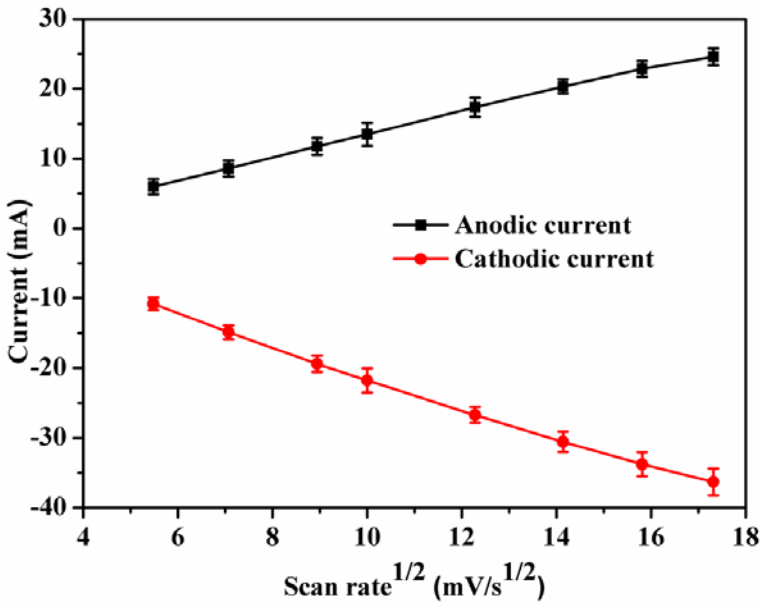

(b)

Figure 4.5: The cyclic voltammograms of PB/MWCNT/Au electrode at different scan rates: 50, 80, 100, 150, 200, 250, and 300 mV/s in PBS (pH 6.8). (b) The dependence of redox peak currents on the square root of scan rates.

www.manaraa.com

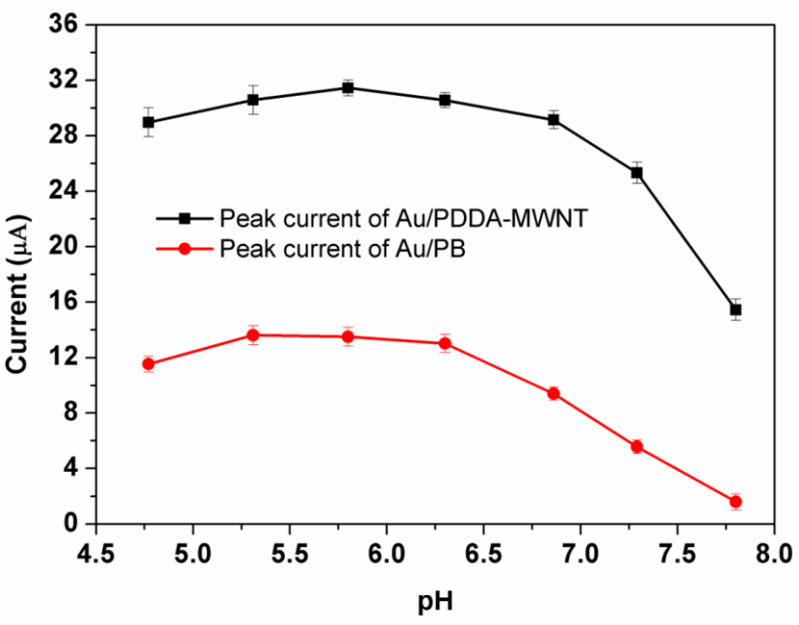

(a)

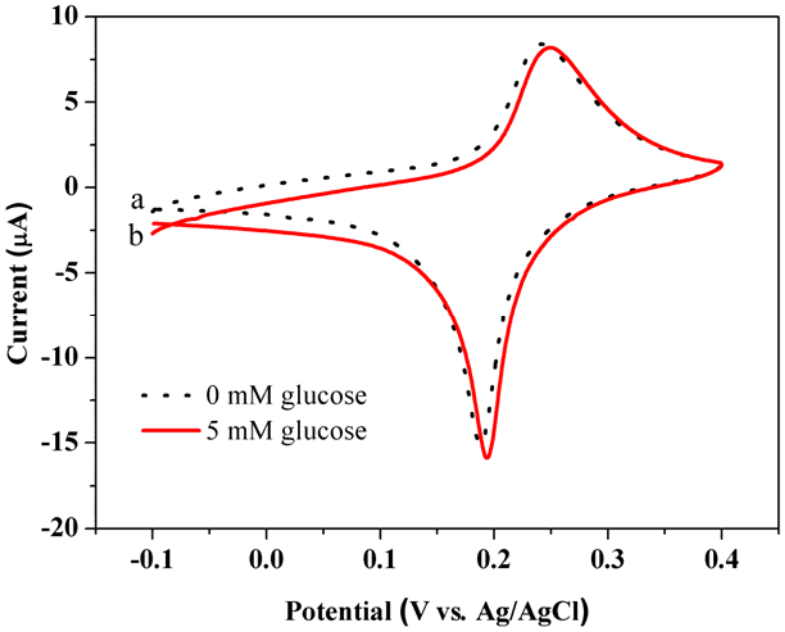

(b)

www.manaraa.com

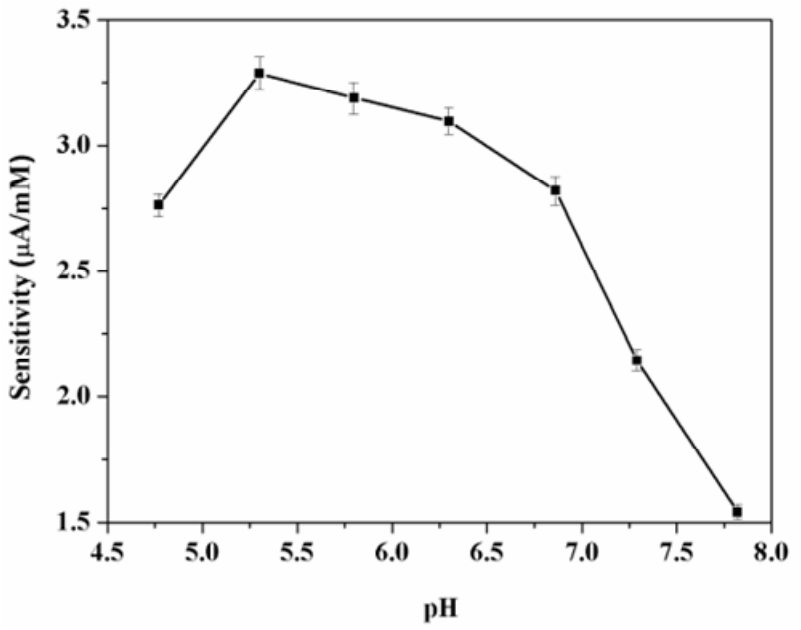

(c)

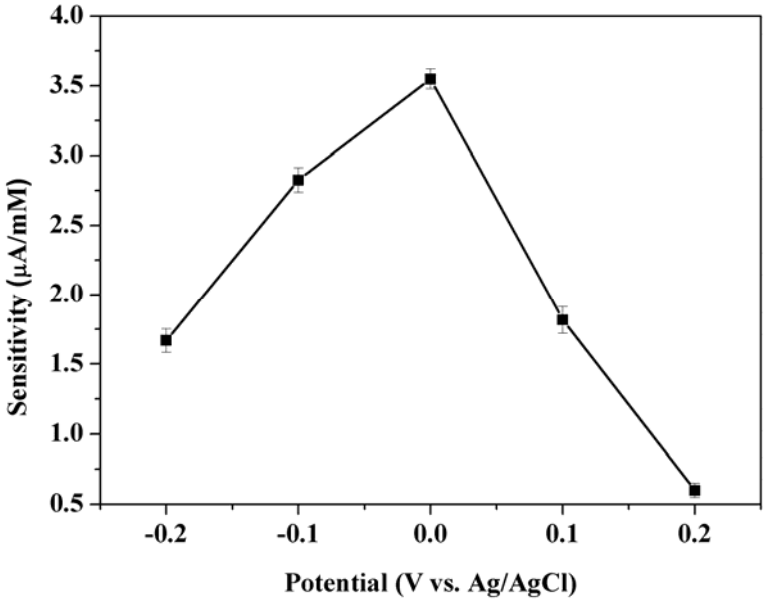

(d)

Figure 4.6: (a) The effects of pH on the oxidation peak current of PB/Au and PB/MWCNT/Au electrodes; (b) Cyclic voltammograms for the biosensor in the absent of glucose and in the presence of 5 mM glucose. Scan rate 50 mV/s; (c) The effects of pH on the sensitivity of the biosensor; (d) The effect of working potential on the sensitivity of the biosensor. Data in (b, c, d) are based on the Nafion/GOx-chitosan/PB/MWCNT/Au biosensors.

www.manaraa.com

4.3.3 Electrochemical behavior of the Nafion/GOx-chitosan/PB/MWCNT/Au biosensor

The biosensor was first characterized in the presence or absence of glucose in a PBS (pH 6.8) (Figure 4.6b). In the absence of glucose, the biosensor only produced the electrochemical response of PB itself. In the presence of 5 mM glucose, the reduction current increased while the oxidation current dropped down, showing an electrocatalytic behavior of PB in response to the reduction of H_2O_2 produced by the enzyme reaction.

The pH effect on the biosensor is twofold: the pH effect on the electrocatalytic property of the PB layer and the pH effect on the bioactivity of GOx. Figure 4.6c illustrates the combined relationship between the sensitivity of the biosensor (Nafion/GOx-chitosan/PB/MWCNT/Au) and the pH values of the glucose solutions. The sensitivity value represents the slope of the calibration curve that was obtained from the typical amperometric response of the biosensor to successive addition of glucose into the stirring PBS at 0 V applied potential. The results showed that the sensitivity increased from pH 4.7 to 5.3 and decreased little in the range of pH 5.3 to 6.8, following a sharp decrease when pH was over 6.8. The maximum sensitivity was observed at pH 5.3 because of the maximum activity of GOx and the stability of PB at this pH level. The decrease of the sensitivity for pH over 6.8 is attributed to the decrease of both PB stability and GOx activity. PBS of pH 6.8 was chosen as bulk solution for the following optimization experiments because this pH value not only provided strong response, but is also closed to the pH value of whole blood sample.

Similar to the optimization process of pH value, the sensitivity of the biosensor was recorded in diverse applied potentials and a fixed pH value (6.8). Figure 4.6d shows that the sensitivity varied in the range from -0.2 to +0.2 V (vs. Ag/AgCl), reaching its largest value around 0 V. The increased sensitivity with applied potential can be attributed to the increased driving force for the reduction of ferric ferrocyanide which was produced

www.manaraa.com

during the redox reaction. Meanwhile, this applied potential also results to a maximum ratio between glucose current and background current (S/B) [50]. Taking into account the high response sensitivity and low background noise, a potential of 0 V was chosen as the applied potential for the following chronoamperometry measurements.

4.3.4 Investigation on the linear range and the sensitivity of glucose biosensors

4.3.4.1 The effect of enzyme immobilization methods

As mentioned in section 4.3.3, GOx was immobilized on the PB/MWCNT/Au electrode using four representative methods to investigate how different methodologies of enzyme immobilization affected the sensitivity and linear range of the glucose biosensors. In the first method, GOx was immobilized in the chitosan matrix through physical absorption, which is a non-specific physical interaction, involving Van der Waals or dispersion forces. This method can be easily performed, and tends to be less poisonous to the bioactivity of enzymes compared to chemical means of attachment. Due to the low strength of the non-specific interaction, desorption of enzymes during the measurement process appears to be a primary problem.

In order to solve this problem, GOx was attached to the support matrix by covalent bonding, which was formed between functional groups on the enzymes and those on the support surface. As chitosan contained abundance of amino that was able to react with aldehyde from glutaraldehyde to form a structure of gel, the GOx-chitosan mixture was cross-linked with glutaraldehyde to provide insolubilized and stable enzyme derivatives that prevented enzymes from leaching into the surrounding solution.

Glutaraldehyde can also lead to the cross-linking of enzyme molecules, creating an insoluble, reticulated, and rigid cluster. The enzyme insolubilization may change the molecular conformation of the enzymes by bonding the active site of enzymes, leading to

www.manaraa.com

the denaturation of the enzyme protein. The cross-linking process can be conducted with the aid of an inert protein to increase the stabilization of the enzymes after it is immobilized. Here, BSA was added into the GOx-chitosan mixture to diminish deactivation during the cross-linking phase and increase GOx stability. Unfortunately, the cross-linking process catalyzed by glutaraldehyde induced the formation of diffusion barriers, which could have impaired the sensitivity of the biosensor. Thus, to thin down the enzyme layer, only the GOx-BSA mixture was cross-linked with glutaraldehyde.

Figure 4.7a shows the current-time response curves of four types of biosensors (Nafion 0.5%, GOx 10U). The sensitivity changed dramatically in the four glucose biosensors because the activity of GOx was varied under different immobilization methods of GOx. The combination of GOx-BSA/glutaraldehyde achieved the highest sensitivity (1.02 μA/mM), while the GOx-BSA-chitosan/glutaraldehyde showed the lowest sensitivity (0.28 μA/mM). However, the linear range of the four glucose biosensors was narrow and changed little (Figure 4.7b). Thus, other factors should be investigated to broaden the linear range of the glucose biosensors.

www.manaraa.com

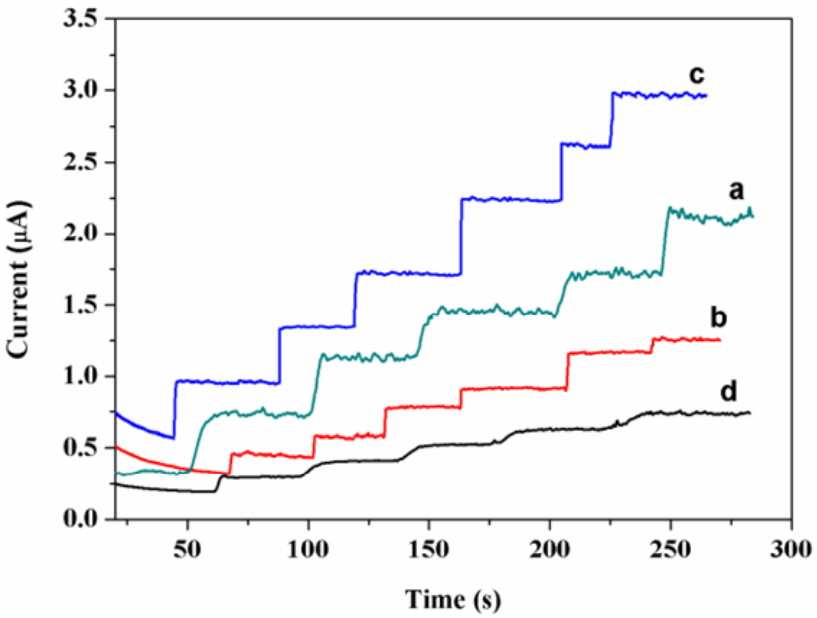

(a)

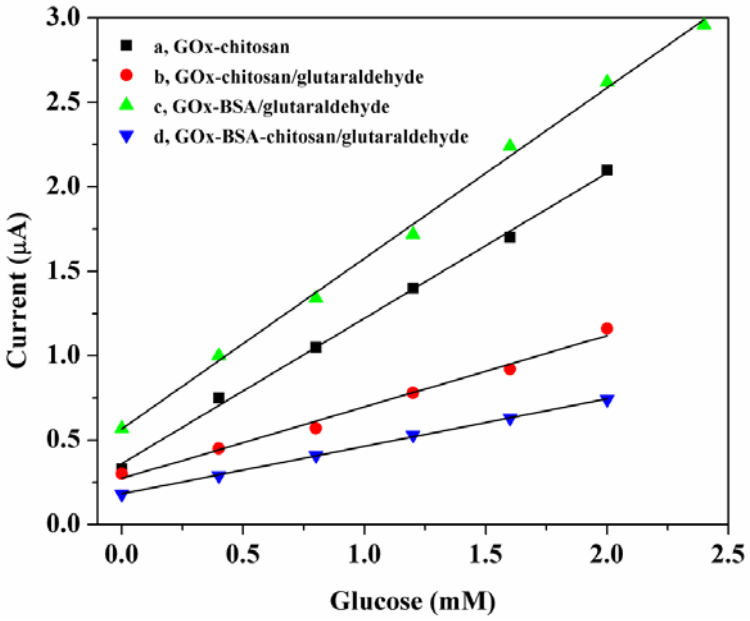

(b)

Figure 4.7: The current-time response curves (a) and their calibration curves (b) of biosensors fabricated using four kinds of enzyme immobilization methods: a GOx-chitosan without cross-linking; b, c and d GOx-chitosan, GOx-BSA and GOx-BSA-chitosan, cross-linked with glutaraldehyde. PBS (pH 6.8) and working potential (0 V) were applied in the experiments.

www.manaraa.com

4.3.4.2 The effect of the amount of GOx

The amount of GOx was reported to influence the performance of glucose biosensors (Tsai et al., 2005). The effect of the amount of GOx on the sensitivity and the linear range of Nafion/GOx-BSA/PB/MWCNT/Au (5 μL 10% Nafion) was investigated in the range of 5 – 15 U (Figure 4.8). The sensitivity of glucose biosensor increased when the amount of GOx increased from 5 U to 10 U. However, the sensitivity decreased when the amount of GOx was above 10 U. This phenomenon could be explained through the inverted relationship between the number of active sites and inhibitors. Increasing the GOx concentration increased the number of active sites and consequently decreased the number of inhibitors. As more active sites were involved in the conversion of glucose molecules into H_2O_2 in a given time period, the sensitivity increased. If the amount of enzymes present had exceeded the amount of glucose molecules in the local surface, the further increase of enzyme concentration would not speed up the enzymatic reaction. On the contrary, the diffusion of H_2O_2 to the catalyst layer would be hindered by the thick enzyme layer, which would decrease sensitivity of the glucose biosensor. Although the amount of GOx could change the sensitivity of the glucose biosensors, it rarely affected their linear range (Figure 4.8b).

www.manaraa.com

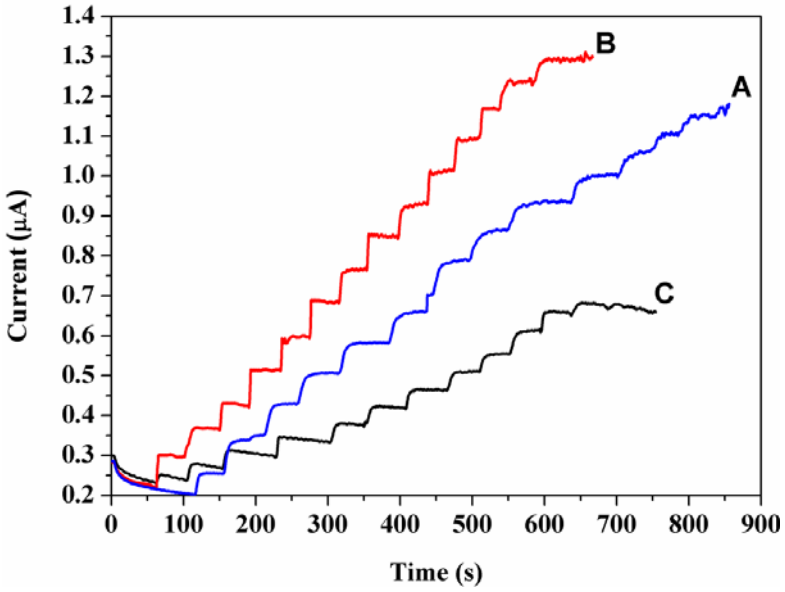

(a)

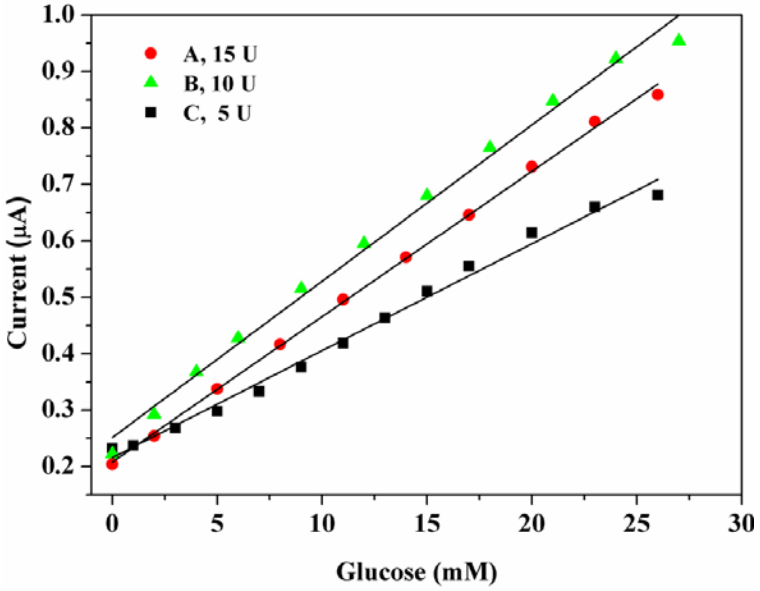

(b)

Figure 4.8: The current-time response curves (a) and their calibration curves (b) for the Nafion/GOx-BSA/PB/MWCNT/Au at the amount of GOx of (A)15 U, (B)10 U and (C) 5 U. PBS (pH 6.8) and working potential (0 V) were applied in the experiments.

www.manaraa.com

4.3.4.3 The effect of diffusion-limited membrane

Nafion has been widely used as an electrochemistry promoting polymeric binder in the fabrication of glucose biosensors to prevent the leakage of GOx and the interference. Nafion can be also used as a diffusion-limited membrane to adjust the diffusion velocity of substrate (here is glucose). The effects of Nafion concentrations, in the range of 0.5% - 10%, on the sensitivity and the linear range of the glucose biosensor (GOx-BSA/PB/MWCNT/Au) were studied. It was shown that the sensitivity of the glucose biosensor decreased rapidly with the increase of Nafion concentration, but the linear range was significantly widened (Table 1).

The enzyme reaction layer and the bulk solution were separated by the Nafion membrane. Prior to reaction the molecules of glucose from bulk solution diffused through the membrane to reach the surface of the enzyme layer. The rates at which the glucose molecules passed over the semi-permeable membrane determined the concentration of glucose in the proximity of enzymes. Based on the response dynamics of enzymes, the response of GOx on glucose is only linearly dependent in low concentrations of glucose. When Nafion was used as a diffusion-limited membrane, the diffusion rate of glucose decreased with the increase of Nafion concentration. The linear range of the glucose biosensor was wider and the sensitivity was lower in a higher concentration of Nafion due to the low concentration of glucose in the enzyme layer. Therefore, the concentration of Nafion could be chosen based on the actual situation. For example, a low concentration of Nafion could be chosen to increase the sensitivity of the biosensor, while a high concentration of Nafion could be chosen to widen the linear range of the biosensor.

www.manaraa.com

Table 4.1: The effect of Nafion concentration on the sensitivity and linear range of the biosensor.

Nafion concentration	Sensitivity (μA/mM)	Linear range up to (mM)	Detection limit S/N=3 (mM)
0.5%	1.02	2.4	0.08
1%	0.17	8	0.1
10%	0.02	20	0.8

4.3.5 Interference

The current response of Nafion/GOx-BSA/PB/MWCNT/Au (1% Nafion, 10 U GOx) to the possible interference was shown in Figure 4.9. The interference from ascorbic acid, uric acid, and lactic acid were negligible. The selectivity of the glucose biosensor was high because Nafion film can effectively prevent the interference of cations and the low working potential of the glucose biosensor, 0 V, prevents the normal interference from oxidation or reduction.

www.manaraa.com

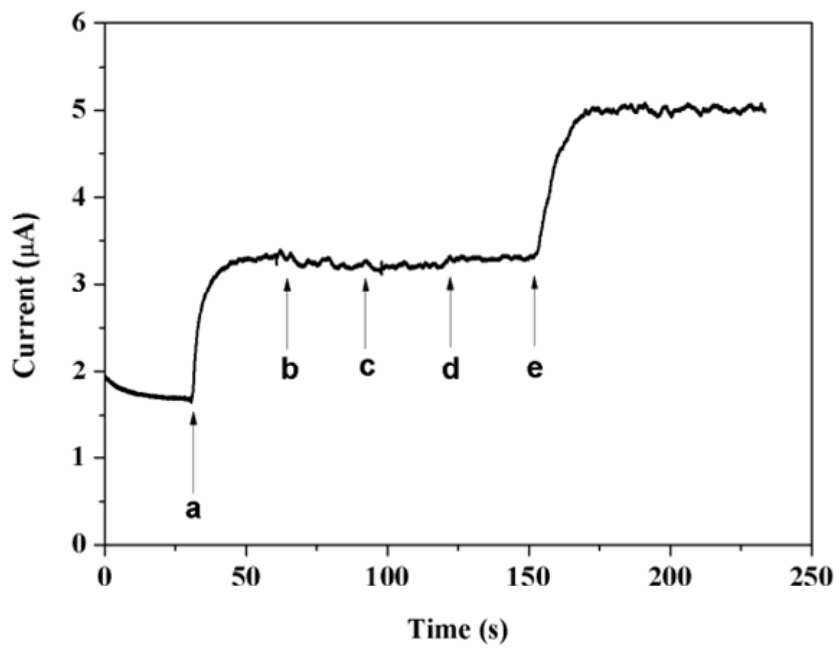

Figure 4.9: Current response of Nafion/GOx-BSA/PB/MWCNT/Au to different substances: (a) 1 mM glucose, (b) 0.6 mM ascorbic acid, (c) 0.6 mM uric acid, (d) 0.6 mM lactic acid, (e) 1 mM glucose. PBS (pH 6.8) and working potential (0 V) were applied in the experiments.

4.3.6 The application of glucose biosensor

The application of the glucose biosensor was evaluated by the presence of glucose in human serum. 0.1 mL of serum was added into 5 mL of PBS. The glucose concentration in the sample was detected as 5.7 mM with a RSD of 5.5% (n = 5). The recovery was obtained by a standard addition method. The glucose biosensor demonstrated satisfactory results with the recovery rate in the range of 98% - 103%. The satisfying results showed that the biosensor has a great potential for practical application, retained its enzyme bioactivity and reproduced 85% of its initial sensitivity after it was stored in PBS at 4°C for two weeks.

www.manaraa.com

4.4 Summary

The linear range of conventional glucose biosensors was normally narrowed under 2 mM, but the blood glucose concentration of diabetes mellitus patients could achieve over 20 mM. The majority of research only focuses on increasing the detective sensitivity of glucose biosensors, and little attention has been focused on their liner range [51]. Although biosensors cannot possess high detection sensitivity and a wide linear sensing range at the same time, their sensing performance should be variable according to practical applications.

This Chapter provides comprehensive information about the PB/MWCNT based glucose biosensors. It was found that MWCNT wrapped by PDDA formed a uniform and porous structure on a Au electrode that increased the response and stability of PB under various pH values and improve the immobilization of glucose oxidase (GOx). The immobilization methods and the amount of GOx mainly influenced the sensitivity of the glucose biosensor, while the concentration of Nafion affected both the sensitivity and the linear range of the glucose biosensor. The widest linear range of the glucose biosensors was from 0.8 mM to 20.0 mM with a sensitivity of 0.02 μA/mM, and the highest sensitivity of the glucose biosensor was 1.02 μA/mM with a linear range of 0.1 - 2.4 mM. The biosensor showed little interference resulting from the possible interferents, including uric acid, ascorbic acid and lactate because of the low operating potential, indicating an excellent selectivity. Finally, the biosensor was used in the determination of glucose in human serum, resulting in 5.5% deviation from the reference value.

As stated above, the measurements of human serum were conducted using PBS (pH 6.8). At this pH environment, the biosensor possesses high sensitivity and strong response, which can provide more information for the optimization of the biosensor. Certainly, there is still a need to improve the performance of the biosensor at pH 7.4 for point-of-care diagnostics.

www.manaraa.com

4.5 Conclusions

An amperometric glucose biosensor based on PB/MWCNT was developed. The effect of enzyme immobilization methods, the amount of GOx and the concentration of Nafion on the sensitivity and linear range of the glucose biosensor was investigated in detail. This study developed a method to manipulate the sensing sensitivity and the linear range of glucose biosensors according to diverse applications.

www.manaraa.com

4.6 References

1. Yoo, E.H. and Lee, S.Y., Glucose Biosensors: An overview of use in clinical practice. Sensors, 2010. **10** (5): p. 4558-4576.

2. Clark, L.C. and Lyons, C., Electrode systems for continuous monitoring in cardiovascular surgery. Annals of the New York Academy of Sciences, 1962. **102** (1): p. 29-45.

3. Heller, A. and Feldman, B., Electrochemical glucose sensors and their applications in diabetes management. Chemical Reviews, 2008. **108** (7): p. 2482-2505.

4. Thevenot, D.R., Tothb, K., Durstc, R.A., and Wilsond, G.S., Electrochemical biosensors: recommended definitions and classification. Biosensors & Bioelectronics, 2001. **16** (1-2): p. 121-131.

5. Wang, J., Electrochemical glucose biosensors. Chemical Reviews, 2008. **108** (2): p. 814-825.

6. Weibel, M.K. and Bright, H.J., Glucose oxidase mechanism: Interpretation of pH dependence. Journal of Biological Chemistry, 1971. **246** (9): p. 2734-2744.

7. Rakhi, R.B., Sethupathi, K., and Ramaprabhu, S., A Glucose biosensor based on deposition of glucose oxidase onto crystalline gold nanoparticle modified carbon nanotube electrode. Journal of Physical Chemistry B, 2009. **113** (10): p. 3190-3194.

8. Ryoo, H., Kim, Y., Lee, J., Shin, W., Myung, N., and Hong, H. G.,Immobilization of horseradish peroxidase to electrochemically deposited gold-nanoparticles on glassy carbon electrode for determination of H_2O_2. Bulletin of the Korean Chemical Society, 2006. **27** (5): p. 672-678.

www.manaraa.com

9. Santos, A.S., Duran, N. and Kubota, L.T., Biosensor for H_2O_2 response based on horseradish peroxidase: Effect of different mediators adsorbed on silica gel modified with niobium oxide. Electroanalysis, 2005. **17** (12): p. 1103-1111.

10. Wang, J., Carbon-nanotube based electrochemical biosensors: A review. Electroanalysis, 2005. **17** (1): p. 7-14.

11. Xu, S.Y., Peng, B., and Han, X.Z., A third-generation H_2O_2 biosensor based on horseradish peroxidase-labeled Au nanoparticles self-assembled to hollow porous polymeric nanopheres. Biosensors & Bioelectronics, 2007. **22** (8): p. 1807-1810.

12. Tsiafoulis, C.G., Trikalitis, P.N. and Prodromidis, M.I., Synthesis, characterization and performance of vanadium hexacyanoferrate as electrocatalyst of H_2O_2. Electrochemistry Communications, 2005. **7** (12): p. 1398-1404.

13. Yu, H., Sheng, Q.L., and Zheng, J. B., Preparation, electrochemical behavior and performance of gallium hexacyanoferrate as electrocatalyst of H_2O_2. Electrochimica Acta, 2007. **52** (13): p. 4403-4410.

14. Che, X., Yuan, R., Chai, Y. Q., Li, J. J., Song, Z. J., and Li, W. J., A glucose biosensor based on chitosan Prussian blue multiwall carbon nanotubes-hollow PtCo nanochains formed by one-step electrodeposition. Colloids and Surfaces B-Biointerfaces, 2011. **84** (2): p. 454-461.

15. Chen, H. L., Zhao, L., Chen, X., Zhuang, Z. X., and Wang, X. R., Development of an amperometric glucose biosensor based on the immobilization of glucose oxidase in an ormosil-PVA matrix onto a Prussian Blue modified electrode. Science in China Series B: Chemistry, 2009. **52** (8): p. 1128-1135.

16. Fu, G.L., Yue, X.L., and Dai, Z.F., Glucose biosensor based on covalent immobilization of enzyme in sol-gel composite film combined with Prussian blue/carbon nanotubes hybrid. Biosensors & Bioelectronics, 2011. **26** (9): p. 3973-3976.

www.manaraa.com

17. Li, J.P., Wei, X.P. and Yuan, Y.H. Synthesis of magnetic nanoparticles composed by Prussian blue and glucose oxidase for preparing highly sensitive and selective glucose biosensor. Sensors and Actuators B-Chemical, 2009. **139** (2): p. 400-406.

18. Liu, Y., Chu, Z. Y., Zhang, Y. A., and Jin, W., Amperometric glucose biosensor with high sensitivity based on self-assembled Prussian Blue modified electrode. Electrochimica Acta, 2009. **54** (28): p. 7490-7494.

19. Ji, X. P., Ren, J. J., Ni, R. X., and Liu, X. H., A stable and controllable Prussian blue layer electrodeposited on self-assembled monolayers for constructing highly sensitive glucose biosensor. Analyst, 2010. **135** (8): p. 2092-2098.

20. Wang, X. Y., Gu, H. F., Yin, F., and Tu, Y. F., A glucose biosensor based on Prussian blue/chitosan hybrid film. Biosensors & Bioelectronics, 2009. **24** (5): p. 1527-1530.

21. Iijima, S., Helical microtubules of graphitic carbon. Nature, 1991. **354** (6348): p. 56-58.

22. Kim, B., Park, H., and Sigmund, W.M., Electrostatic interactions between shortened multiwall carbon nanotubes and polyelectrolytes. Langmuir, 2003. **19** (6): p. 2525-2527.

23. Kim, B. and Sigmund, W.M., Self-alignment of shortened multiwall carbon nanotubes on polyelectrolyte layers. Langmuir, 2003. **19** (11): p. 4848-4851.

24. Wen, D., Liu, Y., Yang, G. C., and Dong, S. J., Electrochemistry of glucose oxidase immobilized on the carbon nanotube wrapped by polyelectrolyte. Electrochimica Acta, 2007. **52** (16): p. 5312-5317.

25. Altug, C., Mengulluoglu, U., Kurt, E., Kaya, S., and Dinckaya, E., A novel biosensor based on glucose oxidase for activity determination of alpha - Amylase. Artificial Cells Blood Substitutes and Biotechnology, 2011. **39** (5): p. 298-303.

www.manaraa.com

26. Zhong, H. A., Yuan, R., Chai, Y. Q., Li, W. J., Zhong, X., & Zhang, Y., In situ chemo-synthesized multi-wall carbon nanotube-conductive polyaniline nanocomposites: Characterization and application for a glucose amperometric biosensor. Talanta, 2011. **85** (1): p. 104-111.

27. Ali, S. M. U., Kashif, M., Ibupoto, Z. H., Fakhar-e-Alam, M., Hashim, U., and Willander, M., Functionalised zinc oxide nanotube arrays as electrochemical sensors for the selective determination of glucose. Micro & Nano Letters, 2011. **6** (8): p. 609-613.

28. Muguruma, H., T. Hoshino, and Y. Matsui, Enzyme biosensor based on plasma-polymerized film-covered carbon nanotube layer grown directly on a flat substrate. Acs Applied Materials & Interfaces, 2011. **3** (7): p. 2445-2450.

29. Barbadillo, M., Casero, E., Petit-Dominguez, M. D., Vazquez, L., Pariente, F., & Lorenzo, E., Gold nanoparticles-induced enhancement of the analytical response of an electrochemical biosensor based on an organic-inorganic hybrid composite material. Talanta, 2009. **80** (2): p. 797-802.

30. Tan, X. C., Tian, Y. X., Cai, P. X., and Zou, X. Y., Glucose biosensor based on glucose oxidase immobilized in sol-gel chitosan/silica hybrid composite film on Prussian blue modified glass carbon electrode. Analytical and Bioanalytical Chemistry, 2005. **381** (2): p. 500-507.

31. Dal Pozzo, A., Vanini, L., Fagnoni, M., Guerrini, M., De Benedittis, A., and Muzzarelli, R. A. A., Preparation and characterization of poly(ethylene glycol)-crosslinked reacetylated chitosans. Carbohydrate Polymers, 2000. **42** (2): p. 201-206.

32. Ahmadalinezhad, A., Kafi, A.K.M. and Chen, A.C., Glucose biosensing based on the highly efficient immobilization of glucose oxidase on a Prussian blue modified nanostructured Au surface. Electrochemistry Communications, 2009. **11** (10): p. 2048-2051.

www.manaraa.com

33. Zhang, Y., Sun, X. M., Zhu, L. Z., Shen, H. B., and Jia, N. Q., Electrochemical sensing based on graphene oxide/Prussian blue hybrid film modified electrode. Electrochimica Acta, 2011. **56** (3): p. 1239-1245.

34. Wang, C., Chen, S., Xiang, Y., Li, W., Zhong, X., and Che, X., Glucose biosensor based on the highly efficient immobilization of glucose oxidase on Prussian blue-gold nanocomposite films. Journal of Molecular Catalysis B: Enzymatic, 2011. **69** (1): p. 1-7.

35. Elliott, J. M., Birkin, P. R., Bartlett, P. N., and Attard, G. S., Platinum microelectrodes with unique high surface areas. Langmuir, 1999. **15** (22): p. 7411-7415.

36. Kannan, R., Parthasarathy, M., Maraveedu, S. U., Kurungot, S., and Pillai, V. K., Domain size manipulation of perflouorinated polymer electrolytes by sulfonic acid-functionalized MWCNTs to enhance fuel cell performance. Langmuir, 2009. **25** (14): p. 8299-8305.

37. Piao, M. H., Yang, D. S., Yoon, K. R., Lee, S. H., and Choi, S. H., Development of an electrogenerated chemiluminescence biosensor using carboxylic acid-functionalized MWCNT and Au nanoparticles. Sensors, 2009. **9** (3): p. 1662-1677.

38. Saito, T., Matsushige, K., and Tanaka, K., Chemical treatment and modification of multi-walled carbon nanotubes. Physica B: Condensed Matter, 2002. **323** (1-4): p. 280-283.

39. Bi, S., Zhou, H., and Zhang, S., Multilayers enzyme-coated carbon nanotubes as biolabel for ultrasensitive chemiluminescence immunoassay of cancer biomarker. Biosensors and Bioelectronics, 2009. **24** (10): p. 2961-2966.

40. Manesh, K., et al., A novel glucose biosensor based on immobilization of glucose oxidase into multiwall carbon nanotubes–polyelectrolyte-loaded electrospun nanofibrous membrane. Biosensors and Bioelectronics, 2008. **23** (6): p. 771-779.

www.manaraa.com

41. Karyakin, A.A., Prussian Blue and its analogues: Electrochemistry and analytical applications. Electroanalysis, 2001. **13** (10): p. 813-819.

42. Karyakin, A.A., Gitelmacher, O.V. and Karyakina, E.E., Prussian Blue-based first-generation biosensor. A sensitive amperometric electrode for glucose. Analytical Chemistry, 1995. **67** (14): p. 2419-2423.

43. Karyakin, A.A., Karyakina, E.E. and Gorton, L., Prussian-Blue-based amperometric biosensors in flow-injection analysis. Talanta, 1996. **43** (9): p. 1597-1606.

44. Karyakin, A.A., Karyakina, E.E. and Gorton, L., Amperometric biosensor for glutamate using Prussian blue-based "artificial peroxidase" as a transducer for hydrogen peroxide. Analytical Chemistry, 2000. **72** (7): p. 1720-1723.

45. Karyakin, A. A., Puganova, E. A., Budashov, I. A., Kurochkin, I. N., Karyakina, E. E., and Levchenko, V. A., Prussian blue based nanoelectrode arrays for H_2O_2 detection. Analytical Chemistry, 2004. **76** (2): p. 474-478.

46. Mattos, I.L., Gorton, L. and Ruzgas, T., Sensor and biosensor based on Prussian Blue modified gold and platinum screen printed electrodes. Biosensors and Bioelectronics, 2003. **18** (2): p. 193-200.

47. Mattos, I.L., Gorton, L., Ruzgas, T., and Karyakin, A. A., Sensor for hydrogen peroxide based on Prussian Blue modified electrode: improvement of the operational stability. Analytical Sciences, 2000. **16** (8): p. 795-798.

48. Ricci, F., et al., Prussian Blue and enzyme bulk-modified screen-printed electrodes for hydrogen peroxide and glucose determination with improved storage and operational stability. Analytica chimica acta, 2003. **485** (1): p. 111-120.

49. Zeng, J. X., Wei, W. Z., Liu, X. Y., Wang, Y., and Luo, G. M., A simple method to fabricate a Prussian Blue nanoparticles/carbon nanotubes/poly(1,2-

www.manaraa.com

diaminobenzene) based glucose biosensor. Microchimica Acta, 2008. **160** (1-2): p. 261-267.

50. Dungchai, W., Chailapakul, O. and Henry, C.S., Electrochemical detection for paper-based microfluidics. Analytical Chemistry, 2009. **81** (14): p. 5821-5826.

51. Tsai, Y.C., Li, S.C. and Chen, J.M., Cast thin film biosensor design based on a nafion backbone, a multiwalled carbon nanotube conduit, and a glucose oxidase function. Langmuir, 2005. **21** (8): p. 3653-3658.

www.manaraa.com

Chapter 5

5 Fabrication of Nanoporous Thin-film Working Electrodes and their Biosensing Applications

As the electrode system is directly embedded in the microfluidic system, it may experience sample flow rates from nl s^{-1} to liter s^{-1} in the centrifugal platform. Here, a nanoporous structure was created on the surfaces of electrodes through an alloying/dealloying process. The nanoporous electrode has an electroactive surface area up to 60 times higher than that of a flat gold electrode of the same size. Abundant catalysts and enzymes were stably entrapped in the nanoporous structure, leading to high stability and reproducibility of the sensor.

5.1 Introduction

Lab-on-a-chip technology has attracted researchers from different disciplines to explore this technology for a wide range of applications [1-5]. Enzymatic electrochemistry is one of the most applied detection techniques used in lab-on-a-chip devices to miniaturize chemical and biological analysis processes due to its low cost, high sensitivity, moderate power requirements, and prominent compatibility with microfabrication technologies [6-8]. Although the miniaturization will not alter the mechanism of biochemical reactions on electrodes, will change fluid mechanics, molecular diffusion and surface to volume ratio in micro scale channels and will require the modification of bulk electrochemical biosensors.

In all types of enzymatic electrochemical biosensors, electrodes (working electrode, reference electrode and counter electrode) perform as transducers, which convert information of the specified amount of a biological analyte into an electrical signal. The biorecognition phenomenon and the redox reaction occur on the surface of the working electrode where the catalyst layer, the enzyme layer and the semi-permeable layer are superimposed. Therefore, the working electrodes employed in microfluidic chips deserve

www.manaraa.com

considerable attention. To fit the electrode in the detection chamber and to minimize the disturbance to fluid movement, the thickness of the embedded planar electrode must be reduced to nanoscale and the surface area must be as small as possible. However, the miniaturization results in several implications that require further improvement. For example, the miniaturization impairs the signal-to-noise ratio and the nanoscale thickness of the metal layer limits the choice of surface functionalization for subsequent coating. Because of the increasing demand for applying electrochemical sensing on Lab-on-a-chip devices, the electrochemical sensing surface is expected to be thinner and possess a higher signal-to-noise ratio.

Efforts have been made to enhance the sensing sensitivity through artificially enlarging the surface area of working electrodes. Recently, porous materials prepared by a sol-gel method have been developed to immobilize enzymes [9-10]. Nanostructured materials have also attracted much attention due to their inherently large surface area. For example, carbon nanotubes, which were randomly or uniformly immobilized with enzymes, were used in the configuration of biosensors [11]. Metal nanoparticles and nanowires were also prevalent selections for substrate materials [12]. However, these matrices have limitations, including fragility, poor adhesion to the electrode surfaces and complicated fabrication procedures, which may lead to the loss of enzyme activity and poor performance in electrochemical biosensors.

Herein, a planar nanoporous thin-film working electrode was introduced for the first time. The nanoporous structure is constructed within a 100 nm thick gold (Au) electrode rather than adding another layer on top, reducing the total thickness of all layers (the metal layer, the catalyst layer, the enzyme layer and the semi-permeable layer) that stack on the electrode surfaces and improving the bonding among layers. This working electrode design was applied in the construction of planar enzymatic electrochemical biosensors. As hydrogen peroxide (H_2O_2) is a common byproduct in oxidase enzyme reactions, Prussian Blue (PB) was used as a redox mediator to enhance the selectivity of H_2O_2

www.manaraa.com

detection on working electrodes [13]. We found that the nanoporous working electrode not only possesses a large surface area, but also is an excellent substrate to hold enzymes and catalysts. In the following sections, the fabrication and characteristics of the nanoporous and planar thin-film electrodes are described, whilst the electrochemical sensing of glucose is reported as an example to demonstrate the superior performance and robustness of such biosensors.

5.2 Experimental Section

5.2.1 Materials and Equipments

D-(+)-glucose, uric acid, sodium L-lactate, ascorbic acid, glucose oxidase (100 - 250 U/mg), Nafion (5 wt. %), human sera (S2257-1ml), glucose (GO) assay kit and benzyl alcohol (anhydrous, 99.8%) were purchased from Sigma-Aldrich. Piranha solution was made using H_2O_2 (30%) and H_2SO_4 (conc) solution in 1:3 vol/vol ratio. All processing solutions were prepared with de-ionized (DI) water from a Milli-Q system (Millipore, Bedford, MA) and all other chemicals were of analytical grade. 20 mM phosphate buffer solutions (PBS) with 0.1 M KCl were adjusted to pH 5.1. Standard samples were prepared through the dissolution of D-(+)-glucose in PBS. The samples were mutarotated overnight, forming an equilibrium mixture that consists of approximately one-third α-D-glucose and two-thirds β-D-glucose. Human serum samples were made by dissolving lyophilized sera with 1 ml DI water. A nanoporous thin-film working electrode, a Ag/AgCl reference electrode in 1 M KCl and a Pt counter electrode comprised the electrochemical sensing system. Electrochemical measurements were conducted using a potentiostat (CHI 1207A, CH Instruments, Austin, TX) at room temperature (22 ± 1°C). A Hitachi S-4500 field emission scanning electron microscope coupled with an energy dispersive X-ray spectroscope (SEM/EDX) and a Veeco atomic force microscope (AFM) were employed to characterize the fine structure of electrodes. A UV-visible spectrophotometer from Varian was employed to provide a reference glucose level in serum samples using a standard glucose assay kit.

www.manaraa.com

5.2.2 Fabrication of Nanoporous Thin-film Electrodes

Nanoporous thin-film electrodes were fabricated by selectively dissolving the less noble metal from a bimetallic alloy. The alloy was made by consecutively depositing Au and Zn (zinc), followed with thermal annealing. Prior to the metal deposition, a silicon wafer was cleaned with piranha solution at 80°C for 20 min. The pattern of the working electrode was defined by a positive photoresist Shipley 1805 on the cleaned wafer, which was then loaded into an electron beam evaporation chamber and successively deposited 5 nm Cr (chromium) and 100 nm Au, where Cr served as an adhesive layer. The sample was taken out, and the lead and conductive pad were covered with a piece of tape. Afterwards, the sputtering technique was applied to deposit 500 nm Zn. After a lift-off process, where the metal in the non-electrode area was removed using a PG remover (N-Methyl Pyrrolidinone), the sample was annealed in benzyl alcohol at 100°C for 60 min and rinsed with isoproponal (IPA) and DI water. Finally, the alloyed samples were dipped into 50% HNO_3 for 2 min to chemically dissolve the Zn.

5.2.3 Deposition of Prussian Blue, Enzyme and Nafion

Electrodeposition of PB was accomplished using cyclic voltammetery (CV) [13]. Before the electrodeposition, the nanoporous electrodes were electrochemically cleaned and activated in 0.5 M sulfuric acid by cycling between 0.4 V and 1.5 V at a sweep rate of 40 mV s^{-1} until a stable voltammogram was obtained. The solution for the electrodeposition of PB comprises 1.5 mM $K_3[Fe(CN)_6]$, 2 mM $Fe(NO_3)$, 1 mM HCl and 0.1 M KCl. The electrode potential was cycled thirty times from 0.6 V to -0.2 V at a sweep rate of 50 mV s^{-1}. Subsequently, the electrodes were rinsed with DI water and activated in 0.1 M KCl + 0.1 M HCl by cycling the applied potential between 0.5 V and -0.2 V with scan rate of 50 mV s^{-1} until stable CV curves were obtained.

Glucose oxidase (GOx) was immobilized onto the PB-modified electrode surface by physical adsorption. The lyophilized GOx powder was dissolved in PBS to form an

www.manaraa.com

enzyme solution with a concentration of 20 mg/mL. 5 μL of the enzyme solution was dropped onto the electrode surface and dried in a fridge (4°C). Nafion solution of 5% was added on top of the enzyme layer to protect against the leakage of the enzymes and reduce the influx of glucose. The Nafion solution dried in the fridge as well. With these steps, the biosensor was completely built and ready to be used immediately or stored in PBS in the fridge.

5.3 Results and Discussion

The results presented here show that the nanoporous electrode is of excellent film quality, large electroactive surface area, and high electrical conductivity. It is these qualities that make it a robust platform for the immobilization of catalyst and enzymes and provides excellent performance in biosensing trials.

5.3.1 Characterization of nanoporous thin-film electrodes

The formation of nanoporous structures on the working electrode layer is the key to their superior performance. The sputtered Zn layer covering the Au layer was shiny and grey before annealing. The sample turned to dark grey at the end of the annealing process, which indicated the successful alloying. Annealing was conducted in benzyl alcohol to prevent the oxidization of Zn to ZnO, which stops the alloying process. In the following dealloying process, the Zn component was dissolved by nitric acid and the remaining Au component gradually diffused to the surface to form bundles, which could further develop into an interconnected porous network. The golden color of the surface turned into a dim copper-like color at the moment the nanoporous structure was formed. As shown in Figure 5.1, the smooth gold film electrode (Figure 5.1a) turned into nanoporous structures (Figure 5.1b) after the dealloying treatment. The nanoscaled ligaments and nanoporous are continuously connected to form a honeycomb structure, which not only enlarges surface area, but also is an excellent substrate for electrode modification. From AFM images (Figure 5.1c and 5.1d), we can see that the roughness was increased from 2

www.manaraa.com

nm for the planar gold to 20 nm for the nanoporous gold. Further, all the Zn atoms should be removed, otherwise, the electrochemical signal would be disturbed by the leftover Zn. In order to remove Zn without destroying the ultrathin nanoporous Au film, EDX analysis was utilized to inspect the composition of the film and optimize the immersion time of samples in the HNO_3 solution. The EDX spectrum in Figure 5.2a shows that only 1.55% Zn remained in the nanopores films after immersing the sample in the HNO_3 solution for 120 sec. The concentration of Zn changed little by further increasing the etching time in the HNO_3 solution. Explanation for this phenomenon is that the porous film containing a small amount of Zn possessed similar corrosion behavior as that of pure gold. Therefore, Zn atoms would not be selectively etched to the extent of 100% without destroying the porous structure [14].

www.manaraa.com

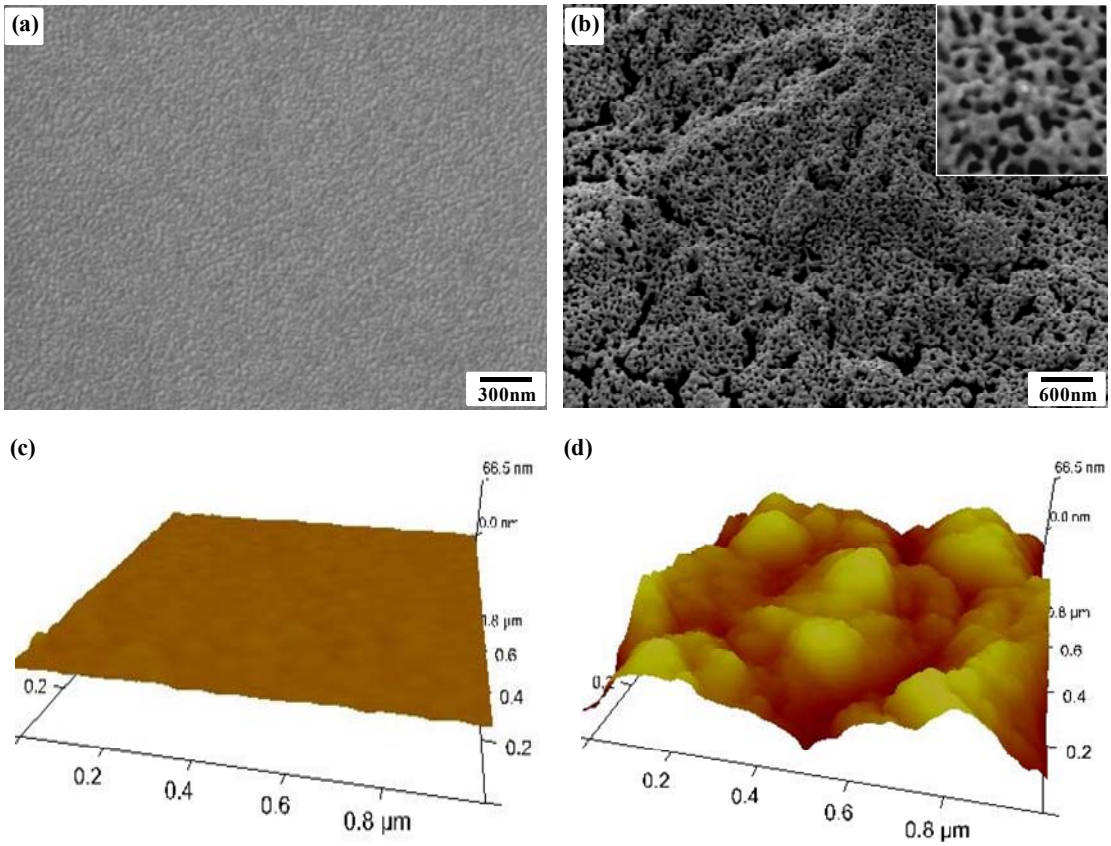

Figure 5.1: SEM and AFM images show (a, c) the smooth and flat surface of a gold electrode before nanoporous treatment; (b, d) the nanoporous surface of a gold electrode after nanoporous treatment.

www.manaraa.com

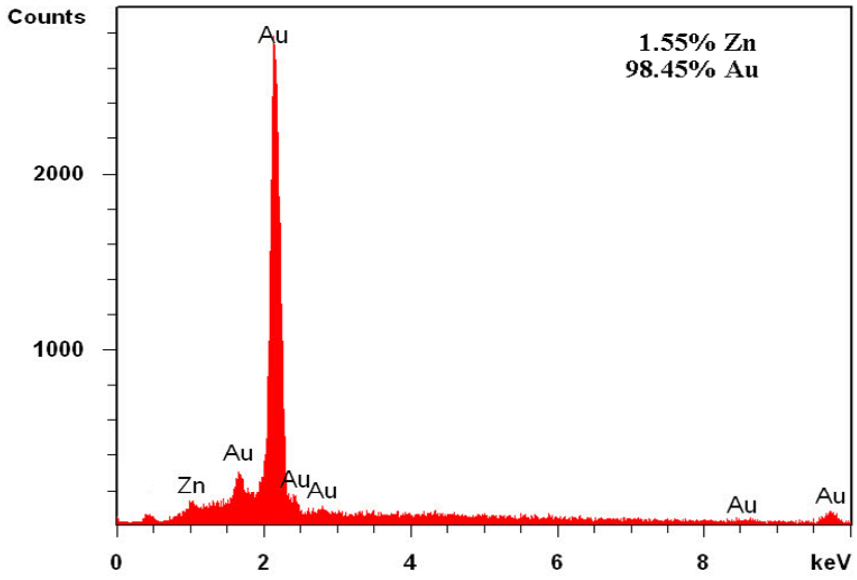

(a)

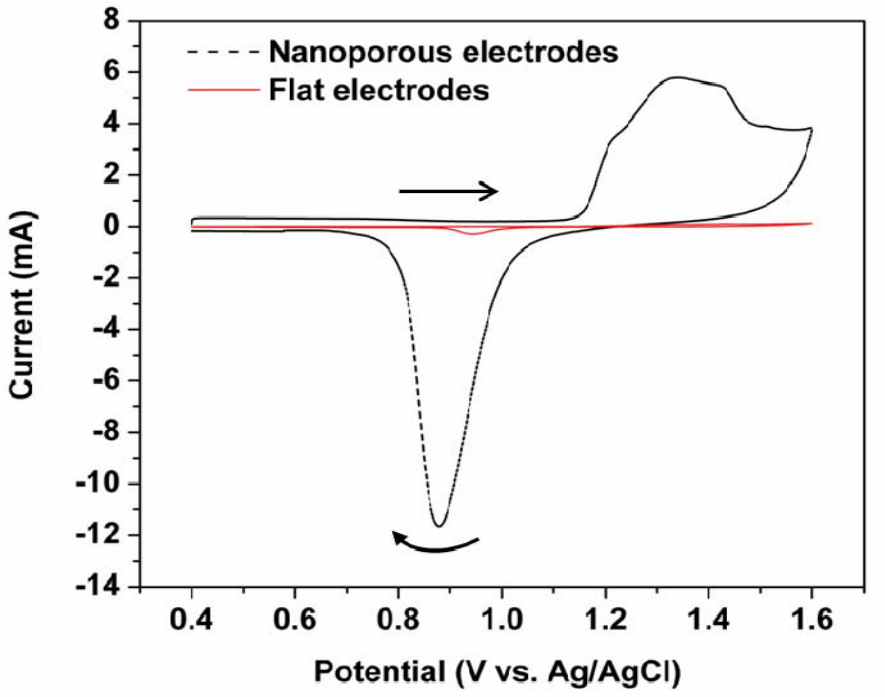

(b)

Figure 5.2: (a) The EDX spectrum of a nanoporous electrode immersed in 50% HNO_3 solution for 120 sec. (b) Cyclic voltammograms recorded in 0.5 M H_2SO_4 for a flat Au electrode and nanoporous Au electrode show that the cathodic peak of the non-porous Au electrode is only one fortieth of that of the nanoporous Au electrode.

www.manaraa.com

It is known that nanoporous electrodes possess larger surface area than flat electrodes. Among various determining methods, the method based on the reduction of gold oxide, the charge of which is proportional to the active surface area, appears to be straightforward [15]. Cyclic voltammograms of a flat Au electrode and a nanoporous Au electrode were recorded in a 0.5 M H_2SO_4 solution and are compared in Figure 5.2b. These voltammograms reveal that the formation of gold oxide results in the peak of the current at the anodic scan, while the reduction of gold oxide induces the cathodic peak at 0.88 V. The electroactive surface area of the nanoporous electrodes was estimated to be about 60 times larger than the flat non-porous Au electrode by measuring the area of the cathodic peaks in the potential-current curves.

The nanoporous structure not only has a larger surface area, but also serves as an excellent substrate for electrode modification. The electrodeposited microcrystalline PB powder was firmly and evenly entrapped and distributed on the nanoporous surface (Figure 5.3a), although the PB film electrodeposited on the flat Au electrode was lumpy and full of cracks (Figure 5.3b). When the electrodes were cycled twenty times in the PBS from 0.5 V to -0.2 V at a scan rate of 50 mV s^{-1}, the majority of PB powder remained on the nanoporous surface (Figure 5.3c), but a large amount of crystallized PB was stripped off from the flat electrode surface (Figure 5.3d). This merit of the nanoporous electrode significantly increases the stability and reproducibility of the biosensor.

www.manaraa.com

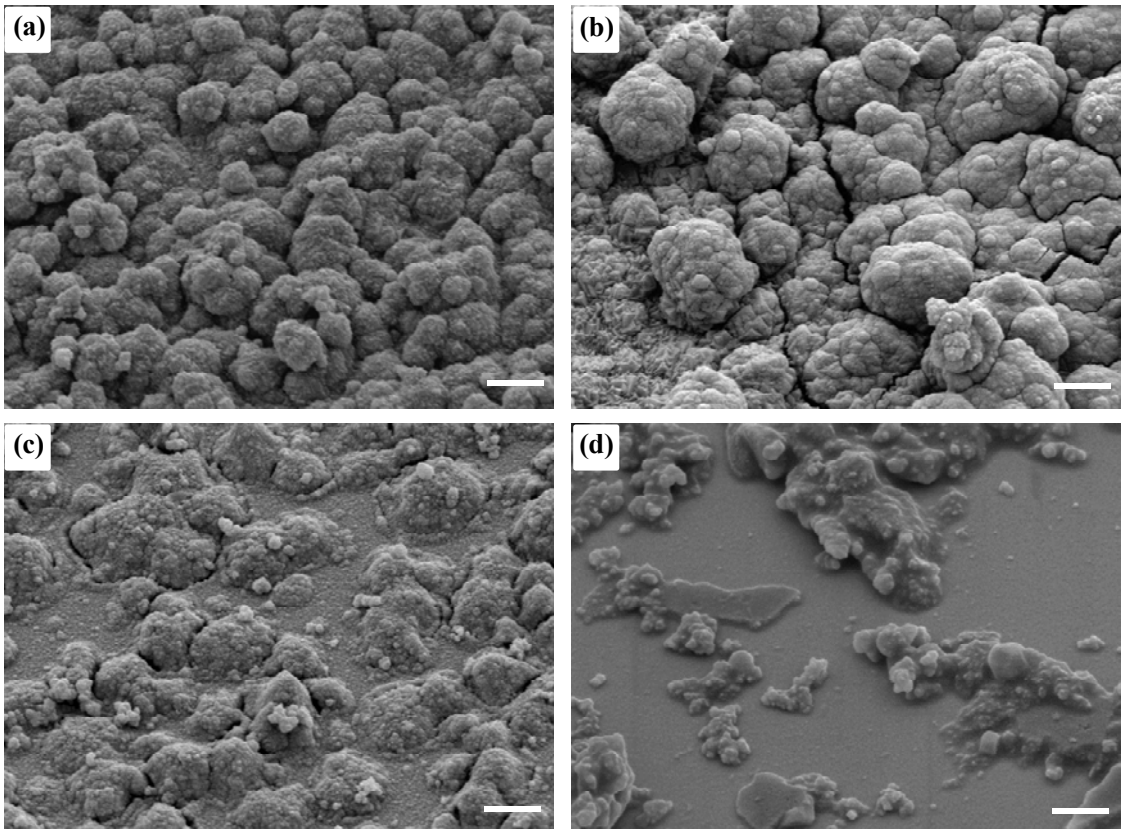

Figure 5.3: SEM images of uniform and compact PB film deposited on a nanoporous electrode (a) and subjected to twenty cycles in a PBS (c); lumpy and loose PB film deposited on a flat electrode (b) and subjected to twenty cycles of potential scan in a PBS (d) All the scale bars are 1 µm.

Before detecting biological samples, the nanoporous electrode with the PB layer was characterized using cyclic voltammetry in the PBS. The PB films were characterized with a benchmark compound Fe^{3+}/Fe^{2+} redox couple and showed electrochemical behavior (cyclic voltammetry) as follows:

$$Fe^{III}{}_4[Fe^{II}(CN)_6]_3 + 4K^+ + 4e^- \Leftrightarrow K_4Fe^{II}{}_4[Fe^{II}(CN)_6]_3 \qquad (5.1)$$

In a forward scan from 0.5 V to -0.2 V with scan rate of 25 mV s^{-1}, ferricyanide was reduced to ferrocyanide and reached a cathodic peak current at 0.16 V. In a return

www.manaraa.com

potential scan, a reversed electron transfer reaction occurred and reached an anodic peak current at 0.26 V (Figure 5.4a). The peak values of the forward and reversed reactions are linearly proportional to the square root of the scan rates in the range from 25 to 500 mV s^{-1} (Figure 5.4b). The linearity implies that the rate of the redox reactions is controlled by the diffusion of potassium ions, which produces a concentration gradient of the electroactive species in the PB lattice on the planar electrode. The rate of the electron transfer step is fast compared to the rate at which potassium ions diffuse from the bulk solution to the electrode surface, so the peak current, i_p, is governed by the Randle-Sevcik relationship [16-17].

www.manaraa.com

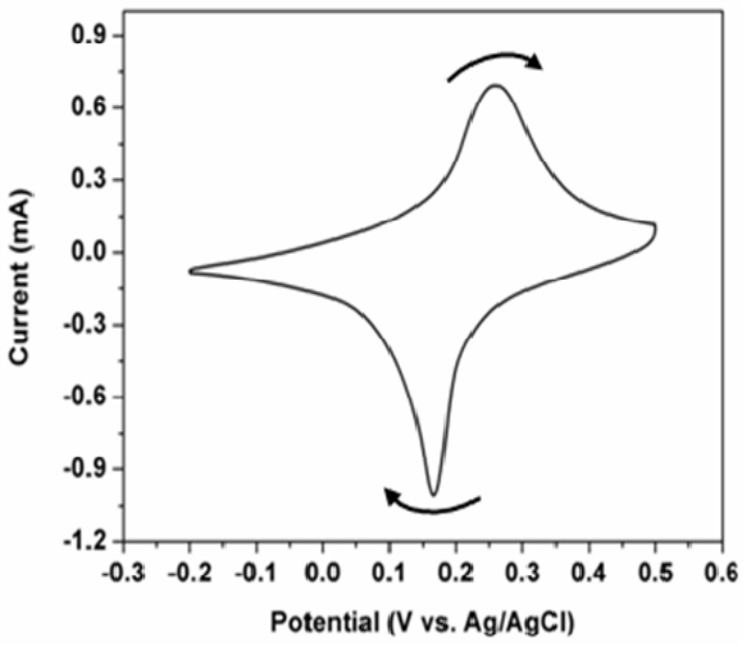

(a)

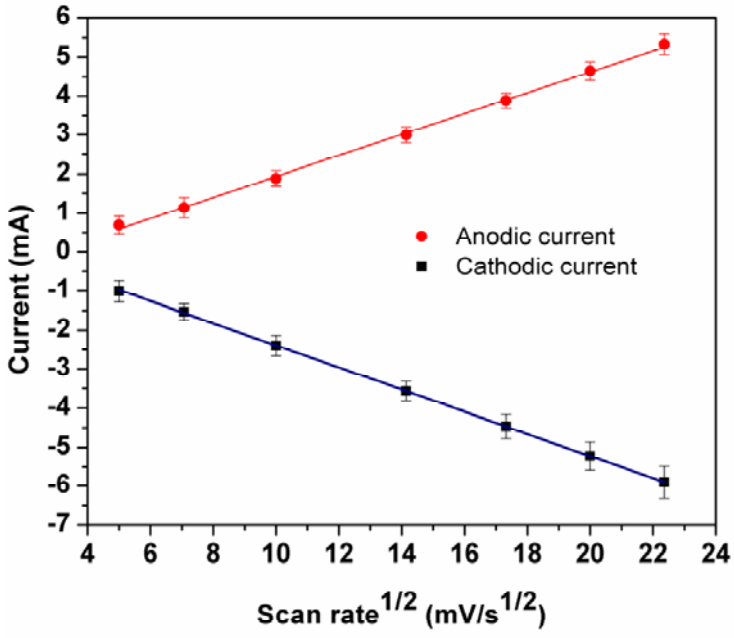

(b)

Figure 5.4: (a) Cyclic voltammogram of the PB-modified nanoporous electrodes at a scan rate of 25 mV s^{-1} in the PBS; (b) The plot of anodic and cathodic currents vs. the square root of the scan rates. The regression equation of the linear fit to anodic response is: y=-0.74+0.26x (R^2=0.9984, n=5), and to cathodic response is: y=0.44-0.28x (R^2=0.9998, n=5).

www.manaraa.com

5.3.2 Calibration of the Biosensor

The mechanism of the sensor involves the electrochemical detection of H_2O_2 generated by the analyte in the enzymatic reaction. Here, we take the specific biorecognition of glucose by the enzyme glucose oxidase (GOx) as an example. GOx, containing two molecules of the cofactor flavine adenine dinucleotide (FAD), is a homodimer with a molecular weight of 160 kD. The sensing process can be elaborated as follows: glucose diffuses from the bulk solution to the GOx layer where it is converted into gluconolactone under the reduction of the FAD prosthetic group (Equation 5.2). The cofactor is oxidized back to its original state, whereby two electrons and two protons are transferred to molecular oxygen, generating H_2O_2 (Equation 5.3). The H_2O_2, which is proportional to the concentration of glucose [18], then catalytically reacts with the Prussian white (PW) by oxidizing PW to PB and PB itself is, in turn, electrochemically reduced back to PW under the applied potential on the surface of the working electrode (Equation 5.4).

$$\mathrm{GOx(FAD)} + \beta\text{-D-glucose} \rightarrow \mathrm{GOx(FADH_2)} + \delta\text{-gluconolactone} \tag{5.2}$$

$$\mathrm{GOD(FADH_2)} + \mathrm{O_2} \rightarrow \mathrm{GOD(FAD)} + \mathrm{H_2O_2} \tag{5.3}$$

$$\mathrm{K_2Fe^{2+}Fe^{2+}(CN)_6} + 2\mathrm{H_2O_2} \leftrightarrow \mathrm{KFe^{3+}Fe^{2+}(CN)_6} + \mathrm{K^+} + 2\mathrm{H_2O} + \mathrm{O_2} \tag{5.4}$$

The biosensors were first calibrated with standard glucose samples using chronoamperometry. In the chronoamperometric measurement, the potential of the working electrode is stepped, so that the Faradic current occurs at the electrode and decays as a function of time. The Faradic current, due to the electron transfer, is proportional to the concentration of analyte, and can be described by the Cottrell equation (for planar electrodes) [19]:

$$i = \frac{nFAC^0 D^{1/2}}{(\pi t)^{1/2}} \tag{5.5}$$

www.manaraa.com

Where i is the current, n is the number of electrons, F is Faraday's constant, A is the area of the electrode, t is the time, C^0 and D are the initial concentration and the diffusion coefficient of the target analyte, respectively.

The potential of 0 V (versus Ag/AgCl) has been optimized for cathodic reduction of hydrogen peroxide aided by PB [16]. Therefore, chronoamperometric measurements were carried out on glucose standard samples with concentrations ranging from 0 mM to 40 mM using 0 V step potential. In Figure 5.5a, the Faradic current occurs right after a large capacitive current and decays as $t^{-1/2}$ until its steady state. The steady state currents at 100 sec were picked up to draw a calibration curve for this biosensor. The mean and the relative standard deviation were generated with a group of data from five biosensors. The calibration curve (square dots) in Figure 5.5b demonstrates the linear relationship between currents and analytes with a concentration of 0 - 30 mM (R^2 = 0.9971, n = 5). The signal for 40 mM is out of the linear range. This linear range has been able to cover the entire normal human blood glucose of 3.5 – 6.1 mM (in whole blood) and abnormal glucose levels (20 – 30 mM). The sensitivity of the glucose analysis is calculated to be 0.50 μA mM^{-1} mm^{-2}, higher than the value (0.43 μA mM^{-1} mm^{-2}) achieved by the electrochemical system built on the porous paper [20]. The limit of detection (LOD), calculated as the concentrations which produced a signal of three times greater amplitude than noise (S/N = 3), is about 0.3 mM, providing better performance compared to the conventional colorimetric methods (LOD, 0.5 mM) and glucometers (LOD, 1 mM) [21-22]. The conventional flat electrodes with immobilized enzymes were also measured using the same condition, and the data were plotted in Figure 5.5b (circular dots). The result of the comparisons clearly shows that the nanoporous biosensor possesses higher sensitivity than conventional biosensors. The increase of electroactive surface area (A) results in sensitivity enhancement, which is supported by the Cottrell equation.

www.manaraa.com

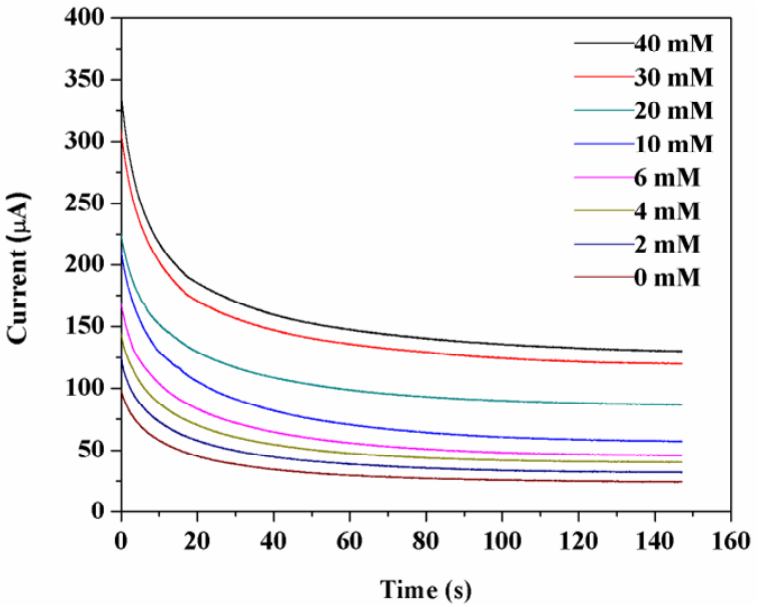

(a)

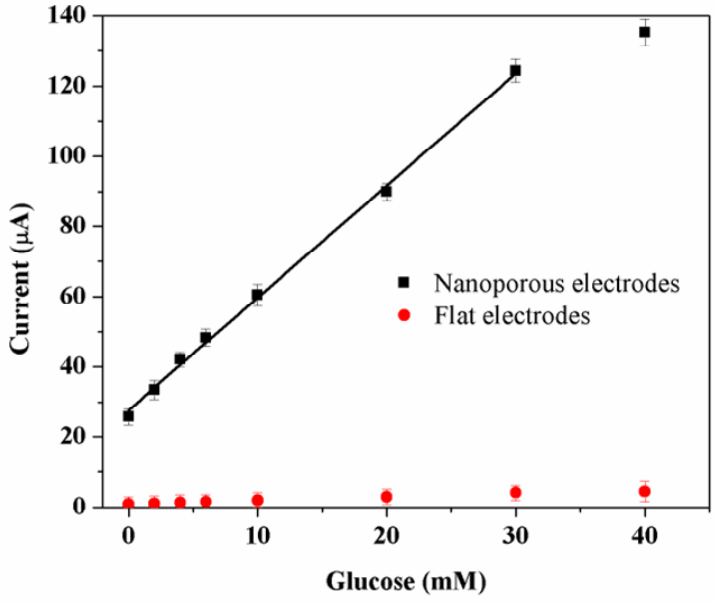

(b)

Figure 5.5: (a) Chronoamperograms of glucose with concentration from 0 mM to 40 mM. The working electrode with a diameter of 3 mm was used to record data at 0 V versus Ag/AgCl. (b) Currents of chronoamperometric curves at 100 seconds plotted as a function of the concentration of glucose. Square dots and circular dots represent data from nanoporous biosensors and conventional biosensors, respectively. The regression equation for the linear fit is: y=25.71+3.19x (R^2=0.9971, n=5).

www.manaraa.com

5.3.3 Analytical performance

Human serum samples were assayed in order to validate that the nanoporous thin-film electrochemical system is beneficial to the practical usage of the glucose biosensor. The glucose concentrations of these serum samples were measured based on a spectrophotometric method using a standard test kit, and used as reference values. The steady state currents of serum samples were then collected in the same condition as in the calibration step, and the glucose concentration was calculated using the previous calibration curve. The measured value with the spectrophotometric method was 5.43±0.08 mM, whilst it was 5.51±0.03 mM with the electrochemical method using the biosensor. The approximation of these two values proves the practical utility of the proposed biosensor. The robustness of the biosensor was further proved by showing the recovery of glucose concentration by a standard addition method. The recovery rates were in the range of 96% - 103% for human serum samples spiked with 0.5 mM glucose. In addition, the biosensor retained its enzyme bioactivity and still had about 80% of its initial sensitivity after 10 days stored in PBS at 4°C.

As an inherent merit of using PB, the biosensor showed little interference to the electroactive interfering compounds commonly present in physiological samples, including lactate (LA), uric acid (UA) and ascorbic acid (AA) due to the low operating potential. The utilization of Nafion as an outermost layer on the electrode surface further ensures its sensitivity to glucose by dramatically reducing the diffusion of interfering compounds to the electrode surface. The normal concentrations of LA, UA and AA in serum are 0.2 mM, 0.3 mM and 0.1 mM, respectively. The amperometric response of the biosensor to successive addition of glucose (0.5 mM) and the interferents into the stirring PBS is shown in Figure 5.6. The current rose only 0.7% and 0.3% during the additions of 0.2 mM lactate and 0.3 mM uric acid (UA), while the presence of 0.1 mM ascorbic acid (AA) slightly depressed the current by about 1.5%. The two additions of 0.5 mM glucose before and after the existence of those interferents produced an equivalent response, so the summation of interferents did not denature the biosensor. These results demonstrated the excellent anti-interference ability of the biosensor.

www.manaraa.com

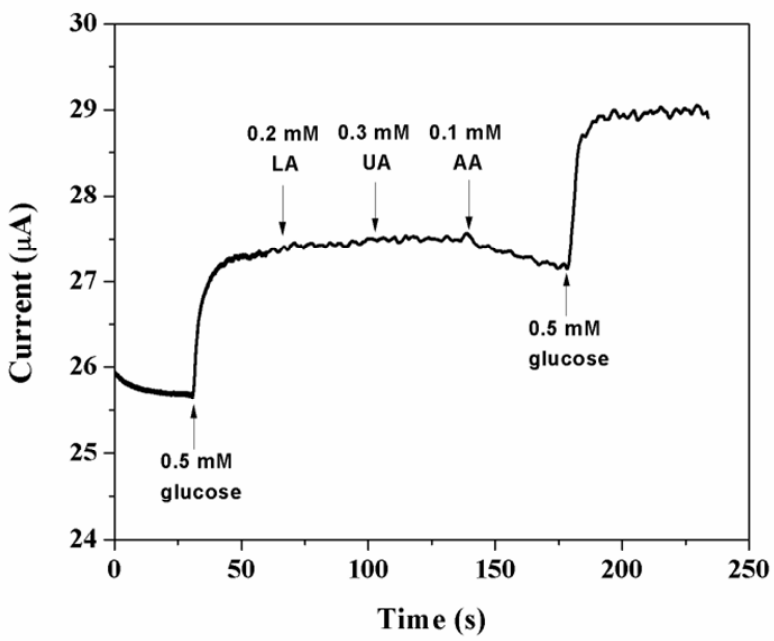

Figure 5.6: Amperometric response to successive adding of glucose and interferents. The experiment was conducted in the stirring PBS at 0 V versus Ag/AgCl. Under this condition, the adding of 0.2 mM lactate (LA), 0.3 mM uric acid (UA) and 0.1 mM ascorbic acid (AA) introduced 0.7% and 0.3% increasing, and 1.5% decreasing, respectively.

5.3.4 Discussion

The fabrication and application of nanoporous structures have been reported in bulk electrodes by other researchers, but the fabrication of nanopores in a thin-film planar electrode and its application in electrochemical detection are conducted here for the first time.

Modification of electrodes through layer by layer assembly of organic and inorganic material possesses the inherent adhesion problem between the assembled layers and the flat electrode surface, and so the risk of the catalysts/enzymes being washed out of the

www.manaraa.com

modified electrodes or leached into the solution is increased, which impairs the stability and performance of the electrode system. It is also known that the PW (the reduced form of PB) at potentials around 0.0 V is unstable and hydroxyl ions produced by the reduction of H_2O_2 in neutral media make the inorganic polycrystal partially soluble, so the electrodeposited PB could easily strip off from the flat electrode surface, leading to the loss of the electrocatalyst [23-24]. In this experiment, blue pigment could be observed by naked eyes due to the detachment of PB from the flat electrode surface whether using the cyclic voltammetric deposition technique or the constant potential deposition technique. However, this rarely happens on nanoporous electrodes, as most of the deposited PB film is firmly entrapped in the nanopores.

The nanoporous structure not only can firmly hold PB particles during the electrode modification process (Figure 5.3), but also benefits from retaining enzymes when the biosensor is integrated in microfluidic system. Sample flow rates in the microfluidic system normally range from nL s^{-1} to L s^{-1} [4]. When it flows across the conventional working electrodes, the sample fluid will continuously bring away portions of the immobilized enzymes, resulting in a decrease of the stability of biosensors. Here, we designed an experiment to compare the performance of a nanoporous biosensor and a conventional (flat) biosensor used in a microfluidic system.

Three electrodes, leads and contact pads were fabricated on a piece of silicon wafer (covered by a 200 nm silicon dioxide layer) using a photolithography method mentioned in Chapter 3. Only the area of the working electrode was made nanoporous and modified with catalysts and enzymes. A tiny drop of Ag/AgCl (AG-500, Conductive Compounds) ink was added on the reference electrode area. These three electrodes form a planar biosensor on the wafer (Figure 5.7a). The design of a microfluidic chip is similar to the previous blood separation design and the detailed fabrication process is available in Chapter 3. The microfluidic chip made of PDMS was cleaned in a 15 minutes UV - Ozone treatment process. Right after this treatment, the PDMS layer was brought into

www.manaraa.com

contact with the wafer layer, and pressed with 10 N force for 2 hours to increase the bonding strength and stored in a fridge (4°C) for testing (Figure 5.7b).

With the propulsion from a syrine pump (BS-8000, Braintree Scientific Inc.), DI water was pumped through the microchannel at a constant flow rate (30 µL s^{-1}) for a specific duration. Then, the flow of DI water was stopped and standard glucose solution (2 mM) was loaded into the system. The sensing chip was connected to a potentiostat to perform chronoamperometric measurements. The comparison involves the nanoporous biosensor and the conventional biosensor, so the steady state currents at 100 sec for both biosensors were picked up and used to calculate the measured concentration. As shown in Figure 5.8, the measured values gradually decreased for both biosensors, but the value of the conventional biosensor deviates from the standard concentration faster compared to that of the nanoporous biosensor. Therefore, it is inferable that the nanoporous structure serves as a better platform to prevent enzyme leakage in a microfluidic system.

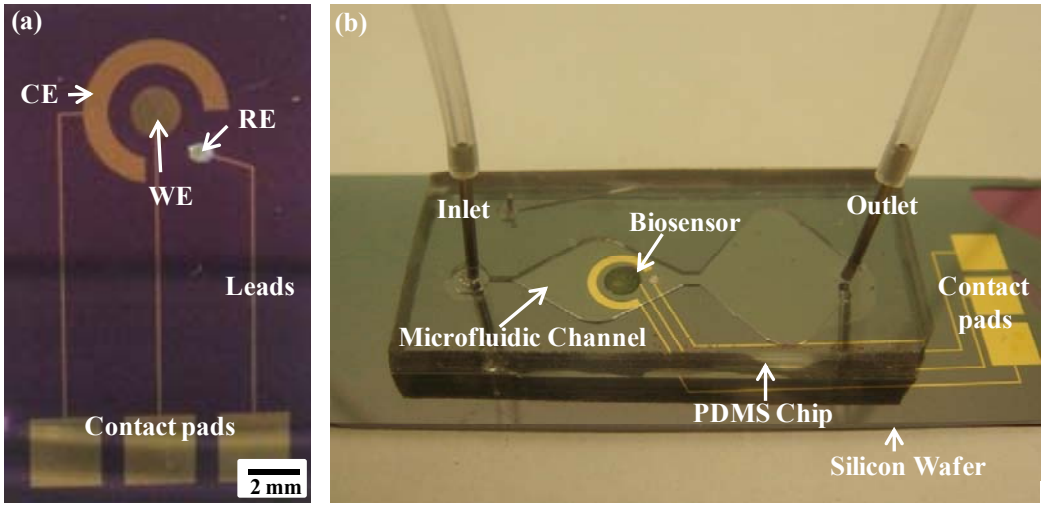

Figure 5.7: (a) A nanoporous, thin film and planar electrode system fabricated on a piece of silicon wafer. The diameter of the working electrode is 3 mm. (b) A biosensor embedded in a microfluidic chip. The depth of the microchannel is 50 µm. Control experiments were conducted using this configuration to show the advantages of nanoporous working electrodes in the microfluidic system.

www.manaraa.com

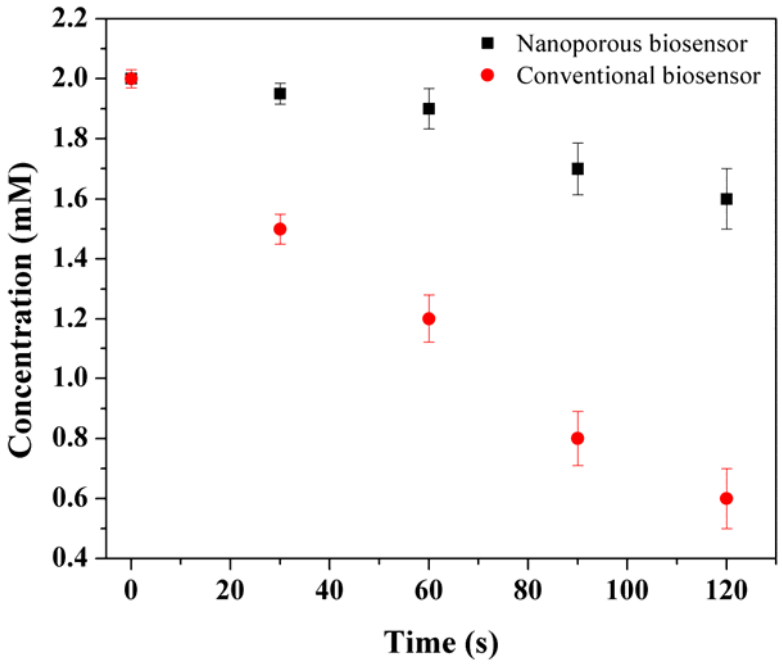

Figure 5.8: The duration of DI water flowing vs. the measured concentrations.

The advantage of the nanoporous electrode is also demonstrated by its superior performance after the enzyme and nafion are entrapped in electrodes. First, the nonporous structure possesses a larger surface area and more active sites, which results in an increase of steady-state Faraday current, compared with the flat electrode surface. Second, immobilization methods based on chemical modification can change the Michaelis-Menten constant of the enzymes because of the steric and conformational alterations [25]. Therefore, physical adsorption and entrapment is a better method to retain enzyme activity. Third, nanoporous metals can enhance the electrochemical transduction of redox enzymes. The continuity of metallic nanoscaled ligaments and nanoporous channels contributes to good electrical conductivity of nanoporous metals. The catalyst and the enzyme are well-dispersed and entrapped in the porous matrix, so that these form a conducting network aiding charge transfer through the film. Therefore, the biosensor has higher response to target analyte due to the high activity of electrocatalysis [26-27].

www.manaraa.com

5.4 Conclusions

We have successfully fabricated nanoporous structures directly on a planar thin film Au electrode, and applied them to configure an enzymatic electrochemical biosensor. Experimental results show that the layer of nanosized metallic ligaments and nanopores complexes possess 60 times more active surface area than a flat layer, and can act as an ideal platform for the immobilization of catalysts and enzymes, with enhanced charge transport and bioelectrocatalytic properties, yielding high electrochemical responses. The use of this sensor in the detection of glucose shows a wide linear range (up to 30 mM), high sensitivity (0.50 $\mu A\ mM^{-1}\ mm^{-2}$) and low interference. This work shows great promise for designing on-chip electrochemical biosensors used in point-of-care diagnostics.

www.manaraa.com

5.5 References

1. Chin, C.D., Linder, V., and Sia, S.K., Commercialization of microfluidic point-of-care diagnostic devices. Lab on a Chip, 2012. **12** (12): p. 2118-2134.

2. Ducrée, J., Haeberle, S., Lutz, S., Pausch, S., von Stetten, F., and Zengerle, R., The centrifugal microfluidic Bio-Disk platform. Journal of Micromechanics and Microengineering, 2007. **17**: p. S103.

3. Huang, Y., Williams, J.C., and Johnson, S.M., Brain slice on a chip: opportunities and challenges of applying microfluidic technology to intact tissues. Lab on a Chip, 2012. **12** (12): p. 2103-2117

4. Madou, M., Zoval, J., Jia, G., Kido, H., Kim, J., and Kim, N., Lab on a CD. Annual Review of Biomedical Engineering, 2006. **8**: p. 601-628.

5. Whitesides, G.M., The origins and the future of microfluidics. Nature, 2006. **442** (7101): p. 368-373.

6. Mir, M., A. Homs, and J. Samitier, Integrated electrochemical DNA biosensors for lab-on-a-chip devices. Electrophoresis, 2009. **30** (19): p. 3386-3397.

7. Vandaveer, I., Walter, R., Pasas Farmer, S.A., Fischer, D.J., Frankenfeld, C.N., and Lunte, S.M., Recent developments in electrochemical detection for microchip capillary electrophoresis. Electrophoresis, 2004. **25** (21-22): p. 3528-3549.

8. Wang, J., Ibáñez, A., Chatrathi, M.P., and Escarpa, A., Electrochemical enzyme immunoassays on microchip platforms. Analytical Chemistry, 2001. **73** (21): p. 5323-5327.

9. Carturan, G., Monte, R.D., Pressi, G., Secondin, S., and Verza, P., Production of valuable drugs from plant cells immobilized by hybrid sol-gel SiO_2. Journal of sol-gel science and technology, 1998. **13** (1): p. 273-276.

www.manaraa.com

10. Liu, Z., Liu, B., Kong, J., and Deng, J., Probing trace phenols based on mediator-free alumina sol-gel-derived tyrosinase biosensor. Analytical Chemistry, 2000. **72** (19): p. 4707-4712.

11. Wang, J., Carbon nanotube based electrochemical biosensors: A review. Electroanalysis, 2005. **17** (1): p. 7-14.

12. Hrapovic, S., Liu, Y., Keith, B., and Luong, J.H.T., Electrochemical biosensing platforms using platinum nanoparticles and carbon nanotubes. Analytical Chemistry, 2004. **76** (4): p. 1083-1088.

13. Karyakin, A.A., E.E. Karyakina, and L. Gorton, Amperometric biosensor for glutamate using Prussian blue-based "artificial peroxidase" as a transducer for hydrogen peroxide. Analytical Chemistry, 2000. **72** (7): p. 1720-1723.

14. Jia, F., Yu, C., Ai, Z., and Zhang, L., Fabrication of nanoporous gold film electrodes with ultrahigh surface area and electrochemical activity. Chemistry of materials, 2007. **19** (15): p. 3648-3653.

15. Trasatti, S. and Petrii, O., Real surface area measurements in electrochemistry. Pure and applied chemistry, 1991. **63** (5): p. 711-734.

16. Dungchai, W., Chailapakul, O., and Henry, C.S., Electrochemical detection for paper-based microfluidics. Analytical Chemistry, 2009. **81** (14): p. 5821-5826.

17. Zakharchuk, N.F., Meyer, B., Henning, H., Jaworksi, A., Scholz, F., and Stojek, Z., A comparative study of Prussian-Blue-modified graphite paste electrodes and solid graphite electrodes with mechanically immobilized Prussian Blue. Journal of Electroanalytical Chemistry, 1995. **398** (1): p. 23-35.

18. Ricci, F. and Palleschi, G., Sensor and biosensor preparation, optimisation and applications of Prussian Blue modified electrodes. Biosensors and Bioelectronics, 2005. **21** (3): p. 389-407.

www.manaraa.com

19. Bard, A.J. and Faulkner, L.R., Electrochemical methods: fundamentals and applications. Second ed. 2001, New York: Wiley.

20. Nie, Z., Nijhuis, C.A., Gong, J., Chen, X., Kumachev, A., Martinez, A.W., Narovlyansky, M., and Whitesides, G.M., Electrochemical sensing in paper-based microfluidic devices. Lab on a Chip, 2010. **10** (4): p. 477-483.

21. Hönes, J., Müller, P., and Surridge, N., The technology behind glucose meters: test strips. Diabetes Technology & Therapeutics, 2008. **10** (S1): p. 10-26.

22. Martinez, A.W., Phillips, S.T., Carrilho, E., Thomas III, S.W., Sindi, H., and Whitesides, G.M., Simple telemedicine for developing regions: camera phones and paper-based microfluidic devices for real-time, off-site diagnosis. Analytical Chemistry, 2008. **80** (10): p. 3699-3707.

23. Itaya, K., Shoji, N., and Uchida, I., Catalysis of the reduction of molecular oxygen to water at Prussian Blue modified electrodes. Journal of the American Chemical Society, 1984. **106** (12): p. 3423-3429.

24. Karyakin, A.A., Karyakina, E.E., and Gorton, L., On the mechanism of H_2O_2 reduction at Prussian Blue modified electrodes. Electrochemistry Communications, 1999. **1** (2): p. 78-82.

25. Guisan, J.M., Immobilization of Enzymes as the 21st Century Begins. Immobilization of enzymes and cells, 2006. **22**: p. 1.

26. Yu, C., Jia, F., Ai, Z., and Zhang, L., Direct oxidation of methanol on self-supported nanoporous gold film electrodes with high catalytic activity and stability. Chemistry of materials, 2007. **19** (25): p. 6065-6067.

27. Zhang, J., Liu, P., Ma, H., and Ding, Y., Nanostructured porous gold for methanol electro-oxidation. The Journal of Physical Chemistry C, 2007. **111** (28): p. 10382-10388.

www.manaraa.com

Chapter 6

6 A Robust Lab-on-a-CD System for High-throughput and Automated Whole Blood Analysis

Based on the blood separation technique and the electrochemical detection method introduced above, a Lab-on-a-CD prototype was built and its performance is evaluated in this chapter. The detections of the concentrations of glucose, lactate and uric acid were employed as examples to prove the robustness of the prototype.

6.1 Introduction

A massive inequality in health exists across the globe. Medical care in low resource areas requires the development of a portable, low cost and effective monitoring and diagnostic method [1-6]. In field blood tests and remote medical care are the best option to provide a comprehensive treatment for patients. Blood tests are the most commonly-used diagnostic methods currently because blood analysis provides definitive information about patients' medical conditions. Comprehensive blood analysis, including sample collection, preparation and detection, is conducted using large-scale blood analyzers and has not become fully point-of-care (POC) yet.

Lab-on-a-chip [7] technology provides an automatic, cost-effective and fast solution for a wide variety of blood analyses. As a main branch of Lab-on-a-chip technology, the Lab-on-CD (compact disc) technique [8] is a promising and attractive option due to the centrifugal force applied during the rotation of the disk. The centrifugal force is able to drive flow from the center of the rotation to the edge of the centrifugal platform, transporting samples and reagents from the inlet reservoirs to the metering, mixing, reaction, detection and waste reservoirs.

www.manaraa.com

The Lab-on-a-CD platform possesses the potential to integrate all conventional blood analysis steps into one continuous process. A large number of research groups have engaged in the exploration of the Lab-on-a-CD system for blood analysis. So far, the major achievement is performing blood separation on the centrifugal platform [9-13]. Sample manipulation, including valving [14], metering [15], and mixing [16], have also been successfully demonstrated on the platform. However, these are only pre-process steps for blood analysis, and their designs are delicate, requiring complicated fabrication steps. Furthermore, quantitative detection of blood samples has not yet been integrated on the centrifugal platform.

Since blood separation is prior to subsequent blood tests in clinical diagnosis [9, 12, 13], our group has demonstrated the robustness of using 3D out-of-plane microvalves for whole blood separation on a centrifugal platform [12]. The microfluidic cartridge was composed of two reservoirs (inner and outer reservoirs), which were connected by the out-of-plane microvalve. This design aims to reduce the complexity of the system by eliminating the step of blood plasma transfer. The inner reservoir served as a sample collection reservoir at the sample loading step, and turned into a detection reservoir at the quantitative analysis step. The electrochemical system embedded in the inner reservoir was pre-loaded with catalyst and enzyme, which risked being washed off under the high speed of the blood flow. We designed and fabricated a type of nanoporous thin-film working electrode to overcome this technical problem (Chapter 5). All the work is dedicated to the developing a low-cost, portable system for multiple and parallel POC blood analyses. In the following sections, the design and fabrication of the completed Lab-on-a-CD system is elucidated in detail, while the performance of the system is demonstrated and evaluated.

www.manaraa.com

6.2 Theory and Design of System

Based on its functions, the Lab-on-a-CD system can be divided into an upstream section for whole blood separation and a downstream section for quantitative analysis. My design employed the centrifugal force as the driving force for blood pumping and separation. The centrifugal force of the Lab-on-a-CD system is ideal for separating blood cells from plasma according to their density difference, because it shares the same mechanism as the conventional bench-top blood separation approach using a large, high-speed centrifuge. The microfluidic structure was created on a centrifugal platform, extending with its inner and outer radial positions of 13 mm and 33 mm, respectively. While the centrifugal platform rotated, blood cells moved outward to the outer reservoirs and plasma was squeezed inward to the inner reservoirs. As the volume percentage of red blood cells in blood (hematocrit) is less than 50% [17] and the volume ratio of the outer reservoir to the inner reservoir is 1.5, the blood cells only accumulated in the outer reservoir. 3D Out-of-plane microvalves were employed to isolate the inner reservoirs and the outer reservoirs, ensuring the purity of plasma in the inner reservoirs [12]. Obviously, the functions of the micropumps and microvalves were realized on the CD platform at the same time without integration of actuation and any auxiliary equipment, which greatly reduces the complexity and the cost of the system. Afterwards, an electrochemical system with high sensitivity and selectivity was placed in the inner reservoirs downstream to extract biological information from the purified plasma. The contents of the plasma reacted with enzymes and produced electroactive species, which were electrochemically oxidized or reduced at metal electrodes. Under the potential provided from a meter, current was generated from the electrons produced in redox. This current was calibrated to measure the concentration of the constituents in whole blood. Without the disturbance from the blood cells, the results from electrochemical detection will have a high accuracy.

Based on the spatial structure, the Lab-on-a-CD system can be exploded into three layers (Figure 6.1). The top layer is a microfluidic cartridge, which was casted from a polymer mold. Microfluidic channels, inlets and vents are arranged in this layer to connect the microfluidic system to the macro-world. The middle layer serves as an insulating layer

www.manaraa.com

that covers the leads and exposes the surface areas of the electrodes and the contact pads. Electrochemical biosensors for quantitative analysis and 3D out-of-plane valves are designed on the bottom layer. The electrochemical biosensors were connected to a potentiostat through the contact pads. In a test, a whole blood sample was loaded into one of the sections through an inlet, and the blood plasma was obtained and retained in the inner reservoir under the centrifugal force field. As it was electrically connected to the biosensor, the potentiostat applied potential between a working electrode and a counter electrode and acquired a relevant electrical signal, which can be used to calculate the concentration of a specific analyte. Multiple sections can be arranged in one circular platform, and each section can independently perform a test. These duplicate sections can either measure different contents for the same blood sample, or detect the same constituents for diverse blood samples. This is a continuous process, including sample collection, preparation and detection, reducing the turn-around time and risk of human errors in processing steps. This is also a miniaturized device, which reduces the consumption of blood samples and reagents.

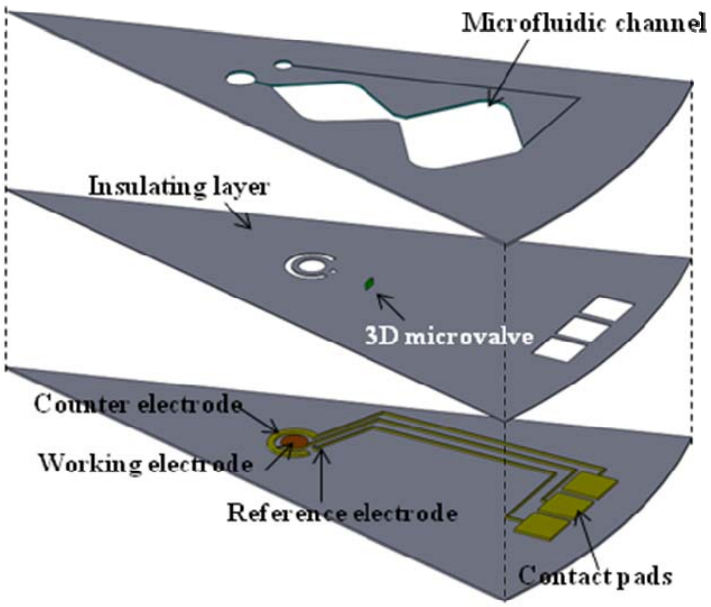

Figure 6.1: Exploded view of the configuration of one Lab-on-a-CD section. It is comprised of a microfluidic layer, an insulating layer and a biosensing layer.

www.manaraa.com

6.3 Experimental

6.3.1 Materials and apparatus

D-(+)-glucose, glucose oxidase (GOx, Type X-S, 250 units/mg), uric acid, uricase (UOx), sodium L-lactate (~98%), lactate oxidase (LOx, ≥ 20 U/g, Sigma), human serum (S2257-1ml), bovine serum albumin (BSA), iron (III) chloride, and potassium ferricyanide (III) ascorbic acid, (100 - 250 U/mg), Nafion (5 wt. %), PDDA (20 wt % in water), glucose assay kit, lactate assay kit, uric acid kit and benzyl alcohol (anhydrous, 99.8%) were purchased from Sigma-Aldrich. Piranha solution was made using H_2O_2 (30%) and H_2SO_4 (conc) solution in 1:3 vol/vol ratio. The multi-wall carbon nanotubes (MWCNT) with 95% purity (purchased from US Research Nanomaterials, Inc) are cylindrical with a diameter in the range 5 – 15 nm. All processing solutions were prepared with de-ionized (DI) water from a Milli-Q system (Millipore, Bedford, MA) and all other chemicals were of analytical grade. 20 mM phosphate buffer solutions (PBS) with 0.1 M KCl were freshly prepared every week. Human serum samples were prepared by dissolving lyophilized sera with 1 ml DI water. All chemicals were employed without further purification. All electrochemical experiments in this experiment were performed on a computer-controlled potentiostat (CHI1200a, CHI Instruments, Inc., USA). A UV-visible spectrophotometer from Varian was employed to provide references of analytes' concentrations in samples using the standard assay kits. A brushless servomotor with a servo drive was employed to control the motion of the Lab-on-a-CD system.

6.3.2 Device fabrication

6.3.2.1 Fabrication of microfluidic cartridge

A microfluidc cartridge was designed using AutoCAD, and its layout was printed on a piece of acetate sheet as a photomask using a high-resolution (2000DPI) printing service from CAD/Art Service Inc.. A polymer mold was fabricated on a silicon wafer using a standard photolithography technique. The microfluidic cartridge made of polydimethysiloxane (PDMS) was replicated from the polymer mold. A large number of

www.manaraa.com

PDMS microfluidic cartridges could be repeatedly replicated from one polymer mold. The details of the fabrication steps are available in my previous publication [12].

As shown in Figure 6.2a, the microfluidic cartridge is comprised of eight parallel sections, and each section is composed of a sample inlet, an inner (sampling and detection) reservoir, an outer (blood cells) reservoir and a vent. The depth of the microfluidic structure is 100 μm, and the volumes for the inner reservoir and outer reservoir are 6.5 μL and 9.5 μL, respectively. Since the PDMS layer is inversely bonded to the biosensing layer, the out-of-plane microvalves were not directly fabricated on the PDMS microfluidic channels. They were arranged on the biosensing layer, and would insert into the microfluidic channels after assembly, serving as out-of-plane valves. (Figure 6.2c)

6.3.2.2 Fabrication of biosensors

The design for the biosensor is based on the electrochemical detection technique. The planar electrochemical system contains a microfabricated Au working electrode, a silver/silver chloride reference electrode and a Au counter electrode (Figure 6.2b). Through an alloy/dealloy process, the working electrode was made to be nanoporous and then was modified with four layers: a multi-wall carbon nanotubes (MWCNT) layer, a catalyst layer (Prussian Blue), an enzyme layer and a semi-permeable layer (Nafion) (from bottom to top). The detailed procedure is as follows:

(1) Defined the surface area of the electrode system on a silicon wafer (with a 1000 nm thick silicon dioxide layer on top) using positive photoresist and deposited a 100 nm thick Au layer over the patterned photoresist layer. Lifted off the photoresist, leaving an area with coated Au to be used for the electrodes, the leads and the conductive pads.

www.manaraa.com

(2) Defined the surface area of the working electrode using positive photoresist and deposited a 500 nm thick Zn layer on top of the Au layer. Lifted off the unwanted Zn area and formed the nanoporous structure on the working electrode (chapter 5).

(3) Defined the surface area of the reference electrode using positive photoresist and deposited a 500 nm thick Ag layer on top of the Au layer. Lifted off the unwanted Ag area and dipped the wafer sample into 50 mM $FeCl_3$, forming a Ag/AgCl standard reference electrode.

(4) Covered the leads with a layer of negative photoresist, only exposing the areas of the electrodes and the conductive pads on the whole wafer.

(5) Physically deposited 10 μL of MWCNT (1 mg/ml) onto the surface of the working electrode.

(6) Electrodeposited a PB layer as a catalyst layer, physically deposited bovine serum albumin (BSA) and enzyme mixture as a biomarker layer, physically deposited 10% Nafion solution as a semi-permeable layer. These layers were all overlaid on the working electrode.

6.3.2.3 Device assembly

The microfluidic layer was washed with isopropanol and DI water, respectively. Next, it was cleaned and hydrophilicly modified in a 15 minute UV - Ozone treatment process. Right after this treatment, the microfluidic layer was placed on the silicon wafer layer, on which the biosensing components and out-of-plane valves were arranged. Alignment marks were designed and fabricated into both layers to assure alignment was accurate. Subsequently, these two assembled layers were pressed together with a force of 10 N for 2 hours to increase the bonding strength. Finally, the Lab-on-a-CD system was completely built up (Figure 6.2c), and stored in a fridge (4°C) for further testing.

www.manaraa.com

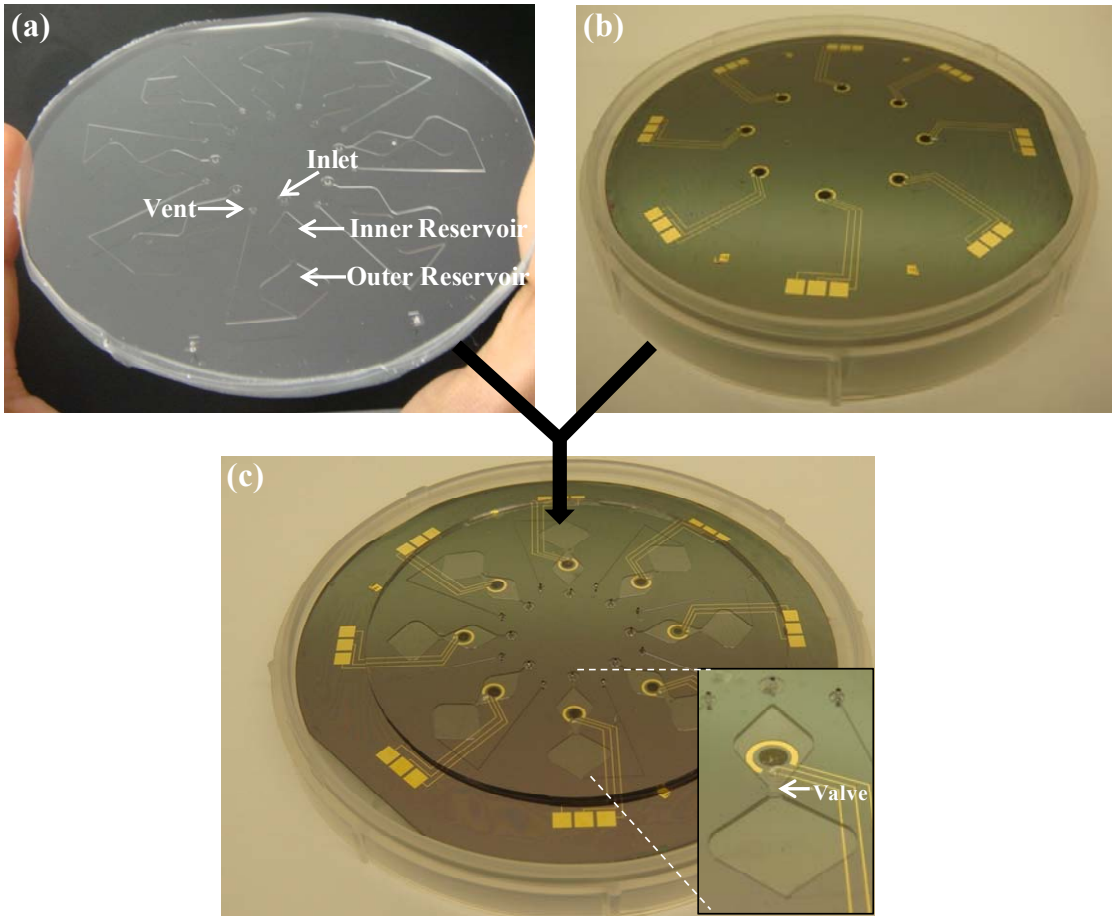

Figure 6.2: Photo of components and assembled device. (a) a microfluidic cartridge made of PDMS; (b) An array of electrochemical biosensors built on a Si wafer; (c) assembly of the PDMS chip and the Si wafer.

6.3.3 Measurements

The Lab-on-a-CD panel was placed on a motor and commands were sent from a graphical user interface to control the motion of the CD panel. The electrochemical results were read by a portable potentiostat and fed into a personal computer.

www.manaraa.com

Human serum sample was formulated by dissolving lyophilized sera with 1 mL DI water, and the concentrations of its analytes were measured based on a spectrophotometric method using three standard test kits. Then serum samples with different concentrations of glucose, uric acid and lactate were prepared by diluting with DI water or adding more analytes. The spiked serum samples were directly loaded in some of the sections of the system without the rotation of the CD panel, and the calibration data was obtained from the potentiostat. Human whole blood was taken from healthy donors at the University Hospital and stored in an anticoagulant (EDTA) treated vacutainer tube. Once the calibration curve was drawn, whole blood samples were loaded into the unused sections of the system, and the testing procedure is shown as follows (Figure 6.3):

(1) A 16 μL blood sample was transferred from the vacutainer tube to the inlet of the cartridge using a syringe.

(2) The Lab-on-a-CD panel was rotated at 2000 rpm for 280 seconds.

(3) The Lab-on-a-CD panel stopped rotating and the leads of the potentiostat were connected to the conductive pads on each section of the CD panel.

(4) Electrochemical measurements were carried out by applying potential from the potentiostat.

(5) Current values vs. time were recorded in a computer through commercial software.

(6) The current values at 150 second were picked up and used to calculate the concentrations of analytes.

www.manaraa.com

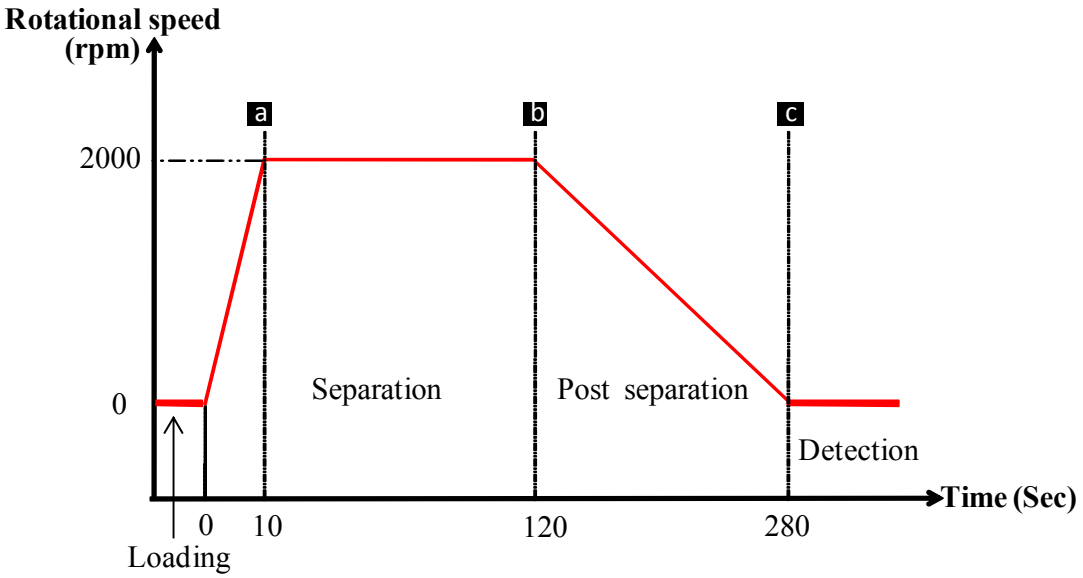

Figure 6.3: Schematics of the experimental steps. A blood sample was loaded into the system at 0 rpm. The rotational speed was ramped from 0 rpm up to 2000 rpm in the first 10 second. The speed was kept at 2000 rpm for 110 seconds, and then slowly decreased to 0 rpm. Electrochemical measurements were conducted when the circular platform was stationary.

6.4 Results and Discussion

6.4.1 Device characterization

Each Lab-on-a-CD panel can continuously accomplish sample collection, preparation (separation) and detection. Figure 6.4 demonstrates the whole system setup. As shown in the insert of Figure 6.4a, the blood sample filled the inner reservoirs and outer reservoirs, and the biosensor was immersed in the sample. The electrochemical reaction will not start until the potential was applied from the potentiostat. Once the panel started rotating, the blood cells with higher density flowed outward to the outer reservoirs, the so called blood cells reservoirs. Meanwhile, the plasma was squeezed inward to the inner reservoirs (plasma reservoirs). When the panel stopped moving, the out-of-plane microvalves broke

www.manaraa.com

the flow in the microfluidic channels, isolating the separated blood cells and plasma (Figure 6.4b).

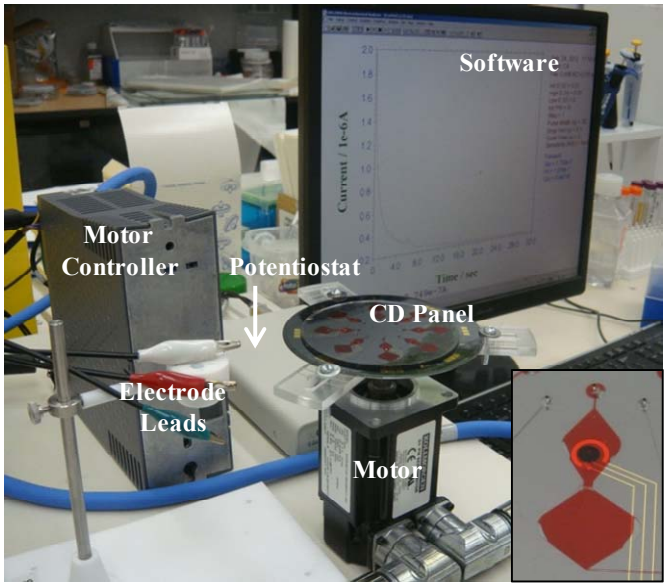

(a)

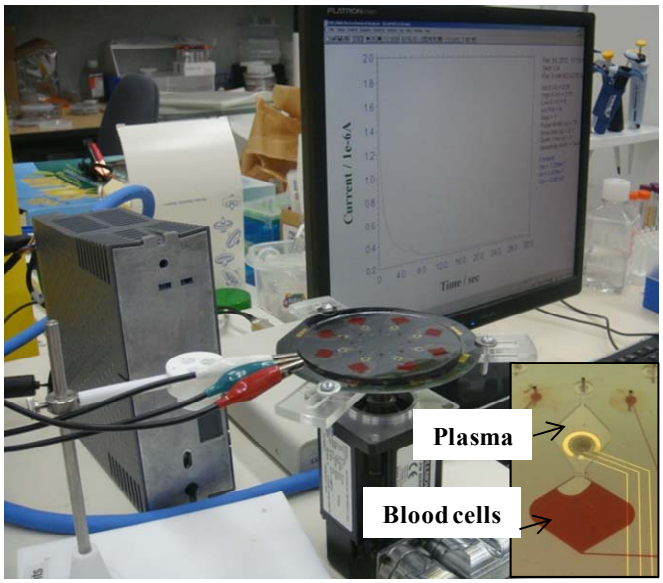

(b)

Figure 6.4: Whole blood analysis using a Lab-on-a-CD system. (a) sample loading and ready for rotation; (b) Rotation ceased and electrochemical signals measured.

www.manaraa.com

The device was first characterized by its bonding strength. For the rotational speed of 2000 rpm, the blood sample with a density of 1125 kg/m^3 exerted approximately 25 kPa to the interface of the outer reservoir's perimeter. The higher the rotational speed, the larger the pressure of blood flow would be. Without enough bonding strength, blood leaked out of the system, resulting in a failed measurement. Two parameters used in the fabrication process to control the bonding strength were the duration of UV-Ozone treatment and the duration of diffusion bonding. Bonding force was optimized at 10 N, avoiding the collapse of the microfluidic structure. At a rotational speed of 2000 rpm, 15 minutes UV-Ozone treatment and 2 hour diffusion bonding can protect the device from leakage. Meanwhile, this bonding is not a permanent bonding, so the assembled layers can be separated and cleaned for further experiments. For disposable cartridges, permanent bonding can be applied by using longer UV-Ozone treatment and diffusion bonding.

6.4.2 Quantitative measurement

Biodetection was carried out when the potential from a potentiostat was applied on these electrodes. We designed this system as a universal system by electrochemically detecting H_2O_2, generated by the analytes in their enzymatic reactions (Equation 6.1 – 6.3) [18-20]. The amount of H_2O_2, which is proportional to the concentration of the analyte, can catalytically react with the Prussian white (PW) by oxidizing PW to PB and PB itself is, in turn, electrochemically reduced back to PW under the applied potential on the surface of the working electrode (Equation 6.4). For a demonstration of the universal property of this system, three enzymes (GOx, UOx, and LOx) were immobilized on different working electrodes to measure glucose, uric acid, and lactate, respectively.

$$\beta - D - \text{glucose} + O_2 \xrightarrow{GOx} \text{gluconolactone} + H_2O_2 \tag{6.1}$$

$$\text{uric acid} + O_2 + H_2O \xrightarrow{UOx} \text{allantoin} + CO_2 + H_2O_2 \tag{6.2}$$

$$L\text{-Lactate} + O_2 \xrightarrow{L\,Ox} \text{Pyruvate} + H_2O_2 \tag{6.3}$$

www.manaraa.com

$$K_2Fe^{2+}Fe^{2+}(CN)_6 + 2H_2O_2 \leftrightarrow KFe^{3+}Fe^{2+}(CN)_6 + K^+ + 2H_2O + O_2 \qquad (6.4)$$

These three kinds of biosensors were first calibrated with spiked serum samples using chronoamperometry. In the chronoamperometric measurement, constant potential (0 V vs Ag/AgCl) was applied between the working electrode and the counter electrode to measure the current due to the cathodic reduction of hydrogen peroxide aided by PB [21]. The current induced by electron transfer is called as the Faradic current and is proportional to the concentration of the analyte. From Figures 6.5 – 6.7, we can see that a large capacitive current is present at the beginning, and then Faradic current occurs and decays as $t^{-1/2}$ until it reaches a steady state. The relationship of the Faradic current and analyte concentration can be described by the Cottrell equation (for planar electrodes) [22].

$$i = \frac{nFAD^{1/2}}{(\pi t)^{1/2}} C^0 \qquad (6.5)$$

Where i is the Faradic current, n is the number of electrons, F is Faraday's constant, A is the area of the electrode, t is the time, D and C^0 are the diffusion coefficient and the initial concentration of the target analyte, respectively. The steady state currents at 150 sec were used to configure the calibration curves for the following analysis. The calibration curve for glucose (Figure 6.5) shows linearity from 0 mM - 25 mM (R^2 = 0.9929, n = 5), while the linear ranges for uric acid (Figure 6.6) and lactate (Figure 6.7) are 0 mM - 5 mM (R^2 = 0.9948, n = 5) and 0 mM – 1.5 mM (R^2 = 0.9950, n = 5), respectively.

The normal level of glucose is from 3.5 to 5.3 mM in whole blood, and the conventional detection limit is 0.5 mM with colorimetric methods and 1 mM with glucometers [23, 24]. The linear range of glucose provided by our Lab-on-a-CD system covers the entire range of normal human blood glucose levels, with a competitive detection limit of 0.3 mM. The Lab-on-a-CD system also shows competitive performance for the detection of uric acid and lactate by covering the normal concentration ranges of uric acid (0.1 – 0.4 mM) and lactate (0.7 – 1.7 mM).

www.manaraa.com

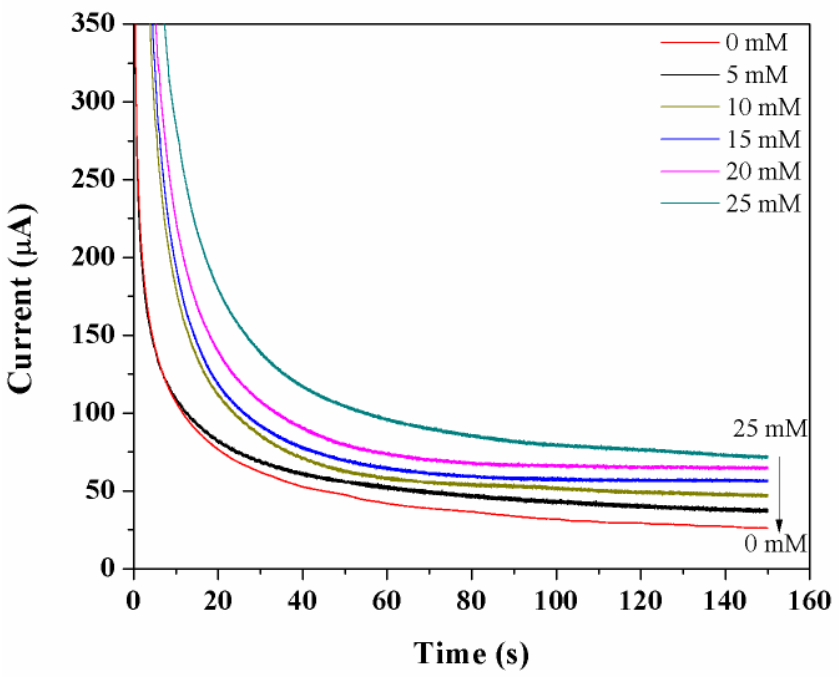

(a)

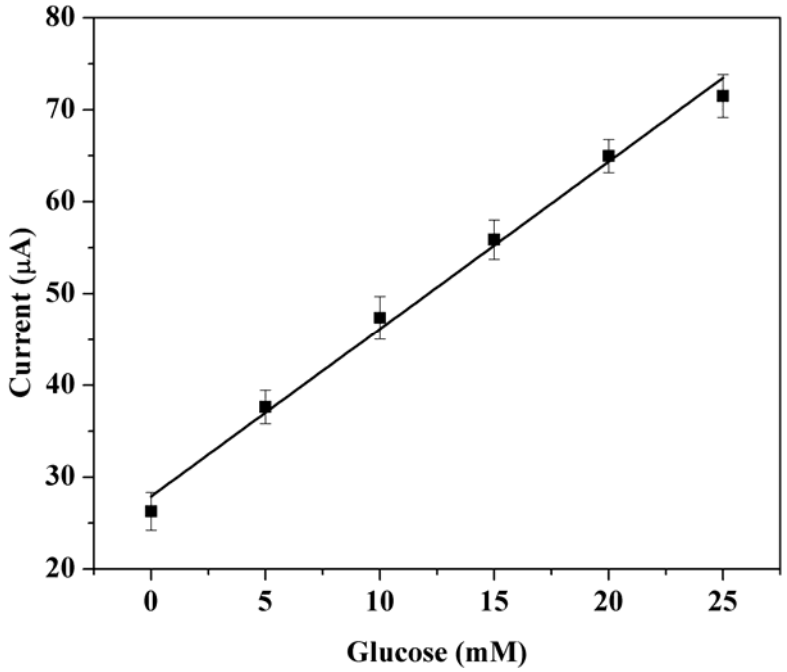

(b)

Figure 6.5:(a) Chronoamperograms of glucose with concentration from 0 mM to 25 mM. (b) Currents at 150th second plotted as a function of the concentration of glucose.

www.manaraa.com

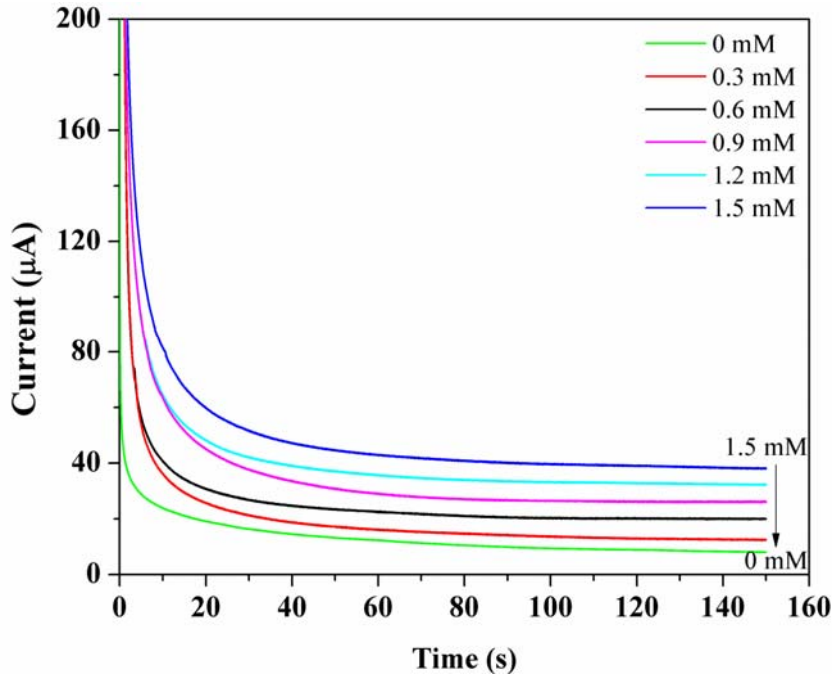

(a)

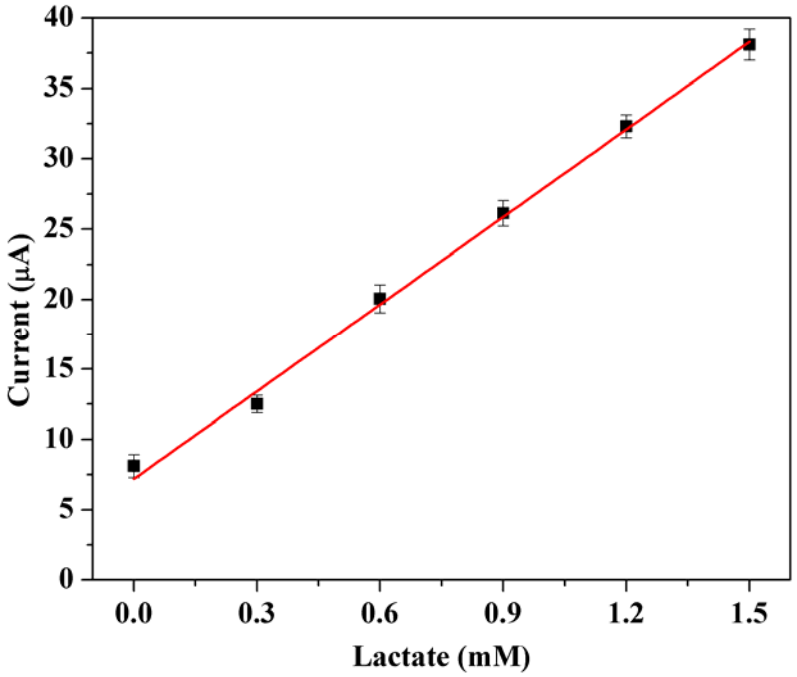

(b)

Figure 6.6:(a) Chronoamperograms of lactate with concentration from 0 mM to 1.5 mM. (b) Currents at 150th second plotted as a function of the concentration of lactate.

www.manaraa.com

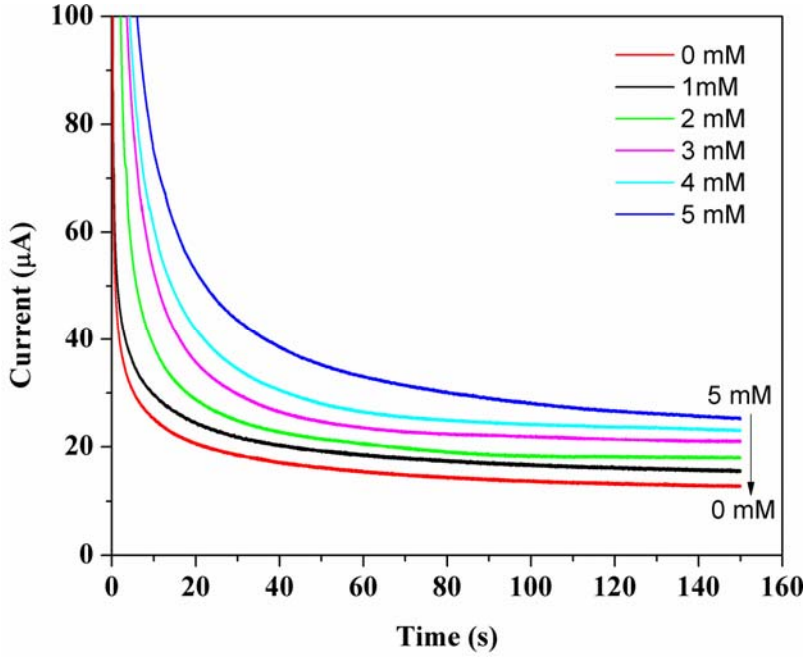

(a)

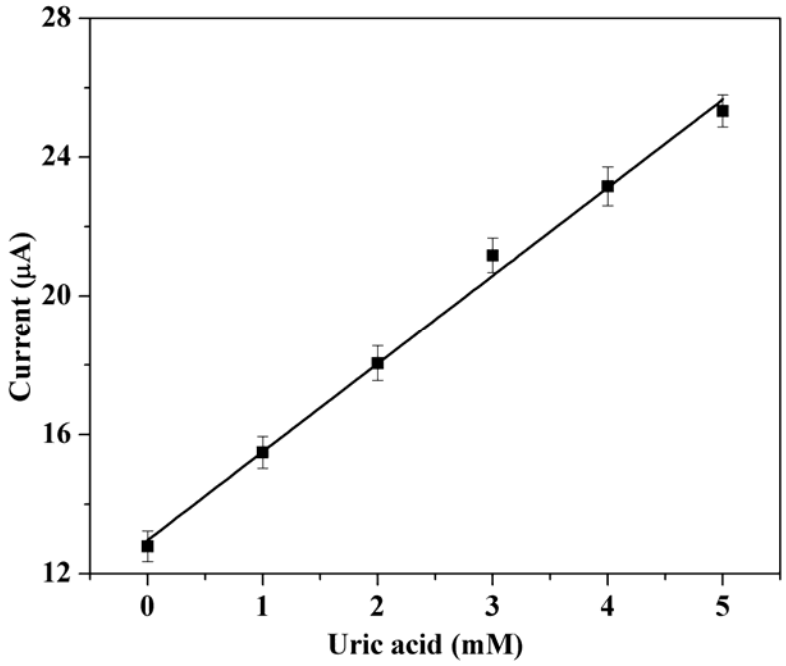

(b)

Figure 6.7:Chronoamperograms of uric acid with concentration from 0 mM to 5 mM. (b) Currents at 150th second plotted as a function of the concentration of uric acid.

www.manaraa.com

By collecting the steady state currents of the separated plasma from unknown human whole blood samples, we can calculate the concentration of the analyte using the calibration curves obtained above. The quantitative results generated by the Lab-on-a-CD system were compared with the reference values that were measured by spectrophotometric method using standard test kits [25].

The measured value of glucose with the spectrophotometric method was 5.43 ± 0.08 mM, whilst it was 5.21 ± 0.03 mM with the electrochemical method using the Lab-on-a-CD system. Only a 4.2% difference exists between these two methods. The differences for lactate and uric acid are 5.2% and 6.0%, respectively (Figure 6.8). This data proves the practical utility of the proposed Lab-on-a-CD system. The robustness of the biosensor was further proved by retaining approximately 85% of its initial sensitivity after a week stored in PBS in a fridge (4°C).

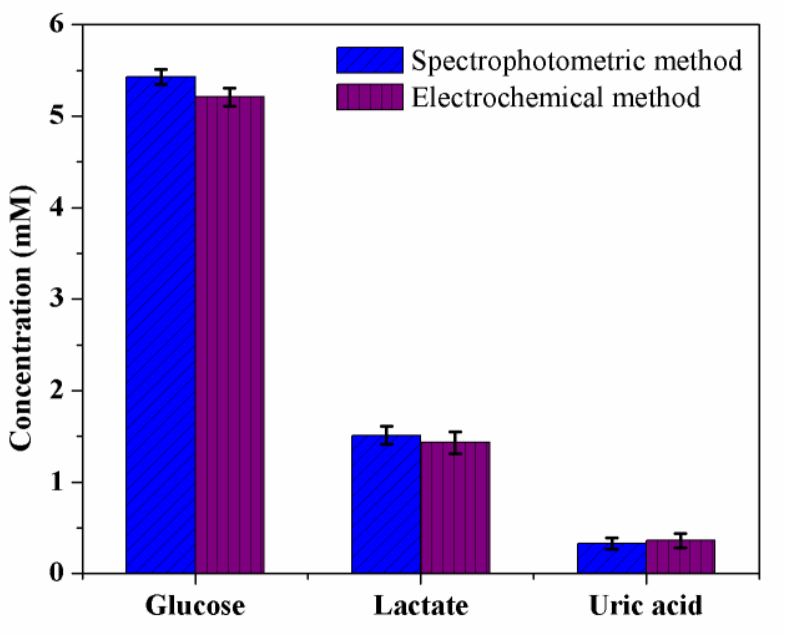

Figure 6.8: The measured concentrations of glucose, lactate and uric acid with the spectrophotometric method and the electrochemical method. The value differences between these two methods are 4.2%, 5.2% and 6.0%, respectively.

www.manaraa.com

6.4.3 Discussion

The Lab-on-a-CD system here integrates three major steps of blood analysis into one continuous process and provides quantitative information about human whole blood.

The nanoporous structure designed on the working electrode plays an important role in the success of the Lab-on-a-CD system. On this centrifugal platform, a large number of blood cells migrated at a high speed, and the resulting momentum was continuously exerted on the enzyme and catalyst layer that were deposited on the surface of the working electrode. Entrapped by the nanoporous working electrode, the deposited materials avoided being washed away.

The measurement using this Lab-on-a-CD system possesses the accuracy to compete with the conventional hospital measurement using sophisticated equipment carried out in large central laboratories. As the disturbance from blood cells is eliminated, the accuracy of the measured signal can be improved by about 10 - 15%, compared to the existing commercial glucometers, which are based on electrochemical measurement with the un-separate whole blood. That is also the reason that hospitals still rely on the results using separated plasma for diagnosis. The results from glucometers are only for monitoring purposes or used as a reference. Furthermore, as this system integrates three separate steps into one process, the possible errors due to human operation can be avoided. For example, mislabelled samples, improper storage environment, etc. This system also provides a visible detection process for patients, which can build their trust in the results. Therefore, the system can give patients fast and straightforward results.

This is a universal platform for blood diagnostics. Besides glucose, uric acid and lactate, we can extract more information from blood plasma by simply changing the enzyme. Only if the enzymatic reaction produces H_2O_2, can the biosensor detect the concentration

www.manaraa.com

of the analyte. This is also a high throughput measurement platform, on which more than ten tests can be performed at a time. Normally, one piece of information from a patient's blood sample is not enough to conclude on his/her medical condition. Multiple tests are necessary for a comprehensive diagnosis. With this system, the efficiency of diagnosis is boosted, and the use of the blood sample is more efficient.

6.5 Conclusions

We designed a Lab-on-a-CD system to automate all of the manual steps of the traditional blood analysis process. In our system, we achieve this automation by designing a microfluidic system around electrochemical biosensors. Although only glucose, lactate and uric acid were analyzed, the Lab-on-a-CD prototype is designed as a universal platform to detect the concentration of analytes in whole blood based on the production of hydrogen peroxide in enzymatic reactions.

www.manaraa.com

6.6 References

1. Girosi, F., Olmsted, S. S., Keeler, E., Burgess, D. C. H., Lim, Y. W., and Aledort, J. E., Developing and interpreting models to improve diagnostics in developing countries. Nature, 2006. 444: p. 3-8.

2. Martinez, A. W., Phillips, S. T., Whitesides, G. M., and Carrilho, E., Diagnostics for the developing world: microfluidic paper-based analytical devices. Analytical Chemistry, 2009. 82 (1): p. 3-10.

3. Iverson, E. and Rabinovich, R., Foreword-Global Access to Health: Legal, Business, and Policy Obstacles. Am. JL & Med., 2008. 34: p. 97.

4. Burgess, D.C.H., Wasserman, J. and Dahl, C.A., Global health diagnostics. Nature, 2006. 444: p. 1-2.

5. Lee, W. G., Kim, Y. G., Chung, B. G., Demirci, U., and Khademhosseini, A., Nano/Microfluidics for diagnosis of infectious diseases in developing countries. Advanced Drug Delivery Reviews, 2010. 62 (4-5): p. 449-457.

6. Urdea, M., Penny, L. A., Olmsted, S. S., Giovanni, M. Y., Kaspar, P., and Shepherd, A.,, Requirements for high impact diagnostics in the developing world. Nature, 2006. 444: p. 73-79.

7. Stone, H.A., Stroock, A.D. and Ajdari, A., Engineering flows in small devices. Annu. Rev. Fluid Mech., 2004. 36: p. 381-411.

8. Madou, M., Zoval, J., Jia, G., Kido, H., Kim, J., and Kim, N., Lab on a CD. Annu. Rev. Biomed. Eng., 2006. 8: p. 601-628.

9. Amasia, M. and Madou, M., Large-volume centrifugal microfluidic device for blood plasma separation. Bioanalysis, 2010. 2 (10): p. 1701-1710.

www.manaraa.com

10. Cho, Y. K., Lee, J. G., Park, J. M., Lee, B. S., Lee, Y., and Ko, C., One-step pathogen specific DNA extraction from whole blood on a centrifugal microfluidic device. Lab Chip, 2007. 7 (5): p. 565-573.

11. Kobayashi, T., Funamoto, T., Hosaka, M., and Konishi, S., Centrifugal separation device based on two-layer laminar flow in microchannels for high-throughput and continuous blood cell/plasma separation. Japanese Journal of Applied Physics, 2010. 49 (7): p. 7001.

12. Li, T., Zhang, L., Leung, K. M., and Yang, J., Out-of-plane microvalves for whole blood separation on lab-on-a-CD. Journal of Micromechanics and Microengineering, 2010. 20: p. 105024.

13. Zhang, J., Guo, Q., Liu, M., and Yang, J., A lab-on-CD prototype for high-speed blood separation. Journal of Micromechanics and Microengineering, 2008. 18: p. 125025.

14. Mark, D., Haeberle, S., Metz, T., Lutz, S., Ducrée, J., and Zengerle, R., Aliquoting structure for centrifugal microfluidics based on a new pneumatic valve. 2008: IEEE.

15. Steigert, J., Brenner, T., Grumann, M., Riegger, L., Lutz, S., and Zengerle, R., Integrated siphon-based metering and sedimentation of whole blood on a hydrophilic lab-on-a-disk. Biomedical Microdevices, 2007. 9 (5): p. 675-679.

16. Grumann, M., Geipel, A., Riegger, L., Zengerle, R., and Ducrée, J., Batch-mode mixing on centrifugal microfluidic platforms. Lab Chip, 2005. 5(5): p. 560-565.

17. Ma, J. Z., Ebben, J., Xia, H., and Collins, A. J., Hematocrit level and associated mortality in hemodialysis patients. Journal of the American Society of Nephrology, 1999. 10 (3): p. 610-619.

18. Dussossoy, D., Py, M., Pastor, G., and Boulenc, X., Development of a two-site immunoassay of recombinant urate oxidase (SR 29142) and its use for determination

www.manaraa.com

of pharmacokinetic parameters in rats and baboons. Journal of pharmaceutical sciences, 1996. 85 (9): p. 955-959.

19. Raab, L. S., Decker, G. L., Jonas, A. J., Kaetzel, M. A., & Dedman, J. R., Glucocorticoid regulation of rat liver urate oxidase. Journal of cellular biochemistry, 1991. 47 (1): p. 18-30.

20. Karyakin, A.A., Karyakina, E.E. and Gorton, L., On the mechanism of H_2O_2 reduction at Prussian Blue modified electrodes. Electrochemistry Communications, 1999. 1(2): p. 78-82.

21. Dungchai, W., Chailapakul, O., and Henry, C.S., Electrochemical detection for paper-based microfluidics. Analytical Chemistry, 2009. 81 (14): p. 5821-5826.

22. Bard, A.J. and Faulkner, L.R., Electrochemical methods: fundamentals and applications. Second ed. 2001, New York: Wiley.

23. Hönes, J., Müller, P. and Surridge, N., The technology behind glucose meters: test strips. Diabetes Technology & Therapeutics, 2008. 10 (S1): p. 10-26.

24. Martinez, A. W., Phillips, S. T., Carrilho, E., Thomas III, S. W., Sindi, H., & Whitesides, G. M., Simple telemedicine for developing regions: camera phones and paper-based microfluidic devices for real-time, off-site diagnosis. Analytical Chemistry, 2008. 80 (10): p. 3699-3707.

25. Lamprecht, W., Trautschold, I. and Bergmeyer, H., Methods of enzymatic analysis. Methods of enzymatic analysis, 1974.

www.manaraa.com

Chapter 7

7 Thesis Summary and Future Work

7.1 Summary

Without a complex integration of the actuating mechanism and associated marco-to-micro interface, a Lab-on-a-CD prototype has been successfully built and tested. It can perform blood delivery, separation and detection in a continuous automated process. The entire blood analysis procedure is completed on a compact Lab-on-a-CD platform developed in this thesis. Whole blood samples were first collected and injected into the system through sample inlets. Blood was delivered into different sections by the universal centrifugal force due to the CD spinning. Blood cells and plasma were separated under the centrifugal force field, and were isolated by the integrated out-of-plane microvalves. Without being transferred to adjacent detection chambers, the extracted pure plasma was analyzed by the electrochemical biosensors underneath. The working electrodes of the electrochemical biosensors were made nanoporous in order to increase the electroactive surface area and firmly confine the coated material. Quantitative information about glucose, lactate and uric acid was obtained. The menu of detectable analytes can be readily expanded to other biochemical reactions where hydrogen peroxide is produced in enzymatic reactions. With modification of the biosensor configuration, the whole panel of blood tests may be realized on such Lab-on-a-CD systems.

7.2 Thesis Contribution

The Lab-on-a-CD system developed here is an integrated platform demonstrating an effective approach to process samples that are appropriate for point-of-care diagnostics, especially for the use in low-resource settings. This design fills the gap between the costly, non-instrumented sample pre-processing steps and the downstream analyte-detection step.

www.manaraa.com

The present design overcomes some limitations in prior works such as blood separation, complexity and the cost. This thesis provides a fully functional Lab-on-a-CD system that integrates whole blood pumping and separation, and quantificational electrochemical detections in parallel. A novel design of out-of-plane microvalves reduces the complexity of the microfluidic networks and flow control, and therefore ensures high yield plasma separation.

The factors that might affect the sensing sensitivity and the linear range of biosensors were analyzed in detail. The results provide a guideline for the practical configuration of biosensors according to diverse applications. Meanwhile, the nanoporous design of working electrodes solves the problems for the embedding of the modified working electrodes in microfluidic systems.

Each Lab-on-a-CD platform is a compact system, built by micro/nano fabrication techniques, so it consumes less sample and reagents. Each mold can be repeatedly used and the microfluidic cartridges are made of low-cost polymer material. Therefore, this system is suitable for POC diagnostics, especially for areas with limited medical resources.

The devices of the invention are suitable for the analysis of any liquid sample, typically a biological sample such as whole blood. It is also useful with numerous other biological samples, such as saliva, semen, sputum, urine, spinal fluid and the like, which need a separation or concentration processing step.

www.manaraa.com

7.3 Future Work

Although a Lab-on-a-CD system for automated and high throughput blood analysis has been built and verified, there is much room for innovation, adaptation, and cost reduction before these technologies can impact health care in the developing world. For example, the circular bio-platform will be designed with a receptacle or other coupling device suitable for mounting on a vertical drive shaft provided by a rotor. It will be appreciated that the bio-platform of the present invention may be adapted for use with all or most types of rotors that are now available on the market. In addition, the portable potentiostat used to perform electrochemical measurements has the potential to be minimized and integrated on the bio-platform. The surface area of the electrodes can be reduced to the micron scale, so each section will take up less area, resulting in more tests that can be done on one panel. Furthermore, more detected functions should be explored on the Lab-on-a-CD system, such as immunoassay for the detection of acute myocardial infarction.

www.manaraa.com

Curriculum Vitae

Name:	Tingjie Li
Post-secondary Education and Degrees:	The University of Western Ontario London, Ontario, Canada 2008-2012 Ph.D.
	Beijing Institute of Technology Beijing, China 2006-2008, M.Sc
	Beijing Institute of Technology Beijing, China 2002-2006, B.Eng
Honours and Awards:	Western Graduate Research Scholarship 2008-2012
	Outstanding Research Thesis Award 2008
	Excellent Student Scholarship 2002-2008
Related Work Experience	Teaching Assistant The University of Western Ontario 2009-2012
	Research Assistant The University of Western Ontario 2008-2012
	Research Assistant Beijing Institute of Technology 2006-2008

www.manaraa.com

Publications:

1. **Tingjie Li**, et al., Nanostructured thin-film electrodes for electrochemical detection in Lab-on-a-chip. (2012, submitted)

2. **Tingjie Li**, et al., Glucose Biosensors Based on Prussian Blue/Carbon Nanotube Electrodes: Design and Optimization of Their Configuration for Practical Applications. (2012, submitted)

3. **Tingjie Li**, et al., Out-of-plane valve for blood separation and metering: towards lab-in-a-tube applications for blood diagnostics. (2012, submitted)

4. **Tingjie Li**, Limin Zhang, Kar Man Leung and Jun Yang, Out-of-plane microvalves for whole blood separation on lab-on-a-CD. Journal of Micromechanics and Microengineering, 2010. **20**: p. 105024.

5. Yaxi Fan, **Tingjie Li**, Woon-Ming Lau and Jun Yang, SU-8 molds modified with copper and flurosilane: design and fabrication of hybrid master molds for rapid prototyping of micro-devices, IEEE/ASME Journal of Microelectromechanical Systems, 2012, 99, 1-7.

6. **Tingjie Li,** Changhua Hu and Gengkai Hu, Experimental study of pull-out test for SMA fiber [J] Mechanics in Engineering, 2008,V30(4): 44-46

Patents:

1. U.S. Provisional Patent, 61/542,885, Fabrication of Free Standing Membranes and Use Thereof for Synthesis of Nanoparticle Patterns.

2. Processing U.S. Provisional Patent, A One-step Photolithographic Method for Engineering of Superoleophobic Surfaces.

3. Chinese Patent, #201010271347.1, Portable system for fast blood analysis based on rotational 3D-microchip. (Pending)

www.manaraa.com

Conference Proceedings:

1. T. Li, F. Jia, Y. Fan, Z. Ding and J. Yang, Nanoporous Thin-film Electrodes for Electrochemical Detection in Microfluidic System, 95th Canadian Chemistry Conference and Exhibition, Calgary, Canada 2012.

2. Y. Fan, T. Li and J. Yang, Fast Prototyping and Small Volume Production of Polymer Devices by Hybrid Molds using Hot Embossing Lithography, 24th Canadian Materials Science Conference, London, Canada 2012.

3. T. Li, F. Jia, Y. Fan, Z. Ding and J. Yang, Nanofabrication of an Electrochemical System and its Application in Lab-on-a-CD, 24th Canadian Materials Science Conference, London, Canada 2012.

4. Q. Zhang, T. Li and J. Yang, Biosensors Based on Prussian Blue/Carbon Nanotube Electrodes: Design and Optimization of Their Configuration for Practical Applications, 95th Canadian Chemistry Conference and Exhibition, Calgary, Canada 2012

5. Li, T., et al., A Centrifugal Lab-in-a-tubing Platform Enabling Automatic Point-of-care Blood Diagnostics, IEEE International Conference on Mechatronics and Automation (ICMA 2011), August 7 - 10, Beijing, China 2011.

6. Qiuquan Guo, Tingjie Li, and Jun Yang, "Design of Enhancing Acoustic Focusing Metamaterials in Conjunction with Tissue Structures for Ultrasound Therapy", International Symposium on Acoustic Metamaterials, May 23-25, Beijing, China 2011.

7. Li, T., et al, "Lab-on-a-CD for Parallel Blood Analysis", ECS Canadian Section Fall Symposium, September 18, London, Canada 2010.

8. Jun Yang, Tingjie Li, "High performance blood separation on lab-on-a-CD: toward parallel and multiple lab-on-a-chip blood testing", International Conference on Cellular & Molecular Bioengineering, August 2 – 4, Singapore 2010.

www.manaraa.com